

**UCGE Reports
Number 20337**

Department of Geomatics Engineering

**Assessment and Attenuation of Movement Disorder
Motion using Inertial Sensors**

(URL: <http://www.geomatics.ucalgary.ca/graduatetheses>)

by

Wesley J.E. Teskey

September, 2011



UNIVERSITY OF CALGARY

Assessment and Attenuation of Movement Disorder Motion using Inertial Sensors

by

Wesley J.E. Teskey

A THESIS

SUBMITTED TO THE FACULTY OF GRADUATE STUDIES

IN PARTIAL FULFILLMENT OF THE REQUIREMENTS FOR THE

DEGREE OF DOCTOR OF PHILOSOPHY

DEPARTMENT OF GEOMATICS ENGINEERING

CALGARY, ALBERTA

SEPTEMBER, 2011

© Wesley J.E. Teskey 2011

Abstract

The research presented is focused on assessment and attenuation of movement disorder motion utilizing inertial sensors (accelerometers and gyroscopes); the major finding of the work is that inertial sensors are well suited for the assessment and attenuation tasks examined. Assessment involves categorizing the motion for patients examined, and techniques utilized to assist with diagnosis of ET (essential tremor) and PD (Parkinson's disease) are included. Common assessment methodologies utilized are based on Fourier and wavelet spectral analysis.

Another focus of the work is tremor attenuation (active mitigation). This involves utilizing two processing methodologies, the first of which is based on understanding along which of the six possible degrees-of-freedom tremor is acting and how tremors along these different six degrees-of-freedom are related in terms of phase. The second methodology is based on designing active and passive systems to mitigate tremor. For active inertial feedback systems, it is helpful to track tremor for removal using an algorithm well suited to the task; preferably a zero phase lag real time filter.

In order to carry out the tasks identified, data were gathered from 9 ET subjects, 30 PD subjects and 11 controls. Firstly, subjects were asked to use a laser mounted on an inertial measurement unit (IMU) to point to targets on a computer screen labeled one through ten.

The subjects moved their hand to direct the laser at subsequent targets in the order in which the targets were labeled. Secondly, subjects were asked to simulate eating using a spoon with an IMU attached to the spoon.

It is important to note that to adequately perform the processing tasks identified above, a Kalman filter and smoother was needed. This filter and smoother, along with subsequent processing, helped to ensure that processed accelerometer data would be representative of mostly lateral tremor motion, and not rotational tremor motion. Rotational tremor motion can influence accelerometer data indirectly as accelerometers are rotated through the gravity field. After the removal of signal components associated with rotational tremor motion, processed accelerometer data could be used to understand lateral tremor. In order to understand rotational tremor, largely unprocessed gyroscope data were utilized.

Preface

There are a number of figures and tables contained in this doctoral thesis that have been previously published, whereby the author of this thesis was lead author for such publications. The author of this doctoral thesis did receive significant support from co-authors (from previous published works) in terms of feedback regarding figures and tables produced; however, all such figures and tables are the author's original work. As well, all permissions have been obtained from co-authors and publishers so that figures and tables can be reproduced within the body of this thesis. Lastly, all such figures and tables are appropriately referenced when they are reproduced from another published source and full citations can be found in the alphabetized references list at the end of this document under the first author name "Teskey" (the last name of the author of this thesis).

Acknowledgements

Most importantly, I would like to thank Maryam Gholamirad, who was during the thesis work, and continues to be, the most important person in my life. It is also very important to thank my family and friends whose love and support helped me during my doctoral work.

I want to express my gratitude towards Dr. Naser El-Sheimy, my supervisor during my PhD work. He provided me great support and encouragement during my thesis work and a lot of latitude to experiment. This experimentation allowed for unique insight into the work presented here and greatly enhanced the quality of the results. I have been given great opportunities to publish and attend international conferences thanks primarily to Dr. El-Sheimy and I thank him very much for this.

I also would like to thank Dr. Mohamed Elhabiby, a collaborator and person providing guidance during my PhD work. He provided very valuable insight for the algorithms presented here and his influence was extremely valuable. Dr. Elhabiby brought a thorough understanding of signal processing with him to any discussions we had about how to appropriately deal with tremor data and he was exceptionally helpful. There were a number of occasions where I would become frustrated after having a paper rejected,

and Dr. Elhabiby was very good at calming me down, putting things in perspective and keeping me on task, and for this I thank him very much.

Dr. Brian MacIntosh was also a very valuable person for the work presented here and is very deserving of thanks; he was on the supervisory committee for the thesis work. Dr. MacIntosh provided his lab space for testing, as well as providing information about test subject recruitment and management. This help likely saved many months for the project and significantly improved the quality for data gathered. Likely the most valuable contribution from Dr. MacIntosh was his insight into movement disorders from the perspective of the movement sciences. This was very valuable insight given that most of the others on the project team were engineers.

Thanks also to Dr. Derek Lichti, my co-supervisor, who provided feedback and insight into the research project undertaken and helped to guide the project direction. I would also like to thank Dr. Yang Gao for being part of my supervisory committee for the work performed. As well, thanks to Dr. Tahir Khan and Dr. Wolfgang Keller, who are on my PhD thesis defense committee.

Ken Grandia helped to recruit test subjects for the project and provided feedback about the project. He is deserving of thanks.

The test subjects themselves are deserving of special thanks because without them the project could not go ahead. As well, thanks to those who helped to recruit the test subjects. Many of the test subjects came from the Parkinson Society of Southern Alberta thanks in large part to the efforts of Marta Vidra, whom is very deserving of thanks.

Thanks to Bruce Wright who built and tested the proprietary IMU used for data acquisition. This was imperative for the project and allowed for the acquisition of inertial data. As well, thanks to Xing Zhao who helped with calibration and debugging for the IMU.

There were three funding agencies who made the work presented here possible. Thanks to Alberta Innovates – Technology Futures, formerly the Alberta Ingenuity Fund (AIF), the Natural Sciences and Engineering Research Council of Canada (NSERC) and Geomatics for Informed Decisions (GEOIDE).

Table of Contents

Abstract.....	ii
Preface	iv
Acknowledgements.....	v
Table of Contents.....	viii
List of Tables.....	xii
List of Figures.....	xiii
List of Abbreviations and Symbols.....	xvii
Chapter 1: Introduction.....	1
1.1 Major Thesis Objectives.....	3
1.2 Novel Contributions.....	3
1.3 Chapter Overview.....	6
Chapter 2: Literature review.....	9
2.1 Movement Disorders Introduction.....	9
2.2 Essential Tremor.....	10
2.2.1 ET Epidemiology.....	10
2.2.2 ET Features.....	11
2.2.3 ET Diagnosis.....	12
2.2.4 ET Pathophysiology.....	12
2.2.5 ET Treatment.....	13
2.3 Parkinson’s Disease.....	13
2.3.1 PD Epidemiology.....	14

2.3.2 PD Features.....	14
2.3.3 PD Diagnosis.....	15
2.3.4 PD Pathophysiology.....	15
2.3.5 PD Treatment.....	16
2.4 Inertial Sensing.....	16
2.4.1 Inertial Principles of Operation.....	19
2.4.2 Common Uses of MEMS Inertial Sensors.....	22
2.4.3 Advantages of MEMS Inertial Sensors.....	23
2.4.4 Disadvantages of MEMS Inertial Sensors.....	24
2.4.5 Inertial Error Sources.....	26
2.4.6 Inertial Sensor Calibration.....	27
2.4.7 Inertial Stochastic Parameters.....	28
2.5 Non-Inertial Motion Capture Techniques.....	30
2.5.1 Optical Sensing.....	31
2.5.2 Mechanical Techniques.....	32
2.5.3 Global Navigation Satellite System (GNSS).....	33
2.5.4 Pressure and Force Sensing.....	35
2.5.5 Magnetic Sensing.....	36
2.5.6 Acoustic Sensing.....	37
2.6 Computational Methods.....	38
2.6.1 Kalman Filtering.....	39
2.6.2 Extended Kalman Filter (EKF) Prediction.....	42
2.6.3 EKF Updates.....	43

2.6.4 Kalman Smoother.....	46
2.6.5 Fourier and Coherence Analysis.....	48
2.6.6 Weighted-Frequency Fourier Linear Combiner.....	50
(WFLC) Filtering	
2.6.7 Wavelet Analysis.....	55
2.7 Summary.....	63
Chapter 3: Experimental Methods.....	65
3.1 Laser Targeting Motion Evaluation.....	66
3.2 Eating Simulation Motion Evaluation.....	71
3.3 Test Subjects Utilized.....	74
3.4 Equipment Utilized.....	76
3.5 Wavelet Chosen to Display Frequency Content.....	77
3.6 Display of Raw Data and Frequency Content.....	81
3.7 Summary.....	89
Chapter 4: Data Analysis using Extended Kalman Filtering.....	91
and Smoothing	
4.1 Need for Kalman Filtering and Smoothing.....	91
4.2 Data Processing to Assist with the Removal.....	94
of Gravity from Accelerometer Data	
4.3 Quaternion Based EKF and Smoother.....	98
4.4 Display of Accelerometer Data with.....	103
and without Gravity's Impact	
4.5 Summary.....	108

Chapter 5: Characterization and Diagnostic Algorithms.....	110
5.1 Auto-Spectral Fourier Analysis of Tremor.....	112
5.2 Wavelet Spectral Analysis of Tremor.....	116
5.3 Cross-Spectral Fourier Analysis of Tremor.....	124
5.4 Summary.....	137
Chapter 6: Attenuation Algorithms.....	138
6.1 Main Axes of Tremor Motion.....	139
6.2 WFLC Based Filtering.....	146
6.3 Summary.....	155
Chapter 7: Conclusions and Recommendations.....	157
7.1 Objectives Realized.....	158
7.2 Strengths and Weaknesses of the Approach Presented.....	160
7.3 Recommendations.....	165
References.....	170

List of Tables

Table 3.1: Inertial sensor specifications.....	76
Table 5.1 (a): Group mean of means ($\bar{x}_Q(20)$) and associated standard deviation of means ($\bar{x}_s(20)$) for wavelet coefficients at scale 20	120
Table 5.1 (b): Group mean of standard deviations ($\bar{x}_s(20)$)..... and associated standard deviation of standard deviations ($s_s(20)$) for wavelet coefficients at scale 20	120
Table 5.2: ET and PD patients with exceptionally high tremor.....	126
Table 5.3: Patterns for auto-spectral and coherence plots..... given x-accelerometer data with gravity removed and y-gyroscope data for the laser targeting motion evaluation	131
Table 5.4: Population mean, standard deviation and p-values for individual coherence peaks for x-accelerometer and y-gyroscope data occurring within the 3-12 Hz frequency band	136
Table 6.1: Population phase lag results in radians for the y-gyroscope..... leading the x-accelerometer at peak coherence for the laser targeting motion evaluation ($\frac{\pi}{2} \cong 1.57$)	140

List of Figures

Figure 2.1: Effect of translational and rotational motion on.....	18
an accelerometer signal	
Figure 2.2: Accelerometer principle of operation.....	20
Figure 2.3: Illustration of Coriolis acceleration.....	22
Figure 2.4: Allan variance plot to find random walk.....	30
Figure 2.5: Acoustic sensing using reflected sound waves.....	37
Figure 2.6: Kalman smoothing flow chart.....	48
Figure 2.7: Derivation of pseudo frequency for a.....	59
Daubechies wavelet of order 2	
Figure 2.8: Cascading high and low pass filters that compose the DWT.....	61
Figure 2.9: Frequency range and number of coefficients for.....	63
different levels of DWT decomposition	
Figure 3.1: A test subject before the initiation of the.....	67
laser targeting motion evaluation	
Figure 3.2: A test subject during the laser targeting motion evaluation.....	68
Figure 3.3: Typical target positioning for the laser.....	70
targeting motion evaluation	
Figure 3.4: A test subject before the eating simulation motion evaluation....	72
Figure 3.5: A test subject during the eating simulation motion evaluation....	73
Figure 3.6: The Coiflets 3 mother wavelet.....	78
Figure 3.7: The Coiflets 3 father wavelet.....	80

Figure 3.8(a): X-accelerometer raw data and time-wise.....	82
spectral distribution (utilizing the Coiflets 3 continuous	
wavelet transform) for a typical control	
Figure 3.8(b): X-accelerometer raw data and time-wise.....	83
spectral distribution (utilizing the Coiflets 3 continuous	
wavelet transform) for a typical ET patient	
Figure 3.9 (a): Y-gyroscope raw data and time-wise.....	84
spectral distribution (utilizing the Coiflets 3 continuous	
wavelet transform) for a typical control	
Figure 3.9 (b): Y-gyroscope raw data and time-wise.....	85
spectral distribution (utilizing the Coiflets 3 continuous	
wavelet transform) for a typical ET patient	
Figure 4.1: Flow chart for the removal of rotational tremor data from.....	93
accelerometer signals	
Figure 4.2: Raw y-accelerometer data before and after Kalman.....	105
smoothing to remove gravity for a typical trial	
Figure 4.3: Population Coiflets 3 spectral magnitudes for.....	108
x-accelerometer data before and after Kalman smoothing	
and subsequent mathematical operations to remove gravity	
Figure 5.1: Population y-gyroscope data continuous Coiflets 3.....	112
spectral distribution	
Figure 5.2: Population auto-spectral distributions using.....	114
Fourier analysis for controls (solid lines)	

and ET patients (dotted lines)	
Figure 5.3: Population wavelet coefficient means and.....	121
standard deviations y-gyroscope data of controls	
(solid lines) and ET patients (dotted lines)	
Figure 5.4: Population means from (5.1) for controls (solid lines) and.....	122
ET (dotted lines)	
Figure 5.5: Population standard deviations from (5.2) for controls.....	123
(solid) and ET (dotted)	
Figure 5.6: Population auto-spectra for x-accelerometer data with.....	127
gravity remove (left) and y-gyroscope data (right) for	
the laser targeting motion evaluation	
Figure 5.7: Representative individual x-accelerometer data with.....	130
gravity removed and y-gyroscope data for the	
laser targeting motion evaluation	
Figure 5.8: Population coherence values for x-accelerometer data.....	134
with gravity removed and y-gyroscope data for the	
laser targeting motion evaluation	
Figure 6.1: The largest two tremor are shown for the laser.....	141
targeting motion evaluation	
Figure 6.2: Flow chart for WFLC data processing.....	149
Figure 6.3: Critically damped filtering to remove.....	150
<i>intended motion</i> depicted using representative data	
from the z-gyroscope	

Figure 6.4: WFLC filtering to track tremor, as depicted using.....151
representative data from the z-gyroscope

Figure 6.5: Coiflets 3 continuous wavelet analysis to.....152
analyze filtering capabilities using representative data
from the x-accelerometer

Figure 6.6: Coiflets 3 continuous wavelet analysis to analyze.....153
filtering capabilities using representative data from
the x-gyroscope

List Abbreviations and Symbols

Abbreviations

AIF	The Alberta Ingenuity Fund
ARW	Angular random walk
CWT	Continuous wavelet transform
DWT	Discrete wavelet transform
EEG	Electroencephalography
EMG	Electromyography
EKF	Extended Kalman filter
ET	Essential tremor
FMRI	Functional magnetic resonance imaging
Galileo	European Union based navigation satellite system
GEOIDE	Geomatics for Informed Decisions
GLONASS	Russian based global navigation satellite system
GNSS	Global navigation satellite systems
GPS	Global positioning system

HP	High pass
IMU	Inertial measurement unit
LMS	Least mean squares
LP	Low pass
MEMS	Microelectromechanical systems
MMSS	Mobile Multi-Sensor Systems Research Group
NSERC	The Natural Sciences and Engineering Research Council of Canada
PD	Parkinson's disease
RTS	Rauch-Tung-Striebel (a type of Kalman smoother)
USB	Universal serial bus
VRW	Velocity random walk
WFLC	Weighted-frequency Fourier linear combiner (filter)

Symbols

\times	Denotes cross product (right hand rule sign convention is followed)
$\tilde{*}$	Notation signifies the complex conjugate of *
$\hat{*}$	Adjusted parameter * (after mathematical optimization)
$ * $	Operator denotes absolute value of *

\int^*	Integral operator for *
$*^{-1}$	Superscript -1 denotes matrix inverse of *
\bar{a}	Measured acceleration vector
$*_a$	Subscript a denotes symbols associated with accelerometer data
\bar{a}_{cor}	Coriolis acceleration vector
A_k	Kalman smoothing weighting matrix
a_r	Adaptive parameter for WFLC filtering
A_{sin}	The amplitude of a sin wave under examination
$A_{sin,l}$	Amplitude for a lateral tremor
$A_{sin,r}$	Amplitude for a rotational tremor
\bar{b}	Inertial signals bias
b_r	Adaptive parameter for WFLC filtering
$c(n_{wav})$	Wavelet approximations coefficients
cl	Represents the 95% confidence limit for statistical testing
\cos	The cosine wave function
$d(n_{wav})$	Wavelet details coefficients
$\frac{d}{dt}$	Differential operator

$d_s(\omega, l)$	Fourier transform of a signal $s(k)$
$E[]$	The statistical operator for expected value
e^*	Exponential operator for *
$\hat{f}_{11}(\omega)$ or $\hat{f}_{22}(\omega)$	Auto-spectral estimate for signals $s_1(k)$ or $s_2(k)$, respectively
$\hat{f}_{12}(\omega)$	Cross-spectral estimate for two signals $s_1(k)$ and $s_2(k)$
F_a	Wavelet pseudo frequency
\bar{f}_a	Error free accelerometer signal
F_c	Wavelet center frequency
\bar{g}	Gravity vector
G_k^{kf}	Kalman filtering noise coefficient matrix
g_{wav}	Low pass filter impulse response for wavelet analysis
\bar{g}_ω	Error free gyroscope signal
H^{kf}	Kalman filtering design matrix
h_{vm}	An exponential parameter for wavelet analysis
h_{wav}	High pass filter impulse response for wavelet analysis
$I_{*,*}$	An identity matrix of size * by *
i	Imaginary number

k	Time step of interest
$*_k$	Subscript k denotes symbols associated with data at time step k
$*_{k-1}$	Subscript $k - 1$ denotes symbols associated with data at time step $k - 1$
K^{kf}	Kalman filtering gain matrix
L	Number of segments for Fourier spectral calculations
l	Segment under evaluation for Fourier spectral calculations
M	Total number of members in the population for statistical testing
M^{wflc}	Represents the maximum harmonic of the fundamental frequency, ω_0 , for WLFC filtering
m_γ	Value of the wavelet scaling used for CWT
N	The total number of time steps evaluated
\bar{n}	Inertial signal noise
N_{av}	The total number of samples for Allan variance
n_{av}	Number of samples in an Allan variance cluster
N_{non}	A matrix to correct for non-orthogonal sensor configurations
N_{sam}	Total number of signal samples under evaluation
n_{wav}	A counter used for the DWT

p	Population member for statistical testing
P^{kf}	Kalman filtering covariance matrix of the state vector
P_0^{kf}	Kalman filtering covariance matrix of the state vector at time zero
$P_{k N}$	Kalman smoothed covariance matrix of the state vector
$P_{k,updated}^{kf}$	Updated Kalman filtering covariance matrix of the state vector
$P_{k+1,not\ updated}^{kf}$	Kalman filtered covariance matrix of state vector before update
\bar{q}	A four element quaternion vector
q_1, q_2, q_3 and q_4	The four elements of a quaternion vector
Q_{av}	Random walk for Allan variance
Q_k^{kf}	Kalman filtering covariance matrix of the system noise
$Q(m_\gamma, t_\sigma)$	Continuous wavelet transform coefficients
$\bar{Q}(\gamma, p)$	Mean for absolute values of continuous wavelet coefficients
R	A three by three rotation matrix
r	Represents harmonics of the fundamental frequency, ω_0 , for WLFC filtering
$ \hat{R}_{12}(\omega) ^2$	Coherence estimate for signals $s_1(k)$ and $s_2(k)$
R_k^{kf}	Kalman filtering covariance matrix of measurement noise

S	A matrix of errors for the linear scale factor
$s(t), s(k)$ or s_k	The signal under evaluation
$s_{av}(T_{av})$	Signal average for the Allan variance cluster
$s_{av,next}(T_{av})$	Signal average for the <i>next</i> Allan variance cluster
$*_{second}$	Denotes parameters for the second iteration of WFLC filtering
\sin	The sine wave function
$s_{\bar{Q}}(\gamma)$	Standard deviation of means for absolute values of continuous wavelet coefficients
$s_s(\gamma)$	Standard deviation of standard deviations for absolute values of continuous wavelet coefficients
$s(\gamma, p)$	Standard deviation for absolute values for continuous wavelet coefficients
t_1	Wavelet time shift parameter
T	Total number of samples under evaluation
$*^T$	Superscript T denotes matrix transpose
t	Time in the continuous domain
T_{av}	Cluster time for Allan variance
t_{σ}	Translational term used for CWT

vm	Vanishing moments for wavelets
\bar{v}_{rad}	Radial velocity vector
\bar{w}_k^{kf}	Kalman filtering noise vector
\bar{x}^{kf}	Kalman filtering state vector
$\hat{x}_{k N}$	Kalman smoothed state vector
$\hat{x}_{k,updated}^{kf}$	Updated Kalman filtering state vector
$\hat{x}_{k+1,not\ updated}^{kf}$	Kalman filtered state vector before update
$\bar{x}_Q(\gamma)$	Mean of means for absolute values of continuous wavelet coefficients
$\bar{x}_s(\gamma)$	Mean of standard deviations for absolute values of continuous wavelet coefficients
y_k^{wflc}	WFLC signal tracking parameter
\bar{z}^{kf}	Kalman filtering measurement updates
γ	Represents whole number wavelet scales for CWT
$\delta(*)$	The Dirac delta function
Δt	Time interval between data samples

ε_k	Error between the tremor tracking parameter, y_k^{wflc} , and signal of interest s_k for WFLC filtering
θ_a	Scalar rotation about a unit vector $\bar{\theta}_u$ (for quaternion analysis)
$\bar{\theta}_u$	The unit vector about which a quaternion rotates
θ_x, θ_y and θ_z	Represent rotations about the x-axis, y-axis and z-axis respectively (for quaternion analysis)
μ_0	Affects the speed of iterative convergence for WFLC filtering
μ_1	Affects the speed of iterative convergence for WFLC filtering parameters a_r and b_r
π	The ratio of the circumference of a circle to its diameter
Σ^*	Summation operator for *
σ	The signal sample currently under evaluation
$\sigma_{av}^2(T_{av})$	Allan variance values for differing cluster times
$\sigma_{av,*,arw}^2(T_{av})$	Angular random walk for * gyroscope (either x, y or z gyroscope)
$\phi(t)$	Father wavelet
$\hat{\Phi}_{12}(\omega)$	Phase shift estimate between signals $s_1(k)$ and $s_2(k)$
$\Phi_{k,k-1}^{kf}$	Kalman filtering discretized state transition matrix
$\psi(t)$	Mother wavelet

$\psi^\#(t)$	The dual function for $\psi(t)$
$\widehat{\Psi}(\omega)$	The Fourier transform of the mother wavelet $\psi(t)$
ω	Radial frequency
$\bar{\omega}$	Measured rotation rate vector
$*\omega$	Subscript ω denotes symbols associated with gyroscope data
ω_0	The fundamental frequency for WLFC filtering
ω_{0t_k}	The fundamental frequency for WLFC filtering updated at each time step t_k
$\bar{\omega}_{cr}$	Circular rotation rate vector
$\Omega(\bar{\omega})$	A four by four matrix representing rotation

Chapter 1: Introduction

Essential tremor (ET) and Parkinson's disease (PD), both of which are movement disorders under examination in this thesis, can be studied and managed much more capably with the advent of inertial technology (accelerometers and gyroscopes). Such use of inertial technology in the formal study of movement disorders is the focus of this thesis, which includes methodologies to improve the quality of life of those afflicted with movement disorders.

Currently, *neither ET nor PD is adequately characterized so that diagnoses can be performed consistently*. ET, for example, has a believed rate of incidence over a very large range (0.008% to 22% (Louis, Ottman and Hauser, 1998)) largely because it is difficult to come up with an objective measure to standardize diagnostic practices. PD, although much better understood than ET, can also stand to benefit from objective diagnostic criteria. Currently, responsiveness to medication is often regarded as a confirmation of a PD diagnosis because it is otherwise difficult to confirm a diagnosis (Koller and Hubble, 1990) and only 75% of PD diagnoses turn out to be true positives when autopsies are carried out (Gelb, Oliver and Gilman, 1999); PD affects approximately 0.15-0.2% of the population at large (Rao et al., 2003).

Usable procedures to assist with diagnosing PD and ET from only inertial data are presented in this thesis. Much of the diagnostic research work carried out using inertial

sensors is still in its infancy and there is no standard inertial technology for objective diagnoses (Louis, 2005).

In terms of quality of life, patients afflicted by either disorder (ET or PD) could benefit from inertial data capture. Utilizing such techniques can help medical practitioners track patient motion over time as medications and other treatment options are explored. Despite all of the advantages of having an objective means of measuring tremor size as well as other significant parameters depicting patient motion, there is no standard technology to perform such a task and there is very little research that has examined this methodological approach (Louis, 2005).

As a final point, ***patients' lives could be made quite a bit better by utilizing tremor attenuation methodologies based on inertial data capture*** and processing, possibly in conjunction with a feedback system. Currently, many movement disorder sufferers (PD and ET) have trouble performing daily tasks such as eating, drinking and writing; as well, ET does not generally have an effective pharmacotherapy based treatment option. As a result, many patients go without any treatment even though 73% of ET patients have a reported disability (Louis et al., 2001). PD is also quite debilitating and has an estimated social cost of \$20 billion annually in the United States (Smaga, 2003). The work presented here details how to mitigate tremor motion while maintaining *intended* patient motion. This information could be used, for example, to design an inertial feedback system for a drinking cup such that the cup handle would move relative to the cup in such a fashion as to limit the ability of tremors felt at the cup handle to spill a beverage in the

cup. There are very few tremor mitigation technologies currently available despite the pressing need, and many of the existing mitigation technologies focus on orthosis based approaches which require patients to wear bulky and difficult to manage exoskeletons in order to dampen tremor motion (Manto et al., 2003).

1.1 Major Thesis Objectives

One of the major objectives of the thesis is to *create diagnostic methodologies for assessment of movement disorder motion*; specifically, differentiating PD and ET motion which is a very common challenge for medical professionals.

Another objective of the thesis is to *process and comprehensively analyze tremor data for six degrees-of-freedom of motion*. This is a very significant undertaking and few if any thorough analyses of tremor in six degrees-of-freedom have ever been undertaken.

Algorithm validation for attenuation (removal) of tremor is also another objective for the work carried out. Tremor is first categorized in terms of its effects along different axes of motion and then a popular mitigation algorithm is utilized to determine how effectively it can cope with tremor.

1.2 Novel Thesis Contributions

The most significant novel contribution for the work carried out was that it is *the first such thorough six degree-of-freedom motion analysis of movement disorders*. It is difficult to overstate how significant and instrumental six degree-of-freedom motion

analysis was for what was accomplished. Without it, coming up with a unique and novel diagnostic methodology to differentiate ET and PD motion may not have been possible. As well, many of the patterns of motion observed in the work would not have been visible.

The second most instrumental novel contribution of the thesis work conducted was that it was *the first such thorough wavelet analysis of movement disorder motion*. Wavelets are quite underutilized for movement disorders research. The work presented for this thesis clearly shows that wavelets are a very important signal processing tool for movement disorder analysis and they deserve much more implementation in future research work.

The *implementation of coherence analysis to different (six degree-of-freedom) movement disorder channels of motion is also a novel contribution* of the thesis work. Coherence analysis is a very important tool for electromyography (EMG) signal analysis and is often used to compare motion data (often inertial motion data) with EMG data. This useful tool was applied in this thesis in a manner such that all six degrees-of-freedom of motion were compared.

One of the results of implementing coherence analysis in the manner depicted in the previous paragraph was that *a new methodology for differential diagnosis of ET and PD was realized*. Such a diagnostic methodology as what was discovered could be very useful for medical practitioners because it is very usable and easily understandable for

differential diagnosis of ET and PD (which is a significant area of research for movement disorders).

Another one of the unique findings of the work is that it is possible to tell the difference between medicated and un-medicated PD motion, using control data as a reference.

Even though to the naked eye medicated PD motion looks like motion of a normal healthy subject, inertial data reveal that a trace of non-control motion still exists even among medicated subjects. This is a very significant research finding because it suggests how medication masks the effects of PD and, more specifically, what motion artifacts this medication fails to mask (or creates). For a researcher studying the pathogenesis of PD, knowing specifically how medication affects motion is very valuable information.

Another valuable and new piece of information regarding movement disorder motion that was realized for the work carried out is that tremor is very similar in frequency for all six degrees-of-freedom. The main difference between tremors for different motion axes were that they were shifted in phase with respect to one another.

The weighted-frequency Fourier linear combiner (WFLC) filtering was carried out for this thesis for the first time using six degree-of-freedom movement disorder data. This algorithm was evaluated for its ability to remove tremor motion while not affecting *intended* motion of test subjects.

The goal of tremor attenuation was more capably pursued given results of the six degree-of-freedom analysis. Given such an analysis, it was conceivable to determine how attenuation might be applied to a real world scenario where, obviously, patients move in six degrees-of-freedom. *The tremor motion axes containing the most amplitude were determined (for the specific type of motion logged), as were the phases shifts for tremors acting along different axes of motion.* Such analysis makes the algorithms developed for tremor mitigation much more useful than they otherwise would have been because they could be realistically implemented in a manner so as to remove the largest tremors.

1.3 Chapter Overview

There are a total of seven chapters for the thesis. The document begins with a literature review in Chapter 2 followed by data collection methods outlined in Chapter 3. After that, Kalman filtering and smoothing are the focus of Chapter 4, where data processing results are examined. Chapter 5 examines diagnosis and assessment of movement disorders, and Chapter 6 details tremor attenuation and mitigation strategies. The conclusion of the thesis is written in Chapter 7.

Chapter 2, as previously mentioned, is a detailed literature review for the research conducted. It begins with an overview of the two movement disorders examined in this thesis (ET and PD) and then focuses on the equipment utilized for motion captured (inertial sensors as well as other equipment that may be useful for future research). At the conclusion of the chapter, the computational methods for the processing carried out in this thesis are examined.

Chapter 3 highlights the two different movement disorder tasks for which data were captured, these are the laser targeting and eating simulation motion evaluations. In the former, test subjects point a laser at targets with their hand while inertial data are logged for the motion under examination, and in the later, test subjects simulate eating with a spoon while inertial data are again gathered for their hand motion. Chapter 3 includes an overview of equipment and test subjects utilized, as well as displays of raw data.

Chapter 4 details the use of Kalman filtering and smoothing for analysis of movement disorder motion. More specifically, a quaternion based Kalman filter utilizes known start and end points of the IMU (inertial measurement unit) along with other parameters as filter updates. The main purpose of the processing in Chapter 4 is to remove the impact of gravity from accelerometer data, and this task is achieved by using results from the Kalman filter and smoothing. By processing accelerometer data in this manner, the impact of rotational tremors can be removed from the data so that the remaining accelerometer data are representative of mostly translational tremor (and not rotational tremor). Since raw gyroscope data are good at depicting rotational tremors, the processed accelerometer data and raw gyroscope data represent, directly, tremor motion for all six degrees-of-freedom analyzed.

Chapter 5 of the thesis details the use of auto-spectral and cross-spectral Fourier based signal processing for the six degrees-of-freedom under analysis; as well, wavelet based spectral processing is utilized. The Fourier based processing proved to be very adept at

diagnosing different tremor types (ET and PD) using a novel methodology developed for the thesis work. The wavelet based processing showed that diagnosed ET tremor has a significant difference in the magnitude of its peak for its spectrum when compared to control data (i.e. more tremor was apparent for ET data).

Chapter 6 details the use of phase based analysis to determine tremor phase data between any two of the six degrees-of-freedom of movement disorders in question, and to verify that tremor tends to be of the same frequency for different degrees-of-freedom examined. The phase data show that tremor along two different channels often have a consistent phase relationship. This information is important for when designing tremor mitigation technologies, such as actuators. The second half of Chapter 6 details how to remove pathogenic tremor in six degrees-of-freedom using a WFLC filter. This is performed here for the first time.

Chapter 7 concludes the analysis that has been undertaken. Objectives that have been realized are discussed in detail; as well, strengths and weaknesses for the approaches utilized are examined. Lastly, recommendations are made pertaining to future research.

Chapter 2: Literature Review

There are three sections in the literature review. The first section introduces the two major movement disorders that are the main focus of the research conducted: essential tremor (ET) and Parkinson's disease (PD). After this, the next section looks at possible methods of logging movement disorder motion, including inertial sensing and optical techniques among others. The last section of the literature review looks at all of the major processing techniques utilized for the signal analysis carried out in this thesis, including Kalman filtering, weighted-frequency Fourier linear combiner (WFLC) filtering and wavelet based techniques.

2.1 Movement Disorders Introduction

Both of the major movement disorders evaluated in the research work presented, ET and PD, have been part of the human existence for many thousands of years; ET has been documented in ancient Israel and Greece and there are biblical descriptions of PD, as well, historical texts thousands of years old describing both of these disorders can be found from Egypt and India (Louis, 2000; Ruiz, 2004). There is more of a pressing need to understand these disorders now than at many times in the past due to an increase in human life expectancy and the aging demographics in western society which will likely cause an increasing incidence of both disorders in the coming decades. For this reason, it is imperative to understand both disorders as much as possible to potentially help limit the rate of incidence and care for those afflicted.

2.2 Essential Tremor

Essential tremor is a very complex movement disorder that is not well understood. It was chosen for evaluation in this thesis because of this fact as well as its high rate of prevalence. The thesis work laid out here does a thorough job evaluating ET motion and suggesting possible means of attenuation, this is a significant advancement for a disorder that the medical establishment has not completely categorized. In the following subsections, what is known about ET is summarized.

2.2.1 ET Epidemiology

ET is the most prevalent action tremor known to exist (Bhidayasiri, 2005). An action tremor is defined as a tremor which manifests itself during voluntary motion.

Unfortunately, the disease is not well understood largely because of its wide ranging and not well defined symptoms (Findley and Koller, 1987; Hubble, Busenbark and Koller, 1989; Louis, 2001; Louis and Greene, 2000). It has been so difficult for medical practitioners to come up with a specific criteria for ET's diagnosis that the rate of prevalence has been quoted as ranging anywhere from 0.008% to 22% of the population at large depending on the study cited (Louis, Ottman and Hauser, 1998). Likely, a more realistic estimate for ET prevalence is 0.4-3.9% based on more thorough investigative studies carried out by experienced researchers (Louis, Ottman and Hauser, 1998).

ET is more common for older individuals (Rajput et al., 1984) and it is often not familial (Bain et al., 1994; Herskovitz and Blackwood, 1969). Known causes of ET are exposure to certain chemical agents (lead and carboline alkaloids); other environmental factors are

thought to increase incidence of ET, but many of these potential causes are not well defined (Louis et al., 2002; Louis et al., 2003).

2.2.2 ET Features

Writing, drinking and eating can all be affected by ET, which causes a tremor in the range of 3-12 Hz (Elble and Koller, 1990). The disorder tends to affect mostly the arms, but can affect any limb or major body segment, including the neck and trunk (Critchley, 1949). Severe cases of ET generally result in postural tremor in addition to kinetic tremor; kinetic tremor, which is unwanted tremor while a patient is intentionally moving, is the hallmark symptom of ET (Brennan et al., 2002). Postural tremor is defined for when a patient is trying to maintain a fixed position while exerting some sort of muscular effort, such as when a subject holds their arm straight in front of them perpendicular to an upright torso. There are also a small number of cases for which patients exhibit rest tremor (Koller and Rubino, 1985; Rajput et al., 1993), which is defined as tremor while a patient is trying to keep muscles in a relaxed state.

ET can have a debilitating effect on one's lifestyle. A large number of sufferers (73%) report a disability (Louis, Barnes, Albert et al., 2001), and for individuals seeking professional medical help, 15-25% retire earlier than desired (Bain et al., 1994) and 60% have reported not applying for a job or promotion because of their condition (Rautakorpi, 1978). ET is also a disorder linked to a patient's physical state such that fatigue and hunger can affect tremor (Critchley, 1949; Critchley, 1972). Although remissions are possible (Kreiss, 1912) ET tends to get worse over time (Critchley, 1949).

Accelerometers were used to log a 29% increase in tremor amplitude over a four year interval for several patients (Elble, 2000).

2.2.3 ET Diagnosis

Because the disease is not well understood, diagnosis of ET is very challenging. The main criterion for diagnosis is kinetic tremor (Louis, 2005) and there is difficulty creating a standard test to confirm a diagnosis with a high degree of reliability (Louis, 2001). A major task for medical practitioners is often differentiating ET from PD (Bain et al., 1994).

There are two standards by which movement disorders are measured. One standard is the Consensus Criteria of the Movement Disorder Society which focuses on whether postural tremor is present for five years or more; this is only valid for diagnosing ET in cases where such a postural tremor can't be explained by the use of drugs, a different neurological condition or other abnormal factors in the background of a subject (Deuschl, Bain and Brin, 1998). The other standard for clinical diagnosis of ET is the Washington Heights-Inwood Genetic Study of ET (Louis et al., 1997; Louis, Ford, Frucht et al., 2001). This diagnostic tool assigns an integer value between 0 (no tremor) and 3 (very large tremor) to quantify the severity of tremor for tasks involving patients pouring water, drinking and eating.

2.2.4 ET Pathophysiology

Similar to many other aspects of ET, its pathophysiology is also not well understood (Louis, 2005). The disease may even be familial, contradicting some previously believed

assertions, based on recent genetic, pharmacological and clinical evidence (Gulcher et al., 1997; Higgins, Pho and Nee, 1997; Higgins et al., 1998; Koller, Vetere-Overfield and Barter, 1989; Louis, Ford and Barnes, 2000). It is not even known for certain what part or parts of the neurological system (including the spinal tissue and portions of the brain) play a significant role in the manifestation of ET tremor (Bain et al., 1994).

2.2.5 ET Treatment

ET generally lacks effective treatment mechanisms and many patients do not report tremor reduction after pharmacotherapy (Louis, 2005). Alcohol is one method of reducing tremor, although it is generally not recommended because of other obvious side effects and the possibility of creating alcoholic addiction (Critchley, 1949; Davis and Kunkle, 1951). Deep brain stimulation (the implanting of an electrode into the human brain by surgical methods) has been effective, but there are many large risks associated with this treatment method including loss of bodily functions (Schuurman, 2000).

2.3 Parkinson's Disease

PD is generally much better understood than ET. This is due in part to the fact that sufferers of PD can't hide its symptoms well given that many of the movement effects it produces are largely involuntary (such as tremor motion while a patient is in a rest position); as such, PD has been afforded a much larger focus in the public and in the media while ET, whose motion is largely based on kinetic tremor, can remain a bit more hidden from the public eye as those who suffer from it can refrain from moving to avoid possible drawbacks of others realizing the effect of their disease.

ET also is as disorder that is very difficult to distinguish from physiological (healthy) tremor which most people share and which also generally grows larger with age; as such, motion tremor is a phenomenon that many people are more familiar with in the context of their daily lives and it seems less foreign to them when they are confronted with it. This is another reason why PD is so well known while ET is not commonly known.

PD can be very difficult to live with for those who suffer from it. It does not only produce tremor effects, but can really slow motion for those who are afflicted. There is still much need for assistance with PD management for medical practitioners because tracking its progress over time (with and without medication and exercise for those suffering from the disorder) can be a significant step forward in research. As well, mitigating PD for patients would help them greatly in coping with having to live with such an affliction.

2.3.1 PD Epidemiology

PD is the most common rest tremor known to exist (Bhidayasiri, 2005) and it affects 0.15-0.2% percent of people (Rao et al., 2003). In the United States, it is estimated that 1.5-2.5% of people aged 70 or older have PD (Mansur et. al., 2007). PD is progressive, and in general, not familial (Bhidayasiri, 2005). The social cost of PD in the United States is about \$20 billion each year (Smaga, 2003).

2.3.2 PD Features

PD is generally described by its capacity to produce rest tremor in those affected (Deuschl et al., 1996; Paulus and Jellinger, 1991; Rajput, Rozdilsky and Ang, 1991); in fact, there is generally only one other disorder (Holmes' tremor) known to commonly

afflict individuals causing rest tremor (Bergman and Deuschl, 2002). PD tremor frequency is in the range of 3-12 Hz (Elble and Koller, 1990). There is also another disease variant for PD which, instead of producing rest tremor, tends to produce akinetic and rigid movement tendencies among those afflicted (Jankovic et al., 1990, Louis et al., 1999). In general, PD both reduces muscle strength (Jordan, Sagar and Cooper, 1992; Stelmach et al., 1989; Stelmach and Worringham, 1988) and limits reaction time (Kutukcu et al., 1999). The disorder is also known in some cases to produce kinetic tremor (Logigian et al., 1991).

2.3.3 PD Diagnosis

The most common method for diagnosis of PD is based on the observation of postural and rest tremor, although any diagnosis is often based on a variety of indicators and relies heavily on the knowledge of the medical practitioner performing the diagnosis (Bhidayasiri, 2005). Bradykinesia (slowness of movement) can also be a telltale sign of PD, as can asymmetric tremor (Bhidayasiri, Waters and Giza, 2005).

As a result of generally limited objective diagnostic criteria, responsiveness to medication is also sometimes used to confirm a diagnosis (Koller and Hubble, 1990). Commonly, the drug levodopa, which boosts dopamine levels in the brain, is used to carry this out.

2.3.4 PD Pathophysiology

PD is caused by a lack of cells producing dopamine resulting in a dopamine shortage in the striatum (Bernheimer et al., 1973; Pifl, Schingnitz and Hornykiewicz, 1991); generally, dopamine producing cells lie within the substantia nigra. The complete

understanding of PD has not yet been realized and there are still many neurological phenomena associated with PD that are not fully understood (Bergman and Deuschl, 2002). It is generally agreed upon the spinal neurological influences do not significantly contribute to PD (Rack and Ross, 1986; Burne, 1987), but contradictory evidence details that the brain (likely the *central oscillator* for PD manifestation) is affected by inputs into spinal tissue (Elble, Higgins and Hughes, 1992). In contrast, the observation that deafferentiation usually does not limit PD tends to support the theory of the brain as the *central oscillator* (Pollock and Davis, 1930).

2.3.5 PD Treatment

Partly because the pathophysiology of PD is so much more understood than ET, PD tends to have much better treatment options when comparing the two disorders. Many PD patients rely on pharmacotherapy aimed at boosting dopamine levels in the brain and levodopa is among the most common drugs prescribed to carry out such a task (Bhidayasiri, 2005). Other commonly used drugs are pramipexole and ropinirole (Navan et al., 2003; Pogarell et al., 2002; Schrag, Keens and Warner, 2002). As with ET, deep brain stimulation can be used in the treatment of PD, but it carries high risk factors such as the loss of bodily functions (Berardelli et al., 2001).

2.4 Inertial Sensing

There are two inertial sensing devices commonly used for navigation applications, these are accelerometers and gyroscopes. Accelerometers measure positioning information by integrating an accelerometer signal twice with respect to time. The first of such integrations provides information about velocity and the second provides information

about position. Gyroscopes only require their signals to be integrated once with respect to time to produce orientation information.

One of the largest difficulties of dealing with inertial sensors is that they are often taking measurements on a moving platform. It would be relatively straight forward to analyze the signal of a single axis accelerometer for a vessel that could only move along the axis of accelerometer measurement. This is rarely the case for most real world applications.

Accelerometers and gyroscopes are generally mounted on devices which move freely in six degrees-of-freedom (three translational and three rotational degrees of freedom).

When six degree-of-freedom motion is permitted, the sensitive axis for each sensor is potentially changing alignment in time with respect to an earth fixed coordinate system.

This creates many complexities when analyzing inertial sensor data and generally all data have to be converted into a consistent coordinate frame so that data processing can take place.

One of the most significant challenges when interpreting inertial results is determining which portion of an accelerometer signal is a product of lateral motion and which portion is a measurement of gravity. Accelerometers do not distinguish between gravitational acceleration and acceleration as a result of lateral motion. This means that for an oscillatory accelerometer signal, either a lateral or rotational tremor could be the cause. The reason this is the case is because a rotational tremor causing a rotation through the

gravity field can generate a tremor signal for an accelerometer. This is illustrated in Figure 2.1.

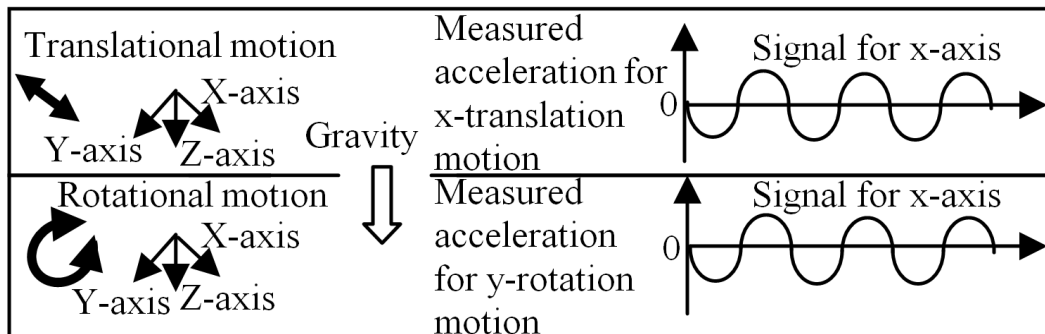


Figure 2.1: Effect of translational and rotational motion on an accelerometer signal

Taken from Teskey et al. (2011)

The phenomenon illustrated in Figure 2.1 is of particular concern for the work carried out in this thesis because much of the data logged is for lateral and rotational tremors. As a result, a great deal of the processing conducted for this thesis was aimed at removing the effect of rotational tremor motion from the accelerometer data so that lateral and rotational tremor could be analyzed separately. This is illustrated in detail in Chapter 4.

Generally when capturing inertial data, three accelerometers and three gyroscopes are utilized because this configuration is ideal for capturing six degrees-of-freedom of motion data. Usually, each of the two sensor triads utilized (composed of three accelerometers and three gyroscopes) have each individual sensor orthogonal to the other two. This makes processing the data much easier, because there is no redundancy in captured data. As well, generally for convenience, one sensor triad will have corresponding individual sensing elements coincident with the elements of another sensor

triad (i.e. the x-accelerometer lies along the same axis as the x-gyroscope, the y-accelerometer lies along the same axis as the y-gyroscope and the z-accelerometer lies along the same axis as the z-gyroscope). There are many other sensor configurations that can also achieve six degree-of-freedom motion capture, such as an all accelerometer sensor set, but these are far less common because they are not as easily implemented. For an all accelerometer configuration in particular, the best results are obtained when accelerometers are mounted a long distance from one another so that good orientation information can be obtained; for many real world applications, this is not practical.

2.4.1 Inertial Principles of Operation

Accelerometers generally operate following Newton's first and second laws. Newton's first law is based on the principle of inertia which describes that objects in motion will tend to remain in motion and objects at rest will tend to remain at rest; this is valid unless there is a force acting on an object so as to change its motion or state of rest. When a force acts upon an object, Newton's second law can be applied. This law states that the net force acting on an object will be equal to its mass multiplied by its acceleration.

Most accelerometers utilize the principles in Newton's first two laws by utilizing a proof mass suspended by a spring or multiple springs. When the proof mass is undergoing acceleration along the sensitive axis of the accelerometer, it is displaced until the force in the spring or springs are enough to counteract the tendency of the proof mass to resist changes in its motion (based on its inertia). This concept is illustrated in Figure 2.2. It should be noted that the sensitive axis of the accelerometer is the axis along which the springs in Figure 2.2 coil and uncoil.

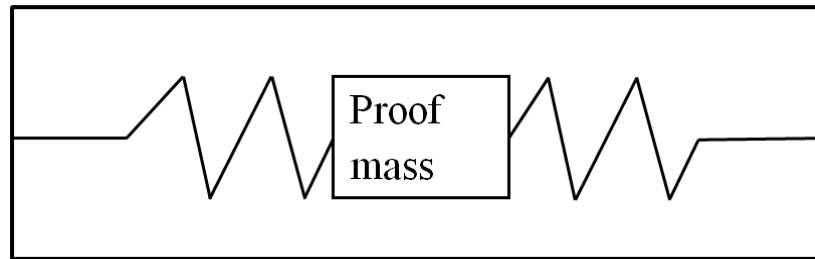


Figure 2.2: Accelerometer principle of operation

Original schematic above is based on a schematic from Goodall (2009)

Microelectromechanical systems (MEMS) accelerometers, such as the ones used for the work carried out in this thesis, generally use the same operational principle as what is depicted in Figure 2.2. The main difference between most MEMS accelerometers and a more traditional accelerometers is that MEMS use very small pieces of material (generally silicon) as a proof mass and as part of the spring mechanism; MEMS also sometimes utilize a closed loop mechanism whereby some signal (often electrical) is utilized to induce a force upon the proof mass to keep it from moving from its central location when an external acceleration is acting upon the proof mass (Yazdi, Ayazi and Najafi, 1998). Such closed loop architectures produce generally better measurement results because they remove many of the difficulties in controlling dynamic effect of the proof mass motion. Closed loop architecture can be compared to the open loop architecture depicted in Figure 2.2 where the motion of the proof mass is allowed and subsequently measured.

MEMS gyroscopes generally utilize a different principle of motion than accelerometers; specifically, they utilize the Coriolis effect (although, strictly speaking, the Coriolis effect follows from Newton's laws). It is important to note that not all gyroscopes operate based on the Coriolis effect, but many MEMS gyroscopes do. The Coriolis effect stipulates that if an object is undergoing uniform circular motion (on a rotating frame of reference) and that object was to move outward radially, then the object would appear to decelerate in the direction of uniform circular motion that it is undergoing with respect to the rotating reference frame. Similarly, for the opposite case, if an object is undergoing uniform circular motion (on a rotating frame of reference) and that object was to move inward radially, then the object would appear to accelerate in the direction of uniform circular motion that it is undergoing with respect to the rotating reference frame. Mathematically, this can be written as follows

$$\bar{a}_{cor} = -2\bar{\omega}_{cr} \times \bar{v}_{rad} \quad (2.1)$$

Where \bar{a}_{cor} is the Coriolis acceleration, $\bar{\omega}_{cr}$ is the circular rotation rate and \bar{v}_{rad} is the radial velocity; all three of these vectors have three elements with the first element depicting x-data, the second element depicting y-data and the third element depicting z-data (this is the convention used throughout this document). Note that the symbol \times denotes cross product and a right hand rule sign convention is followed (such a sign convention is followed throughout this document). Graphically, the Coriolis effect is illustrated in Figure 2.3.

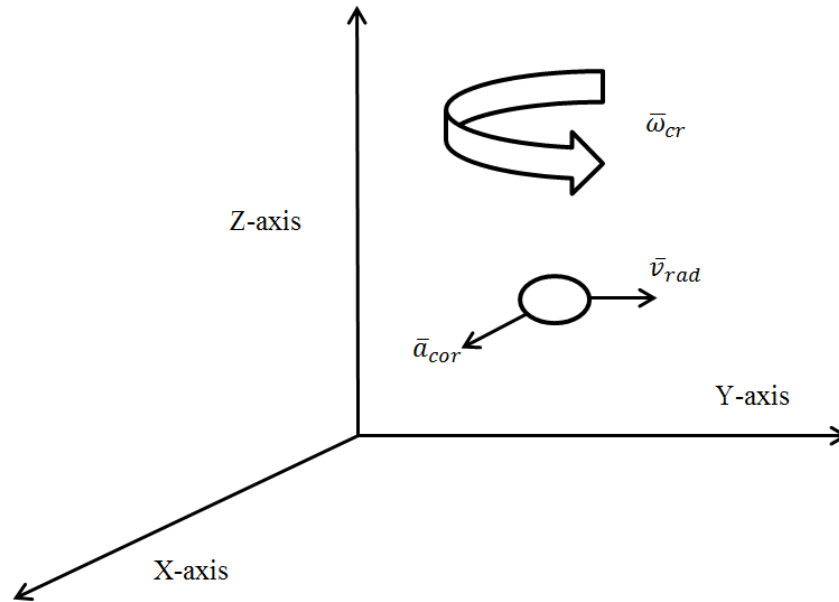


Figure 2.3: Illustration of Coriolis acceleration

Original schematic above is based on a schematic from Goodall (2009)

MEMS gyroscopes utilize a vibrating proof mass which vibrates perpendicular to the direction of rotation. Measuring the force acting upon this proof mass and performing the appropriate calculation, following from Equation (2.1), will yield the angular rate sought (Nasiri, 2005).

2.4.2 Common Uses for MEMS Inertial Sensors

MEMS inertial sensors were popularized in the 1990's due to their use in air bag systems for transportation vehicles (Frost and Sullivan, 2006). The popularization for MEMS for such air bag systems was driven by the digitization of much of the information in a modern automobile, and allowed for the financial resources for large scale development of modern MEMS which offered significantly better in performance than previous generations of MEMS sensors.

Some of the most popular modern uses of MEMS inertial sensors are for personal navigation, camera image stabilization and smart phone based applications (Goodall, 2009). More specifically, many of the newest generations of smart phones have tri-axial accelerometers and gyroscopes built into the devices. MEMS are also becoming popular for computer gaming applications (some of these games are console based and some of these games are smart phone based). Many of the most accurate MEMS inertial sensors have high enough accuracy readings that they are beginning to replace older and more expensive inertial sensing apparatuses for certain navigation applications.

2.4.3 Advantages of MEMS Inertial Sensors

MEMS inertial sensors offer many advantages when compared with other motion tracking technology commonly available. They are very convenient to use because of their low cost (sometimes only a dollar for each sensor), light weight, low power consumption and small size. The particular sensors used in this thesis were not larger than 5 mm along their largest dimension and the accelerometer sensor set had a mass of 0.08 grams based on what is given in ST Microelectronics (2006) and Epson Toyocom (2010) (this data is also presented in Table 3.1 of this thesis). MEMS also can be a non-invasive form of measurement because they can be mounted directly on a subject of interest and they don't necessarily require any data logging cables or power cables; this is because the low power consumption allows for the use of very small batteries to power the MEMS devices and onboard data logging is possible using a small data logging external hard drive device which, like the MEMS sensors themselves, can be smaller than a penny.

2.4.4 Disadvantages of MEMS Inertial Sensors

Previously, in the beginning of Section 2.4, a difficulty in dealing with MEMS inertial sensor data was discussed; this difficulty regarded problems dealing with gravity affecting inertial data and more specifically problems arising from the coupling of rotational and translational motion due to the fact that accelerometers pick up gravitational acceleration. Another significant disadvantage of using MEMS inertial sensors is the large and unrestrained growth in positioning error when processed data are analyzed. This large error growth stems directly from the fact that MEMS inertial signals need to be integrated to obtain positioning information. Such integration can take small errors and amplify them greatly, particularly when multiple integrations are used as is the case when accelerometer data are integrated (twice) to produce displacement information.

One mechanism to try to restrain error growth is to carefully remove biases and scale factors from MEMS inertial data before the data are processed (Lotters et al., 1998). This necessitates a potentially very time consuming calibration process. One problem with such calibration is that bias and scale factor errors can shift in time and with respect to other parameters like temperature, which then necessitates the generation of new calibration parameters that reflect the altered state of the inertial sensors. This can be impractical to perform in many circumstances, so bias and scale factor parameters are often updated in real time using information from aiding sources, such as global navigation satellite system (GNSS) based aiding sources.

The difficulty with using such aiding sources to update the error parameters for inertial data was that processing data with the inclusion of aiding sources greatly increases computational complexity which can be difficult to handle mathematically when designing data processing methodologies. As well, such complex data processing tends to require a lot of computing resources which are not always available in many circumstances. As a further disadvantage, when aiding sources are used, many of the advantages of MEMS can be diminished, such as MEMS' ease of use, small size, low cost and non-invasiveness.

Another disadvantage of inertial sensors is that the positioning information that they offer is only relative in nature and not absolute. This is because inertial sensors measure changes in position and can only reference the current position with respect to previous position locations. In order to obtain absolute positioning information (such as latitude and longitude), an external reference is needed (such as GNSS) which results in MEMS being less useful than they otherwise would have been for many applications because other sensors systems have to, in many cases, have their data fused with MEMS inertial data to produce meaningful results.

Inertial sensors also have difficulty dealing with the Coriolis effects of earth's rotation for many long range navigation applications. This is generally less of a problem for MEMS devices because they tend to be used for more localized positioning which is not as impacted by the Coriolis effect. However, MEMS gyroscopes (like all gyroscopes) can be

influenced by the rotation of the earth whose axis of rotation needs to be kept track of relative to any MEMS gyroscope axis so that the effects of earth's rotation can be removed from the MEMS gyroscope signals.

2.4.5 Inertial Error Sources

There are a number of error sources affecting inertial data, some of which have been discussed in preceding sub-section (2.4.4). The two error sources already explored were bias and scale factor and two significant error sources that have yet to be introduced are non-orthogonally (or sensor triads) and sensor noise. All of these error sources can be represented mathematically as follows for accelerometers and gyroscopes respectively (following from Yang, Niu and El-Sheimy (2006))

$$\bar{a} = (S_a + N_{non,a})\bar{f}_a + \bar{b}_a + \bar{n}_a \quad (2.2)$$

$$\bar{\omega} = (S_\omega + N_{non,\omega})\bar{g}_\omega + \bar{b}_\omega + \bar{n}_\omega \quad (2.3)$$

Where all elements for the above vectors (each with three elements) have subsequent terms representing x, y and z parameters. The terms \bar{a} and $\bar{\omega}$ are measured signals for the accelerometers and gyroscope respectively. The term S with subscript a or ω (for accelerometer and gyroscope data, respectively) denotes a matrix of errors for the linear scale factor; it is populated with non-zero elements only along the main diagonal (and zeros elsewhere). The convention of using subscripts a and ω to denote accelerometer and gyroscope terms is used throughout Equations (2.2) and (2.3). The term N_{non} (with either a or ω appended to it) is a matrix to correct for non-orthogonal sensor configurations. Parameters \bar{f}_a and \bar{g}_ω represent ideal signals with no error for

accelerometer and gyroscope data respectively. Finally, the vectors \bar{b} and \bar{n} represent bias and noise errors.

It is important to note that most of the parameters used in the models for Equations (2.2) and (2.3) can and do shift in time (especially the bias and scale factor terms).

Temperature in particular can cause such shifts to occur and it is often parameterized as part of an error model so that temperature effect on sensor parameters can be adequately quantified.

Another important point is that there are sometime non-linear effects (particularly regarding scale factor errors) that can be modeled as well for any inertial signals under examination. It is sometimes common to have these non-linear effects being modeled as if they were quadratic in nature (Farell, 2007).

2.4.6 Inertial Sensor Calibration

Inertial sensors are commonly calibrated using a level table and a turn table. The level table is used to calibrate the accelerometers. By utilizing a level table and placing accelerometer in the positive and negative direction of gravity, as well as perpendicular to gravity, bias and scale factor terms can be realized as can any non-orthogonal sensor configurations. A turn table can be used to calibrate a gyroscope in a similar manner as to how a level table can be used to calibrate accelerometers. A turn table is operating at a known rotation rate, so placing gyroscope with their sensitive axis along the positive and negative direction of rotation (right hand rule sign convention), as well as perpendicular

to the direction of rotation, can generate bias and scale factor terms, as well as detect any non-orthogonal sensor configurations.

2.4.7 Inertial Stochastic Parameters

It is necessary to model sensor noise for inertial data in many applications. This is particularly the case when inertial data are fused with data from another source as stochastic parameters tend to be utilized to determine which data source should be regarded as more precise. MEMS inertial sensors quite often have their errors approximated as random walks (Goodall, 2009). There exist more complex modeling techniques, but these are not as useful for MEMS data because the modeling parameters often tend to not fit the signal very well, and this is particularly true for short time duration signals where complex error phenomena have very little impact on overall processing results (Brown and Hwang, 1997; Maybeck, 1982; Vanicek and Omerbasic, 1999).

A random walk is generated from the integration of white noise and is commonly named a velocity random walk (VRW) for accelerometer data and an angular random walk (ARW) for gyroscope data. Multiplying a random walk parameter by the square root of time will create an estimate of the standard deviation of the signal change (assuming a stationary inertial sensor); as such, accelerometer and gyroscope errors from random walks are directly proportional to the square root of time.

Both VRW and ARW can be found in a straightforward manner as illustrated in El-Sheimy, Hou and Niu (2008) using Allan variance. A summary is given here, as illustrated using Equations (2.4) through (2.6). To begin the process of determining VRW and ARW, data must be separated into clusters of length T_{av} seconds as follows (using clusters of small fractions of a second up to thousands of seconds)

$$s_{av}(T_{av}) = \frac{1}{T_{av}} \int_{t_k}^{t_k+T_{av}} s(t) dt \quad (2.4)$$

Where $s(t)$ is the signal under evaluation, t_k is the time at sample k , t is time and $s_{av}(T_{av})$ represents the signal average for the cluster. The cluster length T_{av} is the product of the number of samples in the cluster, n_{av} , and the time interval between data samples, Δt . A subsequent cluster average can be defined as

$$s_{av,next}(T_{av}) = \frac{1}{T_{av}} \int_{t_{k+1}}^{t_{k+1}+T_{av}} s(t) dt \quad (2.5)$$

Where t_{k+1} is the next data sample after t_k . Allan variance can subsequently be defined as

$$\sigma_{av}^2(T_{av}) = \frac{1}{2(N_{av} - 2n_{av})} \sum_{k=1}^{N_{av}-2n_{av}} (s_{av,next}(T_{av}) - s_{av}(T_{av}))^2 \quad (2.6)$$

Where N_{av} is the total number of samples for the data captured and $n_{av} < \frac{N_{av}}{2}$. When Allan variance is plotted against cluster length for the lower values of correlation time (T_{av}) chosen, a plot similar to what is depicted in Figure 2.4 is found (the slope of the line shown in Figure 2.4, and its other characteristics are revealed to exist theoretically in El-Sheimy, Hou and Niu (2008)).

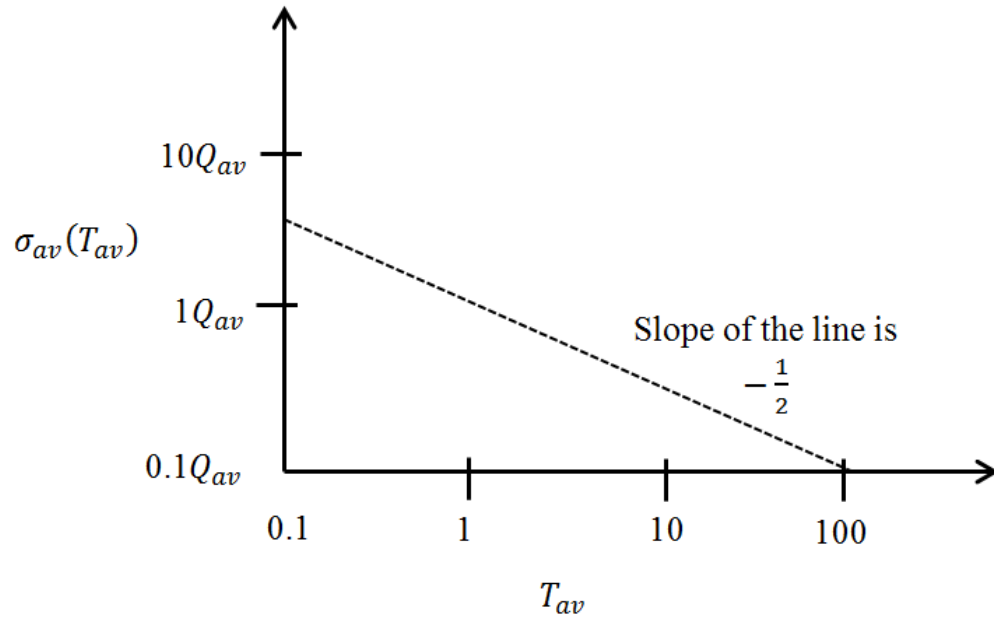


Figure 2.4: Allan variance plot to find random walk (Q_{av})

Based on the analysis from El-Sheimy, Hou and Niu (2008)

From Figure 2.4, it can be seen that the slope when Allan variance is plotted on log scales against cluster time is about minus one half. To obtain both VRW and ARW (using accelerometer data and gyroscope data, respectively) the location on the slope line at the point at which cluster time equals one must be read. Random walk is denoted Q_{av} in Figure 2.4.

2.5 Non-Inertial Motion Capture Techniques

Even though inertial sensing technology was chosen for the motion analysis undertaken in this thesis, it is important to explore other possible motion capture techniques for the benefit of future research. These other techniques are laid out in this section highlighting advantages and disadvantages of each.

2.5.1 Optical Sensing

Any technique that in a broad sense utilizes emitted light is an optical technique. The most common optical involves the use of digital video recording devices. A standard two-dimensional video camera does not usually capture particularly high resolution images, so analysis of only common video data is not going to be likely to generate much useful data. For this reason, passive markers (often circular targets affixed to a subject of interest) are used to try to improve the amount of possible usable data captured from a two-dimensional camera (Cappozzo et al., 1996; Cappozzo et al., 1997; Chang et al., 1998). Using markers can allow for image analysis techniques to derive useful positioning information from captured video data. Without the assistance of markers, it is difficult to derive accurate enough positioning information from two-dimensional video data alone to provide data for meaningful motion analysis.

More advanced image capture techniques utilize multiple digital video cameras and thus have the capability of logging three-dimensional motion information. Many high budget Hollywood movies utilize such a technique to generate the best possible information while maintaining reasonable flexibility for data capture purposes. Common systems for such three dimensional motion capture can have severe limitations. They can be expensive to operate and they generally require a controlled environment whereby there are multiple sight lines towards markers so that it is possible to obtain three-dimensional motion information in a robust and reliable manner. As well, markers on the skin can drift due to sweat and this can create a significant challenge particularly if the motion

being captured requires a person to attempt something physically demanding that may cause them to sweat.

Likely the biggest advantage of optical motion capture (particularly when using markers for three-dimensional motion capture) is the quality of the data captured. Such a motion capture technique can reliably pick up most movement perceptible to the human eye.

For more advanced systems, active markers can emit infrared radiation which is then captured and analyzed. Such systems are even more accurate than passive system which simply log data, but they also require that power be somehow transferred to active markers so that a signal can be broadcast and this is one of the main factors limiting their use.

2.5.2 Mechanical Techniques

It is possible to log motion information utilizing mechanical linkages which are affixed to and move with the human body; such linkages are called goniometers. Goniometers measure angles and changes in angles and electrical versions of these devices, called electrogoniometers, use potentiometers and transducers to log changes in joint angles (Norkin and White, 2003).

Electrogoniometers are more capable than non-electrical goniometers of logging time based motion information and for this reason they tend to be more useful for most

applications. Typically, most goniometers are quite inexpensive and easy to use and these are some of their strongest features.

Goniometers unfortunately have some very large disadvantages which significantly restrict their usage. Likely the most significant disadvantage is that such devices don't create an overall picture of motion since they are only logging motion for one joint at a time and therefore they are very limited in their applications for most research. Multiple goniometers can, of course, be mounted on a subject; however, this often results in discomfort and possibly also can limit the range of motion for a subject under examination (Winter, 1990). Another disadvantage of goniometers is that they don't always move with the body segments they are measuring in an appropriate manner such that they are tracking motion (Bontranger, 1998); in such cases, goniometers can produce data with significant errors.

2.5.3 Global Navigation Satellite System (GNSS)

The modern GNSS systems were first introduced because the United States Department of Defense wanted to improve positioning information for military applications; consequently, the Navstar global positioning system (GPS) program was launched in 1973 (Kaplan, 1996). The GPS positioning system was in time adopted for many civilian applications and is commonly used today for ocean, pedestrian, automotive and aerial navigation.

There are many different GNSS systems currently in operation or development including GPS (the first such system), Galileo (a European Union based system), GLONASS (a Russian global navigation satellite system) and a Chinese system is also currently in development.

GNSS positioning in its basic form uses trilateration for positioning. This positioning methodology relies on time of flight measurement of signals sent from satellites in orbit to receivers on the ground; satellite positions are known in advance. To improve the accuracy of GNSS systems, phase differencing is often used; this generally requires multiple receivers close to one another on the ground.

Likely the most significant drawback of GNSS systems is that they have significantly limited indoor usage. As well, GNSS systems tend to not track small motions well (such as tremor motions which are the focus of the research carried out in this thesis).

The greatest advantage of GNSS based system is their ubiquity in outdoor environments. As well, new GNSS receivers are small enough to easily fit within a cell phone which greatly enhances their usability.

Quite often, inertial data are mathematically fused with GNSS data (usually using a Kalman filter) because these two data sets complement each other very well. Inertial data

provides poor long term motion tracking data but good data when tracking motion from a known location over a short distance. GNSS, on the other hand, does not have the movement resolution of inertial data, but can provide much better absolute accuracy information (i.e. latitude and longitude). By fusing together inertial and GNSS data, the best combination of both data sets can be preserved such that processed data stemming from combined data sets has both good absolute accuracy and movement resolution.

2.5.4 Pressure and Force Sensing

There are many pressure and force sensitive devices commonly available for movement disorder motion monitoring. Most often, these devices are mounted close to a subject (i.e. under to foot) or, in some cases, devices can be mounted in the environment that a test subject is interacting with (such as force plates that a subject can walk over). In some cases, simple switches communicating an on or off state can also be used to log motion, but switches are not nearly as useful as pressure devices because if they are not mounted carefully for a well thought out experiment, they can remain in the on or off stage inadvertently for large duration of a given experiment (Bontrager, 1998).

The main advantages of force and pressure sensitive devices is that they are easy to use and they can communicate a very in depth amount of information to researchers. This is particularly the case for foot pressure sensitive pads, because inadvertent pressure concentrations on the foot can easily be spotted using such a device; it is difficult to conceptualize a device that can perform the function of spotting pressure concentrations as readily (Hausdorff et al., 2004; Herman et al., 2005).

One of the major disadvantages of force and pressure sensitive devices is that they often have to be modified to conform to the particular needs of a given subject. For a foot pressure sensitive device, for example, it may be required to fit the device to the shape of the foot for the person under examination. Another disadvantage of force and pressure sensitive devices is that they don't give an impression of overall motion as readily as optical techniques or inertial data.

2.5.5 Magnetic Sensing

Magnetic sensing devices monitor the local magnetic field; this is commonly carried out in three dimensions and does not require any line of sight observations because magnetic fields are ubiquitous. One of the most popular magnetic sensing systems, a magnetometer, generally utilizes the earth's magnetic field. Such a device is ideal for personal navigation applications because of its small size (smaller than a penny in some cases), light weight, low cost and capacity to operate from a small size battery.

Magnetometers are the perfect complement to inertial sensors because they provide absolute bearing information. Generally, such bearing information is the most critical missing component in an inertial navigation setup because all other orientation information (regarding inertial orientation above the horizontal) can be inferred from stationary accelerometer signals which are partially logging gravity.

The main disadvantage with any magnetic sensing device is that it will pick up magnetic disturbances and therefore its data can't be completely trusted; this is particularly true for indoor applications.

For higher accuracy applications, a multi-coil source is used for generate a local magnetic field. The disadvantage of using this methodological approach is that it can only provide local tracking information (so, for example, the methodology can't be used to track someone as they carry out their daily routine).

2.5.6 Acoustic Sensing

Acoustic sensing techniques utilize timing of flight information for sound (Welch and Foxlin, 2002). One simple technique utilizes reflected sound waves as is depicted in Figure 2.5.

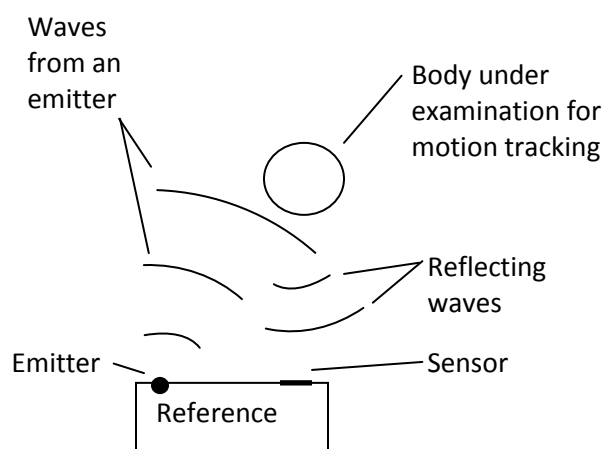


Figure 2.5: Acoustic sensing using reflected sound waves

Taken from Teskey (2007)

It is difficult to use the technique from Figure 2.5 over a range of more than a few meters and the accuracy of such an approach is quite limited. For this reason, carrier phase based approaches have also been implemented whereby a signal is recorded at a location whose position is sought and the phase of the transmitted and recorded data are examined to determine position; unfortunately, such a technique is only good for relative distance measurements unless special procedures for data acquisition are followed (Meyer, Applewhite and Biocca, 1992).

Even though acoustic techniques are easily implemented, they have significant disadvantages. Temperature, pressure and humidity changes in the air, which are common due to changes in weather and indoor climate control settings, can significantly affect any acoustic system. It is possible to mitigate such difficulties, but it involves tracking climatic information over time. Acoustic systems are also strictly line of sight systems and multipath can be a problem. As well, to obtain a broad set of data that are useful for most motion tracking applications, it is necessary to use multiple receivers which can impinge of the ease of use of acoustic systems.

2.6 Computational Methods

There was a wide array of computational methods utilized for processing movement disorders data because of the large number of potential algorithms in the literature. This section begins with an introduction to Kalman filtering and Kalman smoothing; techniques that were utilized to decouple accelerometer data from rotational motion (accelerometer data are coupled to rotational motion due to the influence of gravity as

depicted in Figure 2.1 from Section 2.4 on “Inertial Sensing”). After Kalman filtering and smoothing, Fourier and coherence based processing are introduced. These analysis techniques focus on frequency based analysis, and coherence processing in particular deals with frequency based *closeness* of two different data streams.

At the conclusion of this section, an analysis methods utilized for tremor mitigation (removal) is given; it is the weighted-frequency Fourier linear combiner (WFLC) filtering technique. Later in Chapter 6 of this thesis, the results of using this technique for tremor mitigation will be given.

2.6.1 Kalman Filtering

Kalman filtering is generally used to fuse data streams together taking into account associated statistical information (covariance data) for each of the data streams; one of the most popular such data fusions is the combination of inertial and GNSS data. An advantage of fusing data streams in this manner is that the analysis will tend to improve data quality, robustness and precision (robustness in particular can be materially improved in the case one data stream becomes partially impaired) (Groves, 2008).

Another advantage of Kalman filtering is that if there is a significant blunder in one of the data stream, it will be easier to spot from the results of the Kalman filtering. The Kalman filtering equations that follow here are from Gelb (1974) and Brown and Hwang (1997); specifically, what follows is the extended Kalman filter (EKF) whereby non-linear equations have been linearized (using partial derivatives) so that data processing can be implemented in a much more straightforward manner. The Kalman filtering operations

depicted in this thesis are based on a linearization, and the equations resulting from this linearization are depicted in more detail later in this thesis in Chapter 4.

The Kalman filtering algorithm uses a system model to track changes to the state space variable \bar{x}^{kf} (also known as the state vector, in this case the discrete version of the state space vector is presented). For the purposes of the analysis carried out here, discrete versions of the Kalman variables are presented because this thesis utilizes digital data streams which are more easily processed using discrete analyses. The state vector under examination retains information about the system observed (this often includes, for example information such a position, although Kalman filters can be applied to a multitude of data sources including fluid flow and electrical flow data). It is also common for the state vector to contain information about the derivatives of other state vector elements; for example, if the position of a system was an element of a state vector, it would not be unusual to have velocity (as a derivative of the position examined) as another state vector element.

The state vector is typically updated every time step using a dynamic model of the system under examination. This is done using $\Phi_{k,k-1}^{kf}$, which is the discrete form of the state transition matrix; it must be deterministic (Abeel et al., 2005). The manner in which the state vector is updated (using the discrete form of the state transition matrix) is outlined in the next sub-section of this thesis. The (non-discrete) state transition matrix is based on a linear dynamic model of the system under examination. This model is often obtained

from mathematical and physics based understanding about how the system examined is likely to behave, and the reason that the state transition matrix is non-discrete is because it is generally presented in the form whereby it is taken directly from a system of differential equations. There are many ways to discretize the non-discrete state transition matrix, as given in Strauss (1992).

The difficulty with using solely the state transition matrix to update the state vector is that the system examined can (and does) drift in its behavior from what is considered the ideal case presented in the state transition matrix. For this reason, other data (generally, but not necessarily measurement data) are collected so that the state vector can be updated based on real world events. This other data, or measurement update data, is stored in the vector \bar{z}^{kf} .

When update data are used to correct the state vector, it is not always clear whether the update data are of high quality. If the update data were perfect data, then the state transition matrix could be changed to directly take on the values that would follow from the update data, but the update data are very rarely perfect. The state transition matrix is also not perfect in its assessment of the system under examination, but it is often derived with a very well thought out theoretical development with past experiences in mind. For this reason, the state transition matrix does have some valuable contribution to make to the values of the state vector and should not be ignored.

Because both the state transition matrix and the update data have inherently useful information embedded in them, the Kalman filter attempts to use both of these when obtaining values for the state vector. To do this, various statistical parameters are used to assess the quality of the values produced from the state transition matrix and the update data. These statistical values are examined to determine how much different data streams should be trusted and a weighted average (based on the statistical data) of data streams is used to come up with the best estimate of the state vector. This is outlined further in the next sub-section of this thesis.

2.6.2 Extended Kalman Filter (EKF) Prediction

EKF prediction operations are typically applied at every sample taken to approximate the system under examination. They utilize a mathematical model of the system derived in advance of the filtering operation (this is based on the state transition matrix, as previously discussed). The state can be updated at each time step as follows

$$\hat{x}_k^{kf} = \Phi_{k,k-1}^{kf} \hat{x}_{k-1}^{kf} \quad (2.7)$$

Where subscripts k and $k - 1$ represent subsequent time steps (the convention whereby subscripts k and $k - 1$ represent timing information is used throughout the literature review discussion of Kalman filtering and smoothing in Sub-Sections 2.6.2 through 2.6.4). Often a set of terms including \bar{w}_{k-1}^{kf} (\bar{w}_{k-1}^{kf} has the same number of elements as \hat{x}_k^{kf}) are added onto the end of Equation (2.7) to highlight the fact that the state vector has noise associated with the values it represents; this noise is assumed to have a zero mean and a normal distribution.

The covariance matrix of the state vector, P^{kf} (found indirectly from \bar{w}_{k-1}^{kf} , as shown below), can also be updated for subsequent time steps

$$P_k^{kf} = \Phi_{k,k-1}^{kf} P_{k-1}^{kf} (\Phi_{k,k-1}^{kf})^T + G_{k-1}^{kf} Q_{k-1}^{kf} (G_{k-1}^{kf})^T \quad (2.8)$$

Where superscript T here denotes matrix transpose, as it does throughout this thesis document. The expression $\Phi_{k,k-1}^{kf} P_{k-1}^{kf} (\Phi_{k,k-1}^{kf})^T$ transforms the covariance matrix at time step $k - 1$ into the time step k and $G_{k-1}^{kf} Q_{k-1}^{kf} (G_{k-1}^{kf})^T$ incorporates the covariance matrix of the system noise (Q_{k-1}^{kf}) at time step $k - 1$ into the covariance matrix of the state vector at time step k . The term G_{k-1}^{kf} is the noise coefficient matrix at time step $k - 1$ and represents how noise, \bar{w}_{k-1}^{kf} , is transferred into the state vector; the projection of such noise into the state vector can be taken directly from $G_{k-1}^{kf} \bar{w}_{k-1}^{kf}$. As well, the covariance matrix of the system noise, Q_{k-1}^{kf} , is equivalent to $E[\bar{w}_{k-1}^{kf} (\bar{w}_{k-1}^{kf})^T]$, where $E[]$ is the statistical operator for expected value.

2.6.3 EKF Updates

Kalman filter updates are performed when there is “measurement data” so that the state vector can be adjusted for potential inaccuracies. It is important to note that the fact the term measurement is used here does not necessarily imply that there were physical measurements carried out; the Kalman filtering scheme is flexible enough that physical measurements can be directly implanted into the prediction equations from Sub-Section 2.6.2, as well, measurement data can be representative of other information critical to data fusion other than strictly speaking measurements, such as constraint information for example. The term measurement is only used here to describe updates based on

convention and historical uses of the filter, without necessarily implying limits to the flexibility with which the filter can be used.

Measurement updates are generally not performed at every time step, but instead only at time steps where there is data available. After an update is performed, the adjusted values for the state vector and state covariance matrix are used for the subsequent Kalman filter prediction at the next time step.

Updates are performed by utilizing measurements, \bar{z}^{kf} (as noted in the previous sub-section of this thesis); the measurements are not necessarily directly analogous to values in the state vector. As such, the state vector usually must be transformed utilizing the design matrix, H^{kf} , so that it is differences between state values and measurement values can be directly compared. The mathematical expression $H^{kf} \bar{x}^{kf}$ expresses the state vector in terms of measurements taken. An important point to note is that the design matrix needs to be deterministic (Abeel et al., 2005). The Kalman gain matrix, K^{kf} , is utilized so that measurement data can be used to update the state vector in a manner in which statistical information down-weights observations with high standard deviations and up-weights observations with low standard deviations (this was discussed in the previous sub-section of this thesis)

$$K_k^{kf} = P_k^{kf} (H_k^{kf})^T (H_k^{kf} P_k^{kf} (H_k^{kf})^T + R_k^{kf})^{-1} \quad (2.9)$$

The term R_k^{kf} is a covariance matrix of measurement noise and the superscript -1 here represents matrix inverse, as it does throughout this thesis document. The main diagonal of the covariance matrix of measurement noise can be populated by utilizing VRW and ARW sensor data, which can be found as shown in Sub-Section 2.4.7; the off diagonal terms of the covariance matrix of measurement noise are often presumed to be zeros.

There are, of course, other methods of populating R_k^{kf} when using inertial data, but these can be less reliable because they often depend on more complex and difficult to manage models of inertial errors (Brown and Hwang, 1997; Goodall, 2009; Vanicek and Omerbasic, 1999). The matrix R_k^{kf} is populated using the assumption that the measurement data follow a normal distribution.

Utilizing the Kalman gain matrix, updates can be performed to the state vector as follows

$$\hat{x}_{k,updated}^{kf} = \hat{x}_k^{kf} + K_k^{kf} (\bar{z}_k^{kf} - H_k^{kf} \hat{x}_k^{kf}) \quad (2.10)$$

And updates to the state covariance matrix can be found as follows

$$P_{k,updated}^{kf} = (I - K_k^{kf} H_k^{kf}) P_k^{kf} \quad (2.11)$$

Where I represents an identity matrix (as it does throughout this thesis document) of the appropriate size as to ensure that the subtraction in Equation (2.11) can take place appropriately.

The overall algorithm for Kalman filtering can be summarized using the following instructions:

1. Apply Equations (2.7) and (2.8) at time step k to predict \hat{x}_k^{kf} and P_k^{kf}
2. If measurements are not available advance to the next time step (meaning that data at the current time step k will now be representative of data at time step $k - 1$) and proceed to instruction 1, if measurements are available, proceed to instruction 3
3. Apply Equations (2.9) through (2.11), utilizing measurements and the associated covariance matrix of measurement noise to obtain updated terms $\hat{x}_{k,updated}^{kf}$ and $P_{k,updated}^{kf}$
4. Set \hat{x}_k^{kf} to $\hat{x}_{k,updated}^{kf}$ and P_k^{kf} to $P_{k,updated}^{kf}$ and advance to the next time step (meaning that data at the current time step k will now be representative of data at time step $k - 1$) and proceed to instruction 1

To insure stability for the above iterative steps, it is necessary to ensure good initial estimates of the state vector and covariance; as well, the overall system has to be well modeled, which means the state transition matrix has to be representative of the observed phenomenon (Gelb, 1974).

2.6.4 Kalman Smoother

The Rauch-Tung-Striebel (RTS) Kalman smoother was chosen for implementation because of its fast processing capacity (Shin, 2005). The major disadvantage with this smoother is that the state vector and its associated covariance matrix as well as the state transition matrix information need to be kept for each time step that is evaluated for the Kalman filter (Shin, 2005); this is not a material issue for the analysis because modern

computers have easily enough storage capacity for what is carried out in terms of data processing in this thesis.

The goal of smoothing the data is to remove discontinuities in the processing that occur when measurement and update data cause a large shift in the state vector parameters from one time step to the next. The smoother optimally adjusts data according to covariance information so that if the processing were applied in either the forward (increasing time) or reverse (decreasing time) direction, the end result would be identical (Brown and Hwang, 1997, Shin, 2005).

It is most convenient to run the smoother in reverse (from the end of the processed data to the beginning) and that is what is carried out here. The three equations for the smoothing operation are given below, with all new terms defined after in Figure 2.6

$$\hat{x}_{k|N} = \hat{x}_k^{kf} + A_k(\hat{x}_{k+1|N} - \hat{x}_{k+1,not\ updated}^{kf}) \quad (2.12)$$

$$P_{k|N} = P_k^{kf} + A_k(P_{k+1|N} - P_{k+1,not\ updated}^{kf})A_k^T \quad (2.13)$$

$$A_k = P_k^{kf}(\Phi_{k+1,k}^{kf})^T(P_{k+1|k}^{kf})^{-1} \quad (2.14)$$

For Equations (2.12) through (2.14), N is the total number of time steps, A_k is the smoothing weighting matrix; as well, $\hat{x}_{k+1,not\ updated}^{kf}$ and $P_{k+1,not\ updated}^{kf}$ are the state vector and associated covariance information for the forward (Kalman) filter after the

prediction at time step $k + 1$ is carried out but before the update (for when an update exists at time step $k + 1$).

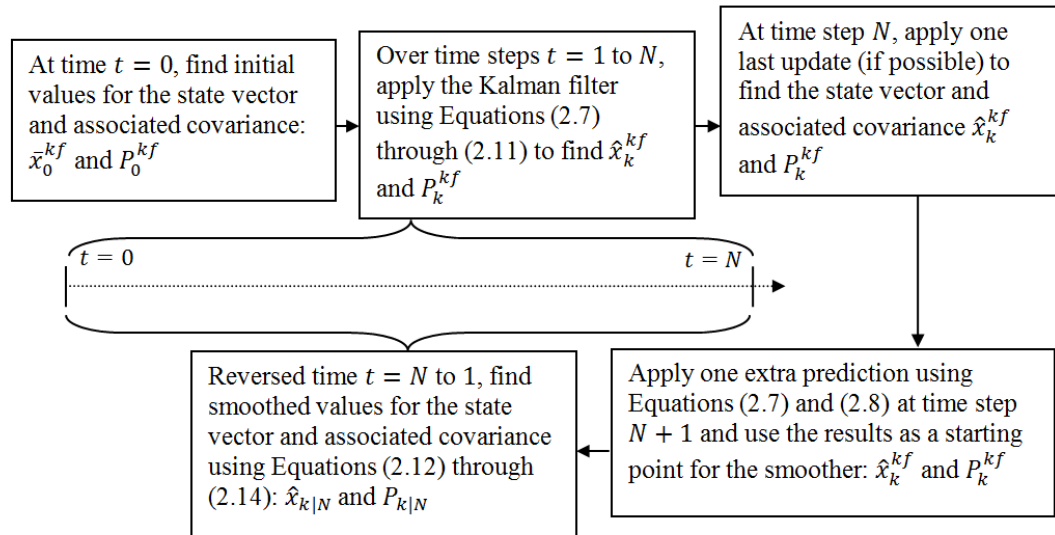


Figure 2.6: Kalman smoothing flow chart

Taken from Teskey, Elhabiby and El-Sheimy (2010a) (slightly modified)

Original figure is available at Sensors and Transducers:

http://www.sensorsportal.com/HTML/DIGEST/P_616.htm

Based on analysis from Shin (2005)

2.6.5 Fourier and Coherence Analysis

The Fourier and coherence analysis here is based on what is given in Halliday et al. (1995). The goal of such analysis is to be able to study frequency based information for an individual signal as well as when comparing two signals to one another; this method of analysis is very popular when comparing movement and EMG data for human test

subjects. During analysis, the frequency spectrum for an individual signal shows how much signal content is present at a given frequency, and this is referred to as an auto-spectrum. When comparing two signals to one another, the cross-spectrum depicts how much signals are matching at different frequencies.

In order to facilitate the implementation of appropriate statistical parameters when evaluating auto-spectra and cross-spectra, inertial data are split into L segments, such that each segment (labeled $l = 1, 2, \dots, L$) has unique non-repeating data; as well, each data segment has an equivalent length of T samples. Based on these parameters, the discrete Fourier transform of a signal $s(k)$ can be estimated as follows

$$d_s(\omega, l) \approx \sum_{k=(l-1)T}^{lT-1} e^{-i\omega k} s(k) \quad (2.15)$$

Where ω represents angular frequency, which is the product of frequency in Hz and 2π ; as well, i is the imaginary unit and e represent the exponential function. Given the above Fourier transform, a cross-spectral estimate ($\hat{f}_{12}(\omega)$) for two signals, $s_1(k)$ and $s_2(k)$, can be found

$$\hat{f}_{12}(\omega) = \frac{1}{2\pi LT} \sum_{l=1}^L d_{s_1}(\omega, l) \overline{d_{s_2}(\omega, l)} \quad (2.16)$$

Subscripts 1 and 2 denote metadata for signals $s_1(k)$ and $s_2(k)$, respectively, and the notation $\overline{*}$ signifies the complex conjugate of $*$. The term $\hat{f}_{12}(\omega)$ signifies how closely related signals $s_1(k)$ and $s_2(k)$ are at each frequency of interest (not taking signal phase shifts into account). If signals $s_1(k)$ and $s_2(k)$ are equivalent, then the cross-spectral

estimate from Equation (2.16) becomes an auto-spectral estimate ($\hat{f}_{11}(\omega)$ or $\hat{f}_{22}(\omega)$). An auto-spectrum is often evaluated to deduce signal frequency distribution; in contrast, the cross-spectrum can be made more useful by scaling it at each frequency to give a coherence estimate

$$|\hat{R}_{12}(\omega)|^2 = \frac{|\hat{f}_{12}(\omega)|^2}{\hat{f}_{11}(\omega)\hat{f}_{22}(\omega)} \quad (2.17)$$

The operator $|*|$ denotes absolute value of $*$. Coherence information lacks any contribution from signal phase shift parameters, however, these can be found as follows

$$\hat{\Phi}_{12}(\omega) = \arg\{\hat{f}_{12}(\omega)\} \quad (2.18)$$

Whereby the phasor angle from cross-spectrum, $\hat{f}_{12}(\omega)$, can be evaluated at each frequency of interest to yield phase shift information.

As statistical parameter can be defined to verify that the coherence from Equation (2.17) is meaningful. A 95% confidence limit, cl , is set up such that a horizontal line can be drawn on a plot of coherence (with frequency on the horizontal axis) to show at which frequencies signals $s_1(k)$ and $s_2(k)$ are independent; data above this line show significant coherence

$$cl = 1 - 0.05^{1/(L-1)} \quad (2.19)$$

2.6.6 Weighted-Frequency Fourier Linear Combiner (WFLC) Filtering

The WFLC algorithm is the most used for tremor removal and it is commonly used with inertial data as well as data taken from a patient writing on an electronic scribe (Rocon et al, 2004). The reason that this algorithm is so common is because it offers zero phase lag

real time tremor tracking for human motion; this is a feat that is very difficult to replicate (Riviere, Reich and Thakor, 1997; Riviere, Radar and Thakor, 1998). This is particularly the case for tracking human tremor, which can vary in both frequency and amplitude (Elble and Koller, 1990). Other techniques, such as Fourier based band pass filtering and auto-regression based filtering, have a difficult time handling human tremor for real time applications (Gonzalez et al., 1995; Prochazka, Elek and Javidan, 1992; Riley and Rosen, 1987). Before WFLC filtering was introduced, Fourier based techniques were the most popular for human tremor analysis (Oppenheim and Schaefer, 1989) but most analyses produce mixed results and in particular frequency spectra were not easily interpreted (Gresty and Buckwell, 1990). Even when using the short time Fourier transform it was difficult to produce quality results because it proved computationally burdensome to find a signal segment that could be treated as stable periodic data without reducing frequency resolution during processing (Cohen, 1989).

There are two iterative sets of operations carried out when performing WFLC filtering, the first set of iterations obtains the frequency for the tremor evaluated (shown in Equations (2.20) through (2.24)) and the second set of iterations matches the amplitude and phase lock of the tremor component of the signal (shown in Equations (2.25) through (2.28)). Unfortunately, frequency realization can't be performed in isolation, so the first set of iterations utilized (at each time step) for the WFLC algorithm provides frequency as well as amplitude and phase lock information; the amplitude and phase lock information is then discarded and the second set of iterations (also performed at each time step) provides new amplitude and phase lock information.

It may seem counterproductive and redundant to perform iterative steps in this way, but it provides more flexibility when implementing the filter. For example, human tremor amplitude can change quickly but tremor frequency does not change as quickly (Riviere, 1995); so having a two stage filter can more easily allow for adjusting filter weights to track both a fast moving amplitude parameter and a slow moving frequency parameter (Gresty and Buckwell, 1990).

The WFLC algorithm is similar to an adaptive notch filter and it uses a least mean squares (LMS) gradient descent algorithm (Widrow and Stearns, 1985). The stability of the algorithm is highlighted in Riviere (1995) and it can be shown that it minimizes mean square error between the signal and the estimated tremor from the filter (Widrow and Stearns, 1985).

What follows here mathematically for the WFLC algorithm is from Riviere, Reich and Thakor (1997) and Riviere, Radar and Thakor (1998). The parameter used to track tremor at time step k , y_k^{wflc} , is given in the following model for the first set of iterations in the WFLC filter

$$y_k^{wflc} = \sum_{r=1}^{M^{wflc}} \left(a_r \sin \left(r \sum_{t_k=0}^k \omega_{0t_k} \right) + b_r \cos \left(r \sum_{t_k=0}^k \omega_{0t_k} \right) \right) \quad (2.20)$$

Where r represents harmonics of the fundamental frequency, ω_0 , used for signal tracking up to a total of M^{wflc} harmonics; because ω_0 can vary from one time step to the next, the term ω_{0t_k} is used to describe ω_0 at a given time step t_k . Terms a_r and b_r change values as optimization is sought for the WFLC algorithm, and in changing values in this manner these terms adapt tremor amplitude and phase.

The error, ε_k , between the tremor tracking parameter and signal of interest (s_k , which is previously denoted $s(k)$) can be found as follows

$$\varepsilon_k = s_k - y_k^{wflc} \quad (2.21)$$

Iterative adjustments to the tremor fundamental frequency are made at each time step

$$\omega_{0k+1} = \omega_{0k} + 2\mu_0\varepsilon_k \sum_{r=1}^{M^{wflc}} r(a_r \cos\left(r \sum_{t_k=0}^k \omega_{0t_k}\right) - b_r \sin\left(r \sum_{t_k=0}^k \omega_{0t_k}\right)) \quad (2.22)$$

The term μ_0 affects the speed of iterative convergence but must not be set to a value which is too high, lest it create iterative instability. Parameters a_r and b_r are iterated as follows

$$a_{rk+1} = a_{rk} + 2\mu_1\varepsilon_k \sin\left(r \sum_{t_k=0}^k \omega_{0t_k}\right) \quad (2.23)$$

$$b_{rk+1} = b_{rk} + 2\mu_1\varepsilon_k \cos\left(r \sum_{t_k=0}^k \omega_{0t_k}\right) \quad (2.24)$$

The term μ_1 is set high if it is desired for each iteration to produce a large change in values of parameters a_r and b_r ; but as with μ_0 , if μ_1 is set too high it may create iterative instability.

For the second set of iterations in the WFLC algorithm, values previously found for ω_0 (now denoted $\hat{\omega}_0$) are kept at each time step t_k , and values for parameters a_r and b_r are discarded. The following equations are then implemented where the subscript second denotes that terms are implemented in the second set of iterative steps and a new iterative parameter μ_2 is utilized

$$y_{k_{second}}^{wflc} = \sum_{r=1}^{M^{wflc}} \left(a_r \sin \left(r \sum_{t_k=0}^k \hat{\omega}_{0t_k} \right) + b_r \cos \left(r \sum_{t_k=0}^k \hat{\omega}_{0t_k} \right) \right) \quad (2.25)$$

$$\varepsilon_{k_{second}} = S_k - y_{k_{second}}^{wflc} \quad (2.26)$$

$$a_{r_{k+1_{second}}} = a_{r_{k_{second}}} + 2\mu_2 \varepsilon_{k_{second}} \sin \left(r \sum_{t_k=0}^k \hat{\omega}_{0t_k} \right) \quad (2.27)$$

$$b_{r_{k+1_{second}}} = b_{r_{k_{second}}} + 2\mu_2 \varepsilon_{k_{second}} \cos \left(r \sum_{t_k=0}^k \hat{\omega}_{0t_k} \right) \quad (2.28)$$

The overall algorithm for performing the WFLC filtering operation is as follows

1. Apply Equations (2.20) through (2.24) at each time step to obtain $\hat{\omega}_0$ and discard values for parameters a_r and b_r
2. Apply Equations (2.25) through (2.28) at each time step utilizing $\hat{\omega}_0$ to obtain parameters a_r and b_r (i.e. parameters $a_{r_{k+1_{second}}}$ and $b_{r_{k+1_{second}}}$)

3. Proceed to the next time step

2.6.7 Wavelet Analysis

Wavelets were first utilized extensively in the mid-1980s and quickly became popular for a number of applications, including imaging processing, data compression, signal noise removal and pattern detection. Wavelets were originally developed with the prospect of evaluating a non-stationary signal (Keller, 2004), and from this desire stems one of the biggest advantages of wavelets: their time and frequency localization properties whereby any desired signal portion can be evaluated with relative ease to study a chosen particular frequency or frequencies. It is difficult to achieve this same localization capacity with Fourier based techniques while preserving computational efficiencies. In part due to the localization capacities of wavelets, they are well suited to removing transient aspects of signal noise or disturbances. Disturbances are common with inertial data, often when a person inadvertently strikes an inertial sensor against a foreign object.

Wavelets also offer other advantages such as a large number of possible base functions from which to pick when analyzing a signal (a base function is utilized as wavelet processing analyzes the *closeness* of a base function to the signal being evaluated).

Fourier based techniques tend to be more restricted in terms of possible base functions as most Fourier based functions are sinusoidal in nature.

A last major advantage of utilizing wavelets is the capacity to easily speed up processing if desired. Discrete wavelets are very well suited for this because they use signal

information very efficiently. In many cases (but not all) there is no redundancy among discrete wavelet coefficients generated when analyzing a signal.

Despite the many advantages cited above, wavelets have not been utilized extensively in movement disorder monitoring, and this is the source of a lot of criticism when movement disorders research is evaluated by those outside the field (Begg and Palaniswami, 2006). One of the major uses of wavelets for motion monitoring is frequency spectrum analysis and filtering. An example of this is research conducted to help extract tremor motion for a prosthesis utilizing wavelet filtering (Popovic and Popovic, 2008). It was found that the wavelet algorithm outperformed a Butterworth filter; this outperformance of wavelets holds for when prior tremor frequency information is not available. Another paper utilized accelerometers and wavelets to analyze PD walking motion by first extracting seven levels of details coefficients and finding variances for each of the seven sets of details coefficients; using these variances (specifically, their progression slope) fractal dimension estimates were obtained (Sekine et al., 2002). The research paper concluded that the analysis carried out was useful for evaluation of PD motion.

There are two research papers (among others) that utilize wavelets for differential diagnosis of ET and PD. One of these papers utilizes a number of parameters as inputs into a back propagation neural network, including motion signal energy parameters from wavelet analysis, extracted coefficients from bispectrum based processing and other

parameters of interest from *empirical mode decomposition* based analysis (Ai, Wang and Wang, 2008). After the initial neural network associated computations were carried out, DS evidence theory was utilized to help differentiate cases of ET and PD with good results; unfortunately, the algorithm lacked computational efficiency. Another paper utilized a similar approach but without DS evidence theory and with the following inputs into a neural network: wavelet based entropy, higher order cumulants and other parameters of interest; the results from this paper were not highly accurate (Engin et al., 2007).

Wavelets generally tend to contain certain properties that help to define them. Such properties tend to include having a zero average, oscillatory tendencies and having a zero value far from the center of the wavelet function (Keller, 2004). Wavelets must follow the following admissibility equation

$$\int_{-\infty}^{\infty} \frac{|\hat{\Psi}(\omega)|}{|\omega|} d\omega < +\infty \quad (2.29)$$

Where the term $\hat{\Psi}(\omega)$ is the Fourier transform of the mother wavelet, $\psi(t)$. The continuous wavelet transform (CWT) provides a very full view signal frequency characteristics and a large amount of redundancy is contained in extracted wavelet coefficients $Q(m_\gamma, t_\sigma)$. The terms m_γ and t_σ scale and translate, respectively, the mother wavelet's complex conjugate, $\tilde{\psi}(t)$; the act of scaling and translating the mother wavelet data in this way produces daughter wavelets (Mallat, 1989). The continuous wavelet transform attempts to measure the degree of *closeness* between a given signal portion and

a scaled mother wavelet and it can be expressed using the following (Goswami and Chan, 1999)

$$Q(m_\gamma, t_\sigma) = \frac{1}{\sqrt{m_\gamma}} \int_{-\infty}^{\infty} s(t) \tilde{\psi}\left(\frac{t - t_\sigma}{m_\gamma}\right) dt \quad (2.30)$$

The term γ (a subscript of m_γ) represents the wavelet scale chosen for a particular analysis (which can take a value of one up to as large as the duration of the signal allows for). Small values of a wavelet scale utilize smaller size wavelets for analysis and consequently wavelets scaled in this way focus on data at higher frequencies. Larger values of wavelet scales produce wavelets for looking at lower frequencies.

It is often desired to look how wavelets correspond to certain frequencies of interest. This is carried out by utilizing pseudo frequencies which are generated to determine the largest possible degree of *closeness* of a particular scaled wavelet with a frequency scaled sinusoidal signal. A constant amplitude sinusoidal signal with a selected adjustable frequency is utilized for this task and pseudo frequencies are taken directly from the frequency of the sinusoidal matching function. An example of a derivation of pseudo frequency parameters is given in Figure 2.7 for a Daubechies wavelet of order 2. Within Figure 2.7, the Daubechies wavelet and the scaled sinusoidal matching data are displayed.

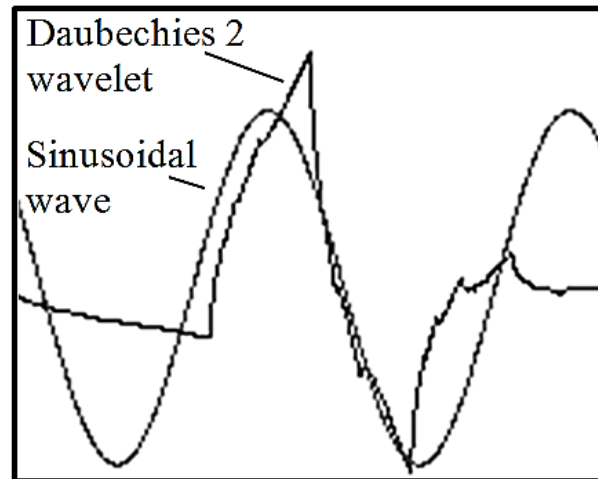


Figure 2.7: Derivation of pseudo frequency for a Daubechies wavelet of order 2

Based on analysis from Matlab (2008)

Mathematically, it would be tedious to derive pseudo frequencies for every daughter wavelet given that identical mother wavelets are used within a wavelet family to create variously sized daughter wavelets. For this reason, each mother wavelet has a derived value called center frequency (F_c in Hz) which can be scaled to find the pseudo frequency values, F_a , of daughter wavelets (Matlab, 2008)

$$F_a = \frac{F_c}{\gamma \Delta t} \quad (2.31)$$

The term Δt is the time interval between samples.

If it is desired to recreate the original signal from the continuous wavelet coefficients (which are found in Equation (2.30)), this can be done by applying the following, but

only in cases where the wavelet under examination is invertible (Goswami and Chan, 1999)

$$s(t) = \int_0^{\infty} \int_{-\infty}^{\infty} \frac{1}{m_{\gamma}^2} Q(m_{\gamma}, t_{\sigma}) \frac{1}{\sqrt{|m_{\gamma}|}} \psi^{\#}\left(\frac{t-t_{\sigma}}{m_{\gamma}}\right) dt_{\sigma} dm_{\gamma} \quad (2.32)$$

In the above, $\psi^{\#}(t)$ is delineated the dual function for $\psi(t)$ and must satisfy

$$\int_0^{\infty} \int_{-\infty}^{\infty} \frac{1}{|m_{\gamma}^3|} \psi\left(\frac{t_1-t_{\sigma}}{m_{\gamma}}\right) \psi^{\#}\left(\frac{t-t_{\sigma}}{m_{\gamma}}\right) dt_{\sigma} dm_{\gamma} = \delta(t-t_1) \quad (2.33)$$

Where t_1 is a time shift parameter and $\delta(t-t_1)$ is the Dirac delta function.

The main advantage of the continuous wavelet transform is that it allows for a full view of the signal under consideration by allowing a user to choose whatever scaling parameters suit their needs. Unfortunately, this flexibility comes at the cost of computational efficiency which is quite poor for the continuous wavelet transform.

The discrete wavelet transform (DWT) attempts to alleviate concerns about computational efficiency while still trying to preserve most of the analysis capacity of the continuous wavelet transform. The manner in which the DWT achieves this is by processing data for wavelet scales which are powers of two (wavelet parameters at other scales are not generated). Many wavelets (including the Coiflet wavelet of order three, which was utilized for most of the processing in this thesis) can capture all signal information when only evaluating a signal using scales that are powers of two. The

process by which this is carried out involves utilization of a series of cascading filters which effectively high pass (HP) and low pass (LP) signal information; this is shown in Figure 2.8 for three levels of decomposition.

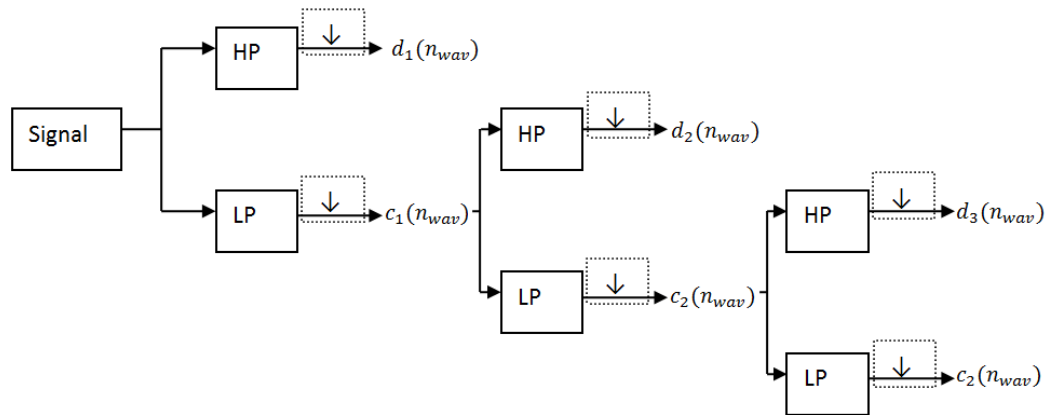


Figure 2.8: Cascading high and low pass filters that compose the DWT

Based on analysis from Matlab (2008)

From each level of decomposition in Figure 2.8, two sets of coefficients are produced, details coefficients ($d(n_{wav})$) hold information for high passed data and approximations coefficients ($c(n_{wav})$) hold information for low passed data to be subsequently processed. For terms $d(n_{wav})$ and $c(n_{wav})$, subscripts 1, 2 and 3 denote the level of wavelet decomposition. The symbolic representation “ \downarrow ” from Figure 2.8 denotes sub-sampling which involves taking only every second data point; this sub-sampling can be performed without the loss of any signal information so that the high and low pass coefficients preserve any signal frequency content. The reason for sub-sampling is so that after data at a frequency band are examined and extracted data components are stored in details and approximations coefficients, the next set of approximations and details

coefficients can be produced to examine data at a different frequency band. High pass and low pass filters, respectively, as shown in Figure 2.8, can be applied as follows for the first level of decomposition using the counter n_{wav} to apply the filters (Chan, 1995; Heil and Walnut, 1989; Torrence and Compo, 1998)

$$d_1(n_{wav}) = \sum_{k=-\infty}^{\infty} s(k)h_{wav}(2n_{wav} - k) \quad (2.34)$$

$$c_1(n_{wav}) = \sum_{k=-\infty}^{\infty} s(k)g_{wav}(2n_{wav} - k) \quad (2.35)$$

Where $g_{wav}(n_{wav})$ is a low pass filter with an impulse response g_{wav} and $h_{wav}(n_{wav})$ is a high pass filter; the two filters have a relation to one another and are delineated a quadrature mirror filter. The term $2n_{wav}$ in both filters ensures the sub-sampling takes place. Subsequent filters for other levels of wavelet decomposition have the same structure as what is given in Equations (2.34) and (2.35), but with inputs and outputs are depicted in Figure 2.8. The manner in which $g_{wav}(n_{wav})$ and $h_{wav}(n_{wav})$ are related to the mother wavelet is described in Burrus, Gopinath and Guo (1998).

As a result of the sub-sampling depicted in Figure 2.8, lower frequencies of signal analysis have less data than higher frequencies for every subsequent level of decomposition carried out. This is depicted in Figure 2.9 by the decrease in the size of the rectangular areas along the frequency axis at progressively lower frequencies. Another feature of the DWT that is depicted in Figure 2.9 is that the initial level of decomposition obtains data for a large frequency range, and subsequent levels of decomposition do not cover such a large range. This is implied by Equation (2.31), which can be used to

highlight the fact that as the number of scales utilized becomes very high, subsequent scales for the next levels of analysis cover only slightly lower values of frequency (this is the case even when increasing scales in powers of two).

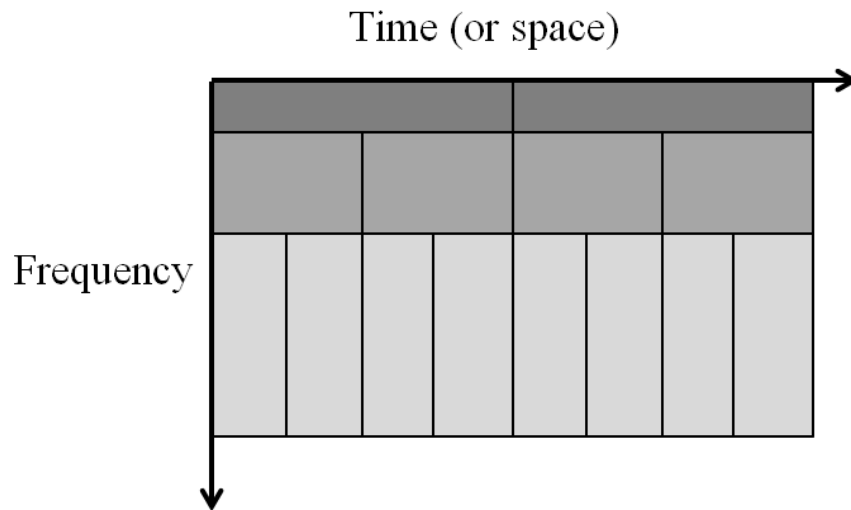


Figure 2.9: Frequency range and number of coefficients for different levels of DWT decomposition

Based on analysis from Griffiths, Higham and Watson (1997)

2.7 Summary

This chapter outlined a thorough overview of different aspects of evaluating movement disorders through the use of inertial sensors. The first part of the chapter looked at the two movement disorders evaluated (ET and PD) and what is currently known about them. It was important to examine this, because given the current state of relatively limited knowledge about movement disorders, there is a lot that can be gained from utilizing inertial sensors in the formal study of these afflictions.

Inertial sensors were then examined to determine how they measure motion and possible errors in their measurements. This knowledge will be utilized throughout the remainder of this thesis. Other possible techniques for evaluation of movement were also examined highlighting benefits and drawbacks of each; these techniques are of significant for future work involving motion monitoring.

The last portion of this chapter examined techniques for processing motion data that will be utilized through the remainder of this thesis. Fully outlining these computational methods is essential for a complete understanding of processed motion data.

Chapter 3: Experimental Methods

This thesis chapter first introduces methods of data logging used to capture tremor data. Subsequently, equipment and test subjects are examined and relevant information about these is given. At the conclusion of the chapter, raw data are plotted and a wavelet based spectral evaluation of the data is performed.

There were two types of experiments carried out to determine the tremor behavior of test subjects and these are both detailed in this chapter. The first of these experiments required test subjects to use their hand to point a laser attached to an IMU at targets on a computer screen. This test was chosen for motion analysis specifically because it required that subjects used their hand and arm in a manner such that they could not easily restrain their tremor by resting their arm on a foreign object. This test was also somewhat similar to what medical professionals use for diagnostic tests in that it allows for unrestrained six degree-of-freedom hand and arm motion. The main difference between the test carried out in this thesis and a test that medical professionals utilize is that the thesis testing utilized a randomized set of targets so that subject motion could be evaluated over a more diverse set of movements. Medical professionals, on the other hand, often utilize tests that require subjects to undergo more repetitive motion, such as first touching ones finger to their nose and then stretching their arm out in a lateral postural motion repeatedly. A more diverse data set was useful for the analysis carried out here because it allowed for

more general description of motion to be stated rather than coming to a conclusion about motion that might only be relevant for one particular type of motion.

The other test carried out, in addition to the laser targeting test highlighted above, was meant to simulate eating using a spoon; this task was chosen because it is one of the tasks that movement disorder patients often cited as being difficult to perform. A major goal of the thesis work is to come up with practical methods of mitigating tremor motion, so logging tremor motion for a difficult to perform task provided the ideal data set for testing tremor mitigation strategies.

3.1 Laser Targeting Motion Evaluation

For the laser targeting motion evaluation procedure, an effort was made to seat test subjects at a consistent distance from the targeted computer screen before the testing procedure was initiated. Subjects were asked to adjust their seat so that when they were sitting in an upright position with their arm outstretched, they would be touching the base to the computer screen. This is depicted in Figure 3.1 (full permission was obtained from the subject shown in Figures 3.1, 3.2, 3.4 and 3.5 for the use of her image in this thesis).

Once the subject had been properly oriented, the testing procedure was initiated. This involved the test subject picking up the IMU data logger from the holster (which is labeled in Figure 3.2) and directing the laser mounted on the IMU at ten targets on a computer screen. These ten targets were labeled “Click 1” through “Click 10” and had randomized positions for ten trials (although the same randomized patterns for each trial

were used for each test subject). Rulers mounted on the computer screen and protruding 0.2 meters towards the subject helped to standardize data collection. Subjects were asked to keep their hand roughly in a plane parallel to the computer screen and defined by points at the end of the rulers utilized.



Figure 3.1: A test subject before the initiation of the laser targeting motion evaluation

Taken from Teskey, Elhabiby and El-Sheimy (2010a) – Sensors and Transducers:

http://www.sensorsportal.com/HTML/DIGEST/P_616.htm

At the conclusion of testing, subjects were asked to place the IMU back into the holster.

This act of placing of the IMU back in the holster at the conclusion of testing was a very

significant part of the instructions given to test subjects because it allowed for Kalman filtering constraints to be determined for the motion analyzed. Such constraints, which define the beginning and end position and orientation for data collection, allowed for a much more accurate analysis of movement once Kalman filtering and smoothing had been implemented.



Figure 3.2: A test subject during the laser targeting motion evaluation

Taken from Teskey, Elhabiby and El-Sheimy (2010a) – Sensors and Transducers:

http://www.sensorsportal.com/HTML/DIGEST/P_616.htm

A typical set of targets for a given trial are shown in Figure 3.3. These targets were placed to lie completely within the computer screen in a non-overlapping manner so as to limit visual confusion for test subjects seeking to find the most appropriate next target of interest.

The laser targeting motion evaluation produced very high quality results and even allowed for a unique diagnostic technique for movement disorders to be created (as highlighted in Chapter 5 of this thesis). One of the strengths of the laser targeting test is that it logged both postural and kinetic tremor for subjects. This is because subjects often had to pause during motion logging as they searched for the next target of interest. When pausing in such a fashion, subjects sometimes produced postural tremor motion because they had to support the weight of their arm as well as the IMU for the duration of time it took to find the next target. The laser targeting motion evaluation also involved the logging of kinetic motion as patients moved between targets of interest.

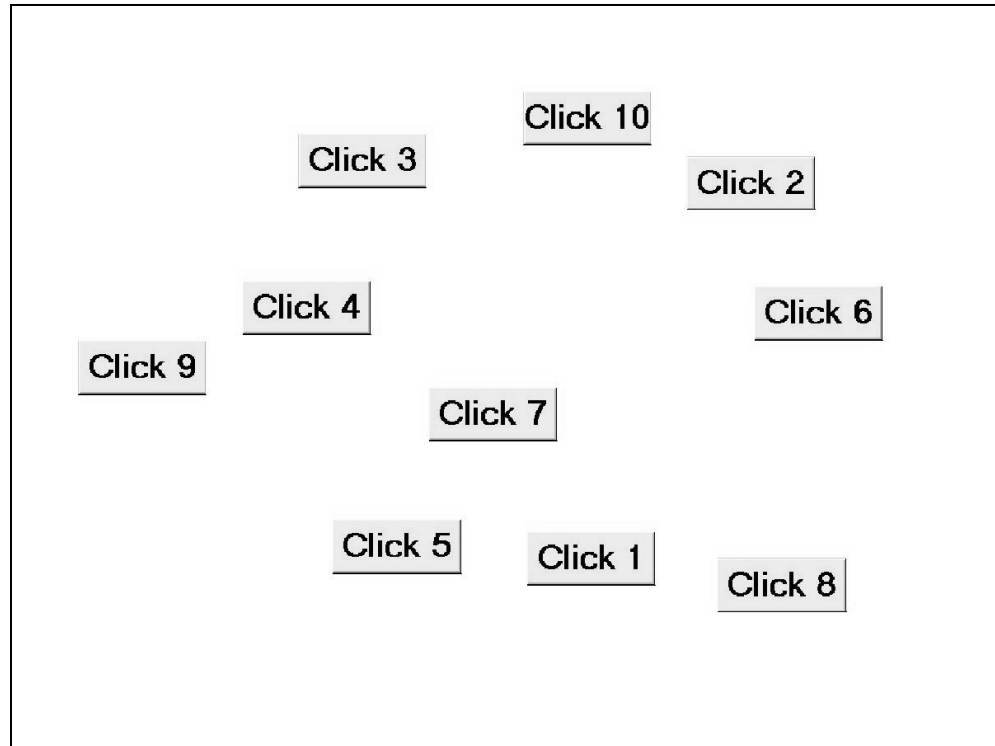


Figure 3.3: Typical target positioning for the laser targeting motion evaluation

By logging both postural and kinetic tremor, the laser targeting motion evaluation provided a rich test bed for tremor analysis. The motion of a patient's arm was not restrained during the test, nor was it easy for patients to rest their arm during the test because, as shown in Figures 3.1 and 3.2, the computer monitor used for evaluation was placed on the edge of the table directly in front of subjects so as to limit the availability of horizontal surfaces that could be used to brace a patients arm during evaluation. Subjects were also specifically instructed not to use both hands in any manner for assistance with the targeting tasks; only one hand was allowed to grip the IMU. Some patients attempted

to brace the arm directing the laser beam with their other arm; when they were told that this was not permissible they subsequently stopped using one arm to brace the other.

3.2 Eating Simulation Motion Evaluation

The other major test conducted for subjects was the evaluation of eating motion. This test was specifically selected because so many subjects had complained about their inability to eat food easily (soup and peas were often cited as among the most difficult foods to eat). The eating test required patients to pick up the IMU from the holster (as was the case for the laser targeting motion evaluation) and, using a spoon mounted to the IMU, simulate eating. A subject is shown in Figure 3.4 directly prior to conducting the eating test.

For the eating simulation, subjects were instructed to dip the spoon into the plate in front of them so as to touch the spoon at the base of the plate (as shown in Figure 3.5).

Subjects were then to lift the spoon towards their mouth in a manner such that they were pretending that soup was inside the spoon (i.e. they were instructed that they should move such as not to spill any fluid that could *theoretically* be inside the spoon). Sterilized spoons were utilized so subjects could touch the spoon to their lips (some subjects had the spoon come within a few centimeters of their lips without actually touching).



Figure 3.4: A test subject before the eating simulation motion evaluation

Taken from Teskey, Elhabiby and El-Sheimy (2011b)

After subjects had simulated ingesting food, they were asked to again dip the spoon into the base of the paper plate as if they were to take a second portion of food (again, this is depicted in Figure 3.5). After dipping the spoon into the base of the paper plate for the second time, subjects were asked to place the IMU back into the holster.



Figure 3.5: A test subject during the eating simulation motion evaluation

Taken from: Teskey, Elhabiby and El-Sheimy (2011b)

This testing procedure was created to give an account of motion during food consumption that would be as close as possible to what realistically takes place in a *real world* scenario. Generally, when someone is eating they repeatedly move a spoon (or other utensil) from the plate to their mouth and back to the plate again. It was not easy to perform this action repeatedly because it was preferred to place the IMU back in the holster at the conclusion of each trial so as to accurately keep track to the IMU position through the use of Kalman filter updates (as described in Section 3.1 on “Laser Targeting Motion Evaluation”). The overall eating simulation experimental protocol was created to balance the need to achieve high accuracy positioning results and the need to maintain a realistic motion profile. This balance was achieved by having subjects perform one full

motion cycle before returning the IMU into the holster (i.e. dipping a spoon into a plate, simulating ingesting food and then again dipping a spoon into a plate).

The eating simulation motion evaluation produced very good results for *typical* test subject motion in a simulated *real world* scenario. The test results depicted a lot of tremor motion and subjects stated that they felt that what was simulated was generally similar to their dining experiences.

3.3 Test Subjects Utilized

Test subjects were recruited through movement disorder societies (particularly, the Parkinson Society of Southern Alberta) and through contact persons associated to the research project who would contact friends and relatives to participate. A total of 11 controls (people without any inherent movement disorder) were utilized, along with 9 ET patients and 30 PD patients. There were 4 male controls along with 6 male ET patients and 10 male PD patients; as well, the mean age for controls was 64.1, the mean age for ET patients was 64.8 and the mean age of PD patients was 66.1. Associated standard deviations for the mean ages are 7.2, 16.2 and 9.2, respectively. Given these statistics, it is clear to see that different groups evaluate shared similar demographic characteristics. This is important because both ET and PD are highly age dependent disorders.

Many of the patients were medicated (2 ET and 27 PD) and it was not possible to have them discontinue medication for the tests carried out because none of the members of the team charged with data collected had an adequate medical background. If complications

resulted from medication not been taken it could have caused a very serious professional and medical difficulties. The fact that so many patients were medicated did not pose nearly as much of a problem as would at first glance seem to be the case. For one thing, almost all ET patients noted that medication was largely ineffective and the largest factor limiting the size of tremor for ET patients (based on conversations with the patients) was the fact that their disorder was not so pronounced in the first place.

For PD patients, the effect of medication sometimes wore off quickly. Many patients stated that towards the end of the period of time for which they had taken medication its effects were almost completely absent. Since PD patients tend to take medication during regular intervals (which did not coincide in any way with the testing intervals utilized for data collection) the data that were collected represented a group of patients on various levels of medication (some were effectively medicated, but many effectively were not). When the data collected is analyzed in subsequent chapters of this thesis, effort is taken to split off the group of patients whose tremor suggested limited or ineffective medication was used during the time interval for which data was collected (i.e. those with a large amount of tremor); this group is separated (for analysis) from the group of patients who were well medicated or had limited natural tremor (i.e. those with small or insignificant tremor).

All subjects utilized gave written consent as per the documentation approved by The Conjoint Health Research Ethics Board at The University of Calgary.

3.4 Equipment Utilized

The IMU utilized was designed and fabricated by the Mobile Multi-Sensor Systems (MMSS) Research Group at the University of Calgary, in the Department of Geomatics Engineering. The unit was designed to be held easily in a hand and had on board data logging capabilities using a USB (Universal Serial Bus) compatible data logging card. Using such a set up allowed for very fast collection and download of data, it also helped to limit the use of wires during data collection which can significantly complicate the process of capturing data (the IMU that was utilized is labeled in Figure 3.1). The sensors utilized included three accelerometers that were orthogonally mounted (LIS3LO6AL from ST Microelectronics (2006)). As well, three gyroscopes were utilized, these were also orthogonally mounted (XV-8100CB from Epson Toyocom (2010)). Accelerometers and gyroscopes had coincident x, y and z axes as labeled in Figures 3.1 and 3.4. The specification for the sensors are given in Table 3.1.

Table 3.1: Inertial sensor specifications

Parameter	LIS3LO6AL (accelerometer data)	XV-8100 CB (gyroscope data)
Range	$\pm 2g^*$ or $\pm 6g^*$	± 100 degrees/s
Non-linearity	$\pm 1.5\%$ of full scale	$\pm 0.5\%$ of full scale
Noise	$50 \mu g^*/\sqrt{Hz}$	$0.004(\text{degrees/s})/\sqrt{Hz}$
Size	$5 \times 5 \times 1.6$ mm	$5 \times 3.2 \times 1.3$ mm
Mass	0.08 grams	Not given
Temperature range	-40°C to 85°C	-40°C to 85°C

Taken from ST Microelectronics (2006) and Epson Toyocom (2010) *g is gravity

IMU data were logged at 130 Hz. No on board data filtering was used before analog to digital conversion. Care was also taken to design simultaneous signal acquisition capabilities for the different IMU sensors, so that all data collected for a given time were extracted at precisely the same time instant. It is easier to design the IMU hardware if simultaneous signal acquisition capabilities are not utilized, but it would have a very negative effect on data quality. Since the data captured is utilized later in this thesis (Chapter 5) for cross-spectral analysis, it was imperative that simultaneous signal acquisition was used. Without this technological capability, many of the data processing techniques used in this thesis would not have yielded the significant results that they did because cross-spectral analysis generally requires simultaneous signal acquisition. Without simultaneous signal acquisition, partial signal reconstruction would need to be attempted to be able to use cross-spectral analysis (or another complex mathematical technique would need to be used); it is not completely clear if such data processing would produce viable results.

3.5 Wavelet Chosen to Display Frequency Content

The frequency content for the thesis tremor data is often displayed by utilizing wavelets (first introduced in Sub-Section 2.6.7). The particular wavelet chosen for analysis is the Coiflets 3 wavelet. This wavelet was selected after an extensive search of all possible wavelets given for the Matlab programming environment (Matlab, 2008) showed that the Coiflets 3 wavelet often matched well with the tremor signal often under evaluation. The Coiflets 3 mother wavelet is given in Figure 3.6).

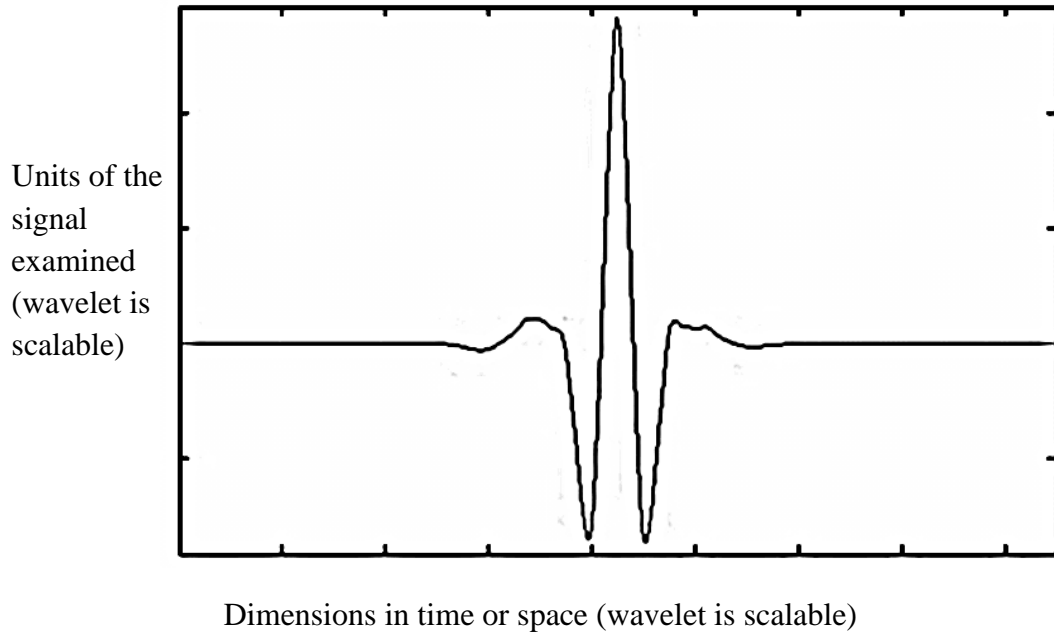


Figure 3.6: The Coiflets 3 mother wavelet

From the shape of the mother wavelet, it is easy to see why it might be good at capturing tremor motion given that its shape is similar to a tremor pulse. The mother wavelet, $\psi(t)$, is effectively used for the continuous wavelet analysis in such a manner that its complex conjugates' closeness with the signal under evaluation is utilized to determine wavelet coefficients $Q(m_\gamma, t_\sigma)$, as depicted originally in Equation (2.30). It should be noted that since the Coiflets wavelet is not complex, the complex conjugate of the mother wavelet is equivalent to the mother wavelet; the term complex conjugate is only used here for sake of generalization for when complex wavelets are used.

Given the manner in which the mother wavelet is used (as described in the previous paragraph), it would follow intuitively that a mother wavelet with a shape similar to a

tremor signal would be the best candidate for extracting tremor motion from a signal (and this is indeed what was found to be the case).

For discrete wavelet analysis, the mother wavelet is not directly utilized, but instead a high pass filter, $h_{wav}(n_{wav})$, is utilized to find details coefficients $d_1(n_{wav})$ as depicted in Sub-Section 2.6.7 on “Wavelet Analysis”

$$d_1(n_{wav}) = \sum_{k=-\infty}^{\infty} s(k)h_{wav}(2n_{wav} - k) \quad (2.33)$$

There exists a relationship between $h_{wav}(n_{wav})$ and the mother wavelet function, $\psi(t)$, as they essentially perform the same operation on the signal of interest (the former performs this operation in the discrete domain, and the latter in the continuous domain).

The father wavelet function, $\phi(t)$, allows for efficiency during discrete wavelet processing because it ensures that processing at different levels of decomposition process data in a non-redundant manner. Conceptually, if the complex conjugate of the mother wavelet can be thought of as been utilized to measure *closeness* for the signal under evaluation, the father wavelet can be thought of as representing what is left over after data *close* in shape to the mother wavelet have been extracted from the signal. The Coiflets 3 father wavelet is shown in Figure 3.7 (also sometimes called the scaling function).

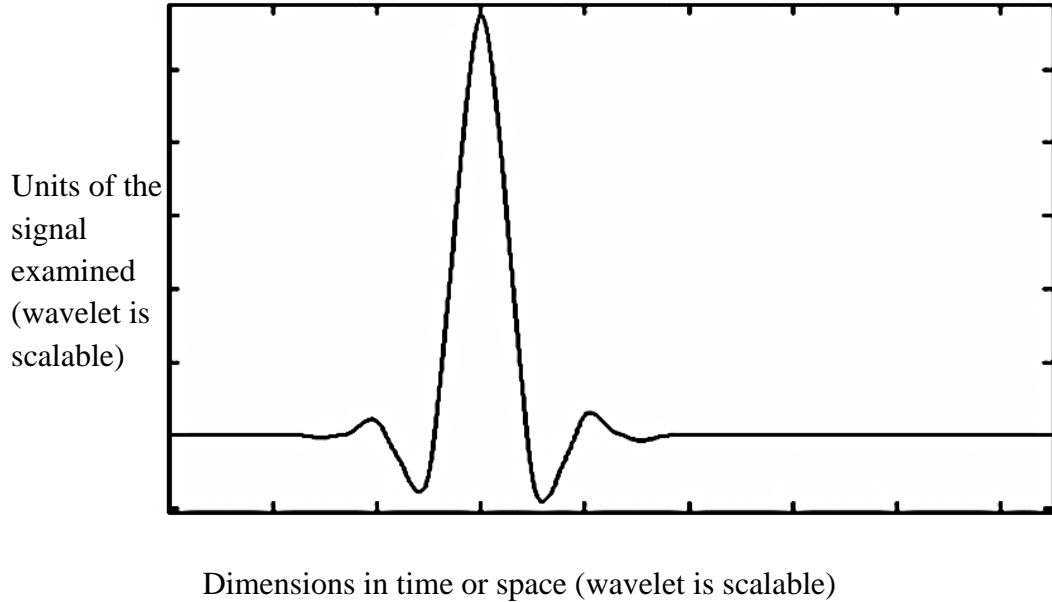


Figure 3.7: The Coiflets 3 father wavelet

Just as how there is a relationship between the mother wavelet and the high pass filter $h_{wav}(n_{wav})$, there is also a relationship between the father wavelet and the low pass filter $g_{wav}(n_{wav})$ which is utilized in discrete wavelet analysis to produce approximations coefficients $c_1(n_{wav})$ (as described in Sub-Section 2.6.7)

$$c_1(n_{wav}) = \sum_{k=-\infty}^{\infty} s(k)g_{wav}(2n_{wav} - k) \quad (2.34)$$

The Coiflets 3 wavelet has some very specific properties that can be used to define it. The mother wavelet must have minimum support size given vm vanishing moments and the father wavelet needs to contain a specified number of vanishing moments. Vanishing moments are defined for the mother and father wavelets, respectively, as follows (Mallat)

$$\int_{-\infty}^{\infty} t^{h_{vm}}\psi(t)dt = 0 \quad \text{For } 0 \leq h_{vm} < vm \quad (3.1)$$

And

$$\int_{-\infty}^{\infty} t^{h_{vm}} \phi(t) dt = 0 \quad \text{For } 1 \leq h_{vm} < vm \quad (3.2)$$

Where h_{vm} is an exponential parameter. The father wavelet also needs to satisfy the following (Mallat, 1999)

$$\int_{-\infty}^{\infty} \phi(t) dt = 1 \quad (3.3)$$

Another property of Coiflets mother wavelets is that they are nearly symmetric.

3.6 Display of Raw Data and Frequency Content

Raw data displayed in Figures 3.8 and 3.9 ((a) and (b)) depict typical motion for controls and ET patients (PD data are similar to ET data). Figure 3.8 shows typical accelerometer data and Figure 3.9 shows typical gyroscope data; both figures show data for the laser targeting motion evaluation carried out. For the displays in the figures, x-accelerator and y-gyroscope data, respectively, were chosen, because these are two axes of motion which depicted among the most tremor data (the x-axis and y-axis, of course, move with the inertial sensors that are gathering the data). Eating simulation motion evaluation data contained tremor similar to what is depicted for the laser targeting motion evaluation.

One thing that is clear from both Figures 3.8 and 3.9 is that control data depicted less tremor than ET data. This is clear looking at both raw signals as well as the signals analyzed utilizing a Coiflets 3 wavelet scalogram (at the bottom half of both Figures 3.8 and 3.9); whiter shades in the scalogram indicate greater frequency content and darker shades indicate an absence of frequency content. The scalogram is constructed using a continuous wavelet transform. The data depicted in the scalograms clearly illustrate that the Coiflets 3 wavelet chosen for evaluation is capable of picking up tremor at the

appropriate frequency range (3-12 Hz), given the more frequency rich content in the figures for this range.

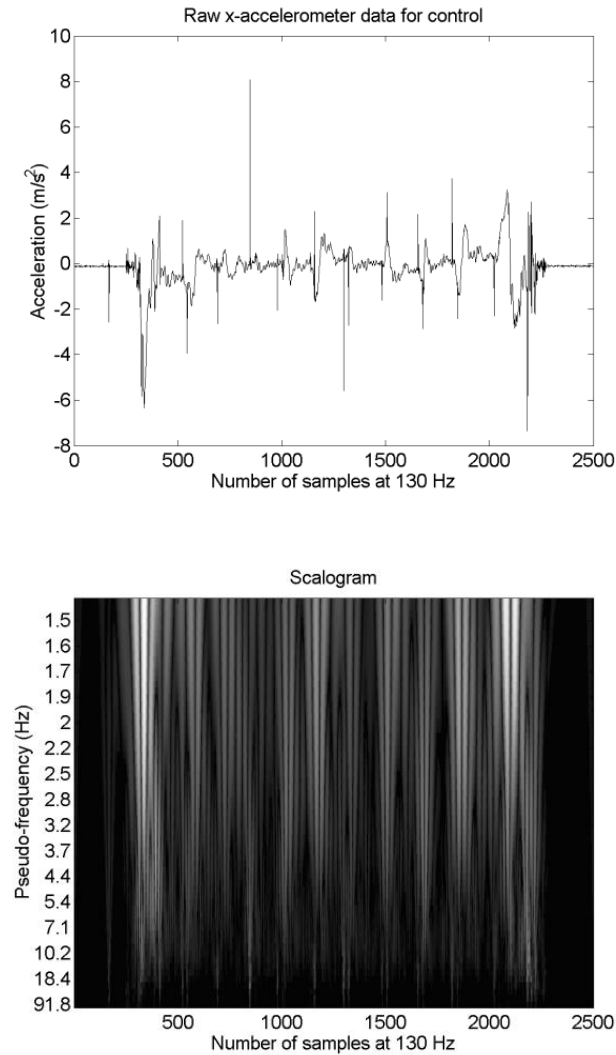


Figure 3.8 (a): X-accelerometer raw data and time-wise spectral distribution (utilizing the Coiflets 3 continuous wavelet transform) for a typical control for the laser targeting motion evaluation

Taken from Teskey, Elhabiby and El-Sheimy (2011a)

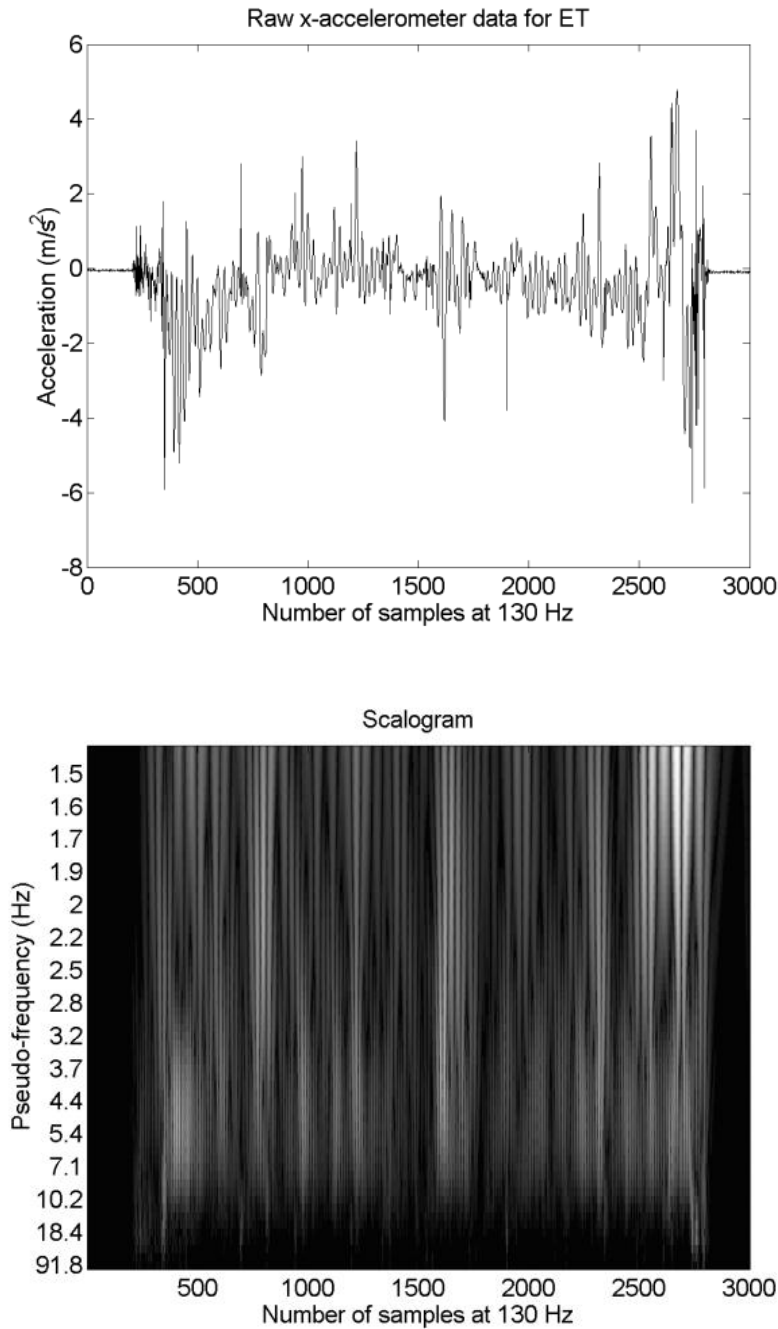


Figure 3.8 (b): X-accelerometer raw data and time-wise spectral distribution (utilizing the Coiflets 3 continuous wavelet transform) for a typical ET patient for the laser targeting motion evaluation

Taken from Teskey, Elhabiby and El-Sheimy (2011a)

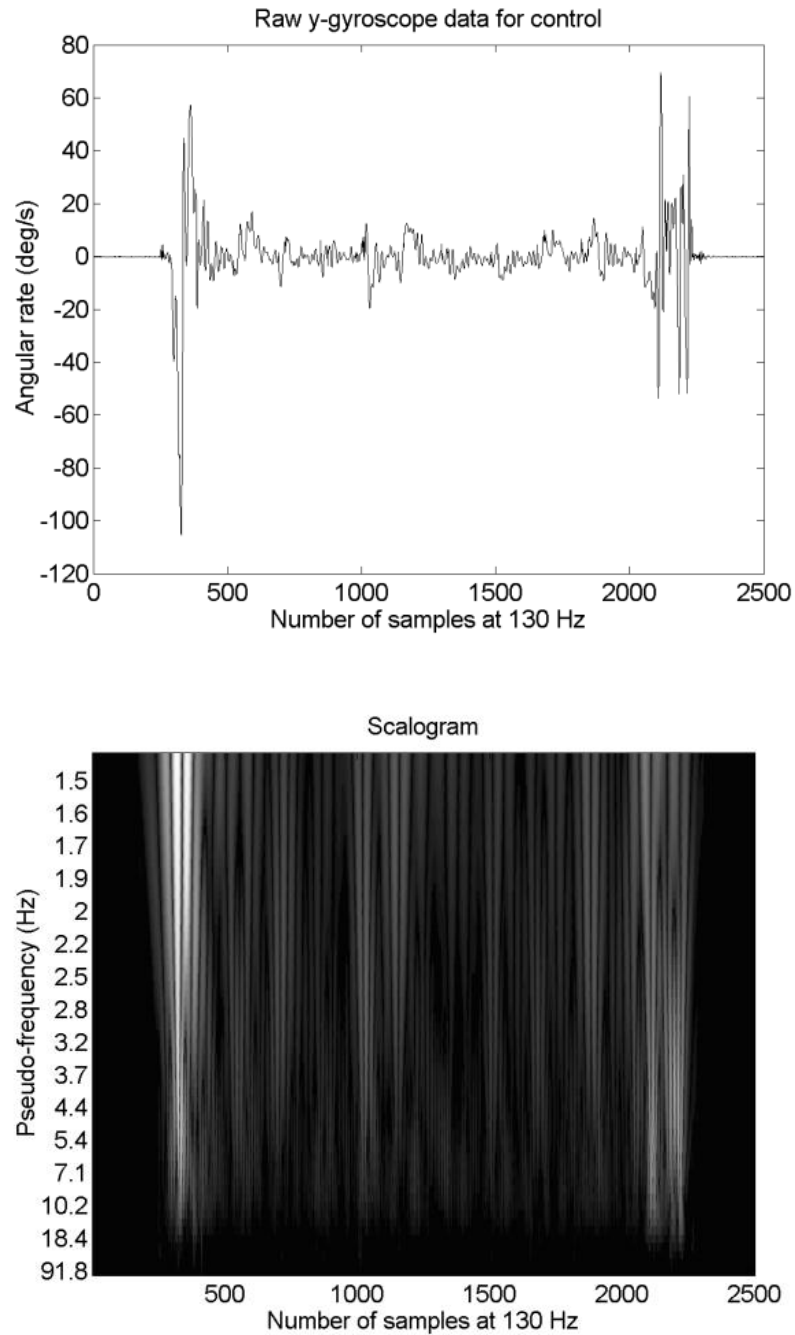


Figure 3.9 (a): Y-gyroscope raw data and time-wise spectral distribution (utilizing the Coiflets 3 continuous wavelet transform) for a typical control for the laser targeting motion evaluation

Taken from Teskey, Elhabiby and El-Sheimy (2011a)

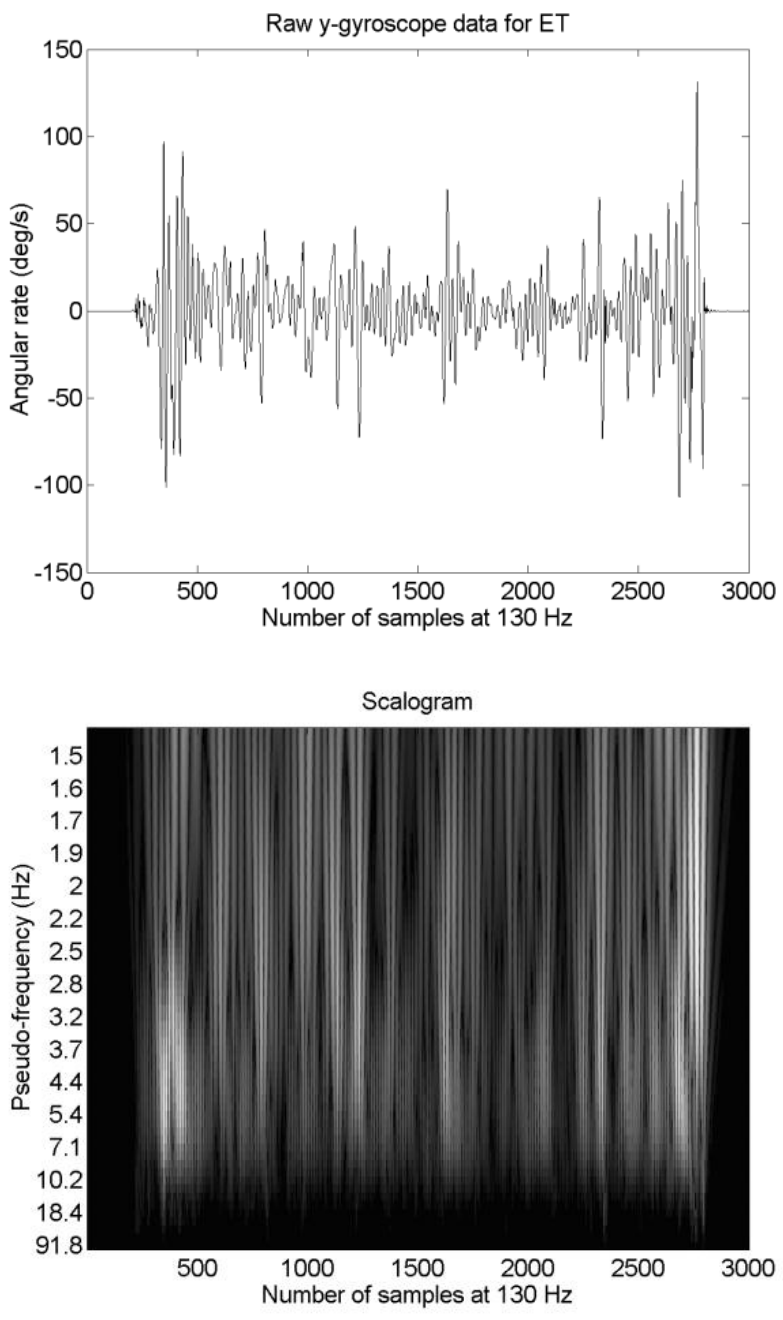


Figure 3.9 (b): Y-gyroscope raw data and time-wise spectral distribution (utilizing the Coiflets 3 continuous wavelet transform) for a typical ET patient for the laser targeting motion evaluation

Taken from Teskey, Elhabiby and El-Sheimy (2011a)

Another important point when looking at data in the scalograms for Figures 3.8 and 3.9 is that tremor seems to have a high variation (in terms of amplitude) over the duration of the signals studied. This was very typical of data captured for the laser targeting motion evaluation because as patients moved between targets of interest and subsequently ceased moving for a few seconds when arriving at a target of interest; inertial data logged both kinetic motion (generally larger tremor when moving between targets) and postural poses (generally less tremor when stationary at a target). These different motion phases can be seen to a certain extent in Figures 3.8 and 3.9 for ET data. For the ET motion in Figures 3.8 and 3.9, the tremor signal portions generally indicate kinetic motion and the signal portions with fewer tremors tend to indicate a postural pose.

The data given in Figures 3.8 and 3.9 tend to suggest very particular types of motions for the subjects examined. X-accelerometer tremor data tends to suggest a motion whereby a subject moves their hand in front of them from right to left in an oscillatory fashion. Y-gyroscope tremor data tends to suggest a motion whereby a subject has a tremor that manifests itself such that it is as if they are turning a door knob back and forth continuously. Both of these suggested motion profiles (and their inter relationship) are explored in detail in Chapter 6 of this thesis; and Figure 6.1 (also in Chapter 6) displays the motion profiles described above.

Large signal spikes are evident in the accelerometer data in Figure 3.8 ((a) and (b)), and these occurred as a result of patients inadvertently striking the IMU on the table in front

of them during data collection. These signal spikes often represent only one data point and for the purposes of most of the signal processing carried out, these unitary data points representing signal spikes could easily be ignored during subsequent processing and did not pose a significant challenge. Such signal spikes are shown here to help illustrate some of the challenges of motion captured using inertial sensors. It is generally easier to log data with signal spikes and then remove the signal spikes during processing than it is to try to log data without any signal spikes (given that it is difficult to restrain patient motion adequately so as to remove signal spikes).

The gyroscopes used have a much lower bandwidth than accelerometers (this is typically the case for MEMS sensors); and as a result, gyroscopes were less sensitive to signal spikes. This simplified the processing of the gyroscope data.

Another important factor in evaluating the accelerometer data in Figure 3.8 is that the accelerometer signals depicted can spend long durations of time at quite a distance from zero acceleration because accelerometers pick up gravitational acceleration. Any orientation of an IMU that does not align the accelerometers perpendicular to gravity can generate a signal offset from zero. Much of the processing in the next chapter of this thesis attempts to deal with this tendency of accelerometers to pick up gravitational acceleration (which not only affects the accelerometer long term signal offset from zero but also the ability of an accelerometer to distinguish between rotational and lateral tremors).

Gyroscopes don't contain long term signal offsets from zero in the same way as accelerometers do because they are not, for the most part, sensitive to gravity. However, gyroscopes are sensitive to the rotation of the earth; but this is a very weak signal and one the MEMS sensors often lack the capacity to resolve in a consistent manner.

The accuracy of the tremor data logged (after accelerometer data are processed to account for gravitational acceleration) is quite high. Most sources of error have been removed from the tremor data largely because of the manner in which the data were logged. For example, by having known start and end orientations for data logging (as is highlighted by the use of a holster during the trial start and end) it is possible to remove most signal biases from the inertial data. This removal of signal biases is possible because when inertial sensors are stationary in a fixed known position, there expected signal reading can be anticipated and any deviation from this expected signal reading can be assumed to be a signal bias. Another major source of error for inertial data, signal noise, does not affect tremor data to a large degree because tremor motion tends to produce oscillatory data. The signal noise may have a small impact on the magnitude of peaks and valleys of the oscillatory motion (without affecting the overall pattern of motion logged very much); this has a very small impact on the overall ability of inertial sensors to track oscillatory motion. In contrast to the analysis given in this thesis, when inertial sensors are used to describe long term (as opposed to oscillatory) position movement for motion tracking applications (such as walking), noise tends to be a very large problem because inertial signals (and thus noise) are integrated to produce position data for motion tracking. Integration of noise tends to dramatically increase errors in processed results.

The only major source of inertial signal error affecting the motion tracking capability of the sensors when tracking oscillatory motion is scale factor error. There is not complete data from manufacturers regarding the size of scale factor errors for the sensors used, however, based on a calibration of the sensors carried out just before experimentation to gather data, scale factor errors are at most in the low single digit percentages. This suggests that the accuracy of the oscillatory motion peaks and valleys is in the neighborhood of the low single digit percentages, which is more than adequate for assessment and attenuation of movement disorders (this is shown to be adequate for assessment in particular later in this thesis when it is shown that ET and PD data are different than control data based on objective analysis of the inertial signals captured).

A last important point to note in Figures 3.8 and 3.9 ((a) and (b)) is the large dynamic range motions logged directly at the beginning and end of each trial. These motions are due to patients pulling the IMU of the holster or placing the IMU back in the holster and are not generally representative of the movement disorder motion that the experiments conducted were set up to capture. For this reason, the beginning and end of each trial are not examined for most of the processing carried out for the remainder of this thesis.

3.7 Summary

Laser targeting and eating simulation motion evaluations were reported on at the beginning of this chapter. These evaluations allowed for the capture of relevant inertial data that contained tremor motion, so that subsequent data analysis could be performed (as will be depicted in subsequent chapters of this thesis).

Test equipment was also reported on in this chapter and relevant information about the data capture hardware was also given. The most important aspect of the hardware is that data are captured from all sensors at exactly the same time for each data logging event. This allows for cross-spectral signal evaluation in the subsequent chapters of this thesis; and it also allows for Kalman filtering and smoothing to take place, as Kalman filtering presumes data are logged for each sensor at the same time instant.

After data logging tests and equipment were presented, the wavelet utilized to evaluate tremor data was introduced. This wavelet was chosen largely based on its *closeness* in shape with the tremor motion under evaluation. When raw data were presented just before the conclusion of this chapter, it was clear that the wavelet chosen for evaluation was capable of capturing tremor motion in the 3-12 Hz tremor frequency range of interest for movement disorder motion. This wavelet will be used throughout this thesis to evaluate signal spectral information.

Chapter 4: Data Analysis using Extended Kalman

Filtering and Smoothing

This chapter of the thesis examines the quaternion based EKF used to carry out a portion of the data processing for this thesis. The main aim of this EKF is to remove large processing errors in orientation of the IMU used for data logging. Commonly, an EKF is used with inertial data to constrain both lateral errors and rotational errors, however, the former is not particularly relevant for that analysis in this thesis because tremor motion is the main focus of the work and, as such, large errors in overall position are not particularly relevant as they don't affect the lateral tremor signal logged.

On the other hand, rotational errors in the processed IMU data are quite relevant because accelerometers pick up gravitational acceleration, which makes isolating translation tremor from rotational tremor difficult. This will be further explored in Section 4.1 below.

4.1 Need for Kalman Filtering and Smoothing

Without appropriate information regarding IMU orientation, it is not possible to differentiate lateral tremor and rotational tremor logged by an accelerometer; it is essential to differentiate lateral and rotational tremor so that subsequent data processing conducted will have a greater capacity to track motion. This is principally why an EKF is utilized to correct IMU orientation information for the analysis carried out in this thesis;

gyroscopes provide some orientation information, but the gyroscope data has too much noise to provide accurate results, and thus Kalman filter updates are utilized along with smoothing to improve orientation data.

Accelerometers log lateral tremor directly and log rotational tremor indirectly; the latter is logged as an accelerometer is rotated about any given vector perpendicular to gravity, as shown in Figure 2.1 (in Chapter 2 of this thesis). The logging of rotational tremor by accelerometers is caused by the fact that accelerometers are sensitive to gravity induced acceleration measurements which vary as a result of rotation.

Accelerometer data can be corrected so that rotational tremor is removed, as shown in Figure 4.1, which depicts the processing needed to create a variable only containing translational accelerometer data, \bar{a}_t . However, the removal of rotational tremor data from accelerometer signals relies on accurate knowledge of the IMU orientation. This knowledge is difficult to obtain from only gyroscope data because of noise in the gyroscope signal which tends to make long term orientation tracking difficult.

The processing of gyroscope data with an EKF and appropriate supplementary data can greatly increase the accuracy of orientation information. For the experimentation conducted in this thesis, it is known that the IMU start and end orientation are identical as the IMU is situated in a holster at the beginning and end of each trial, which is described

in Sections 3.1 and 3.2. The known relative start and end positions of the IMU provides Kalman filtering updates which can help to contain long term growth of errors in orientation (other updates are also taken for when the IMU is relatively stationary during a trial, as explained later in this section).

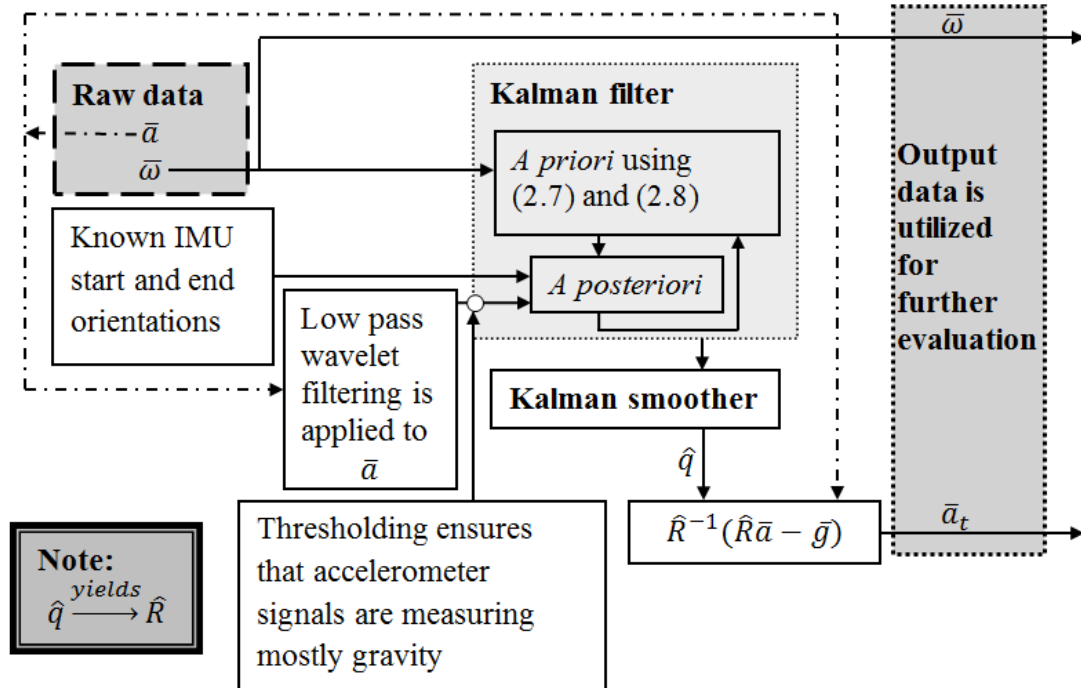


Figure 4.1: Flow chart for the removal of rotational tremor data from accelerometer signals

Taken from Teskey et al. (2011) (modified slightly)

In Figure 4.1, the term \hat{q} represents a four element quaternion vector (where $\hat{\cdot}$ depicts that adjusted quaternion values are utilized) and the term \hat{R} represents adjusted values for a three by three rotation matrix. Quaternions are examined in detail in Section 4.3 of this

thesis, titled “Quaternion Based EKF and Smoother” and Equations (2.7) and (2.8), which are referenced in Figure 4.1, are also explained in more detail in Section 4.3 for the purposes of applying a quaternion based EKF. As well, the terms in \hat{R} can be found directly from the terms in \hat{q} (and vice-versa), as shown in (Altmann, 1986; Kuipers, 1999)).

4.2 Data Processing to Assist with Removal of Gravity from Accelerometer Data

The manner in which \hat{R} is applied in Figure 4.1 (in the expression $\hat{R}^{-1}(\hat{R}\bar{a} - \bar{g})$) is intended to remove rotational tremor from accelerometer data. The expression $\hat{R}\bar{a}$ is utilized to rotate raw accelerometer data into a consistent coordinate frame. For the experimentation conducted, this consistent coordinate frame is typically defined by the orientation of the IMU in the holster at the beginning and end of testing (refer to Sections 3.1 and 3.2 on “Laser Targeting Motion Evaluation” and “Eating Simulation Motion Evaluation”, respectively, for the experimental procedure utilized during data capture, as well as IMU axes labels).

Once accelerometer data are in a consistent coordinate frame, gravity, \bar{g} , can be removed directly by subtraction ($\hat{R}\bar{a} - \bar{g}$ in Figure 4.1). After the impact of gravitational acceleration is removed from the accelerometer data, the remaining data are rotated back into the coordinate frame of the IMU at the time step for which processing is being carried out by utilizing \hat{R}^{-1} , as shown in Figure 4.1 (the superscript -1 denotes matrix inverse).

Data processing results improved significantly when more data (updates) were utilized to restrain the growth of orientation errors; these updates were used for Kalman filtering. One source of update data (in addition to updates based on the known start and end orientation of the IMU) was accelerometer signals when accelerometer data showed limited motion during a trial (i.e. for when a subject was relatively stationary when holding the IMU). There is no way to definitively separate accelerometer data based on whether no motion exists or a state of constant velocity exists, but generally human motion implies a lot of signal variation, even if relatively constant velocity human motion is being logged; this tendency of human motion to produce variability in accelerometer data is what was utilized to be able to use accelerometer data for orientation updates. Thresholding was applied to low passed accelerometer data, as shown in Figure 4.1, to ensure that during the period of limited motion, accelerometers were mostly measuring gravitational acceleration and thus accelerometer signals could be used to help orient the IMU about axes perpendicular to gravity. The thresholding applied was utilized for low passed accelerometer signals to ensure they were showing little change in magnitude over a period of time (thus implying the IMU was stationary); this thresholding was carried out using a standard deviation of each inertial signal for a set number of samples. Specifically, data within a set number of samples of the current sample under examination were used to compute a standard deviation measure (i.e. only data closest in time to the sample under examination were used for the evaluation). If the standard deviation measure was greater than the threshold chosen, then the current sample would not be used as an update, otherwise it would be used as an update. Thresholding criteria were not set firmly and were adjust somewhat for different subjects (with different

motion profiles) and then end results were checked visually to ensure that only accelerometer data during limited motion were used for updates. Motion profiles of subjects still affected the signals during relatively still motion segments, and this is why an adaptive thresholding criterion had to be used.

As well, a second thresholding criterion ensured that the magnitude of low passed accelerometer data (using all three signals) was roughly equal to the magnitude of gravity to further help ensure that accelerometer signals were measuring principally gravitational acceleration. Typically, a range of plus or minus 0.5 m/s^2 would be used as a tolerance limit such that the accelerometer data signal norm (magnitude for all three accelerometer sensors at a given time step) would need to be within 0.5 m/s^2 of gravitational acceleration for this second thresholding criterion to determine that the signal samples examined were appropriate to use for updates. Both of the above mentioned thresholding criteria would need to be satisfied so that accelerometer data at a given time step could be used as an update of orientation information.

The low pass filtering that was applied for the thresholding as described above (and as shown in Figure 4.1) utilized the discrete wavelet transform at scale $\gamma = 2^5 = 32$, corresponding to a pseudo frequency, F_a , of 2.87 Hz based on Equation (2.31). The low pass filter cut off of 2.87 Hz was chosen because it was just below the 3-12 Hz range of interest for movement disorder tremor, and thus data low passed in this manner would have most patient tremor motion removed. This is important because the thresholding

applied, as depicted in Figure 4.1, is more effective when utilized with data lacking tremor motion.

To apply the filter, discrete wavelet details and approximation coefficients were created for each level of decomposition. When the fifth level of decomposition was reached (corresponding to a scale of $\gamma = 2^5 = 32$), the details coefficients were zeroed for only the first five levels of decomposition and the signal was reconstructed using the zeroed details coefficients and non-zeroed values for all other approximations coefficients created during the decomposition. Refer to Sub-Section 2.6.7 on “Wavelet Analysis” for the necessary background information needed to carry out the filtering operation.

One important point to note for the Kalman filtering evaluation carried out in this thesis is that the state vector utilized only contains values for the quaternion terms and not biases in the gyroscope data. It is common to use a Kalman filter that utilizes in the state vector (and thus adjusts) both quaternion terms and gyroscope biases. However, this is not necessary for the experiment conducted here because the duration of experiments rarely exceeded twenty seconds and biases therefore did not change substantially for the duration of a trial; as such, a model of gyroscope signal bias drifts was not necessary.

As well, since we know in advance that the IMU is stationary in a holster directly before and after a trial, any non-zero (bias) signal elements could be subtracted directly from the

stationary gyroscope signal. As well, IMU orientation is known for the beginning and end of each trial and therefore biases can be subtracted from accelerometer data after orientation dependent gravitational accelerations are taken into account. Signal bias drifts in both gyroscope and accelerometer data sets are assumed linear when comparing computed bias values for a signal directly before and after a trial (computed bias values are based on stationary data for the IMU in the holster). In practice, for a trial duration of twenty seconds, assuming signal bias drifts were linear was adequate to remove most of the signal bias error affecting processing results because many other (non-linear) signal bias components do not show up in a twenty second sampling interval (they only show up for a much longer sampling interval).

4.3 Quaternion Based EKF and Smoother

A quaternion formulation for orientation tracking is based on the fact that any orientation in three dimensions can be represented by a scalar rotation, θ_a , about a unit vector $\bar{\theta}_u$.

$$\theta_a = \sqrt{\theta_x^2 + \theta_y^2 + \theta_z^2} \quad (4.1)$$

$$\bar{\theta}_u = \left[\frac{\theta_x}{\theta_a}, \frac{\theta_y}{\theta_a}, \frac{\theta_z}{\theta_a} \right]^T \quad (4.2)$$

The terms θ_x , θ_y and θ_z represent rotations about the x-axis, y-axis and z-axis respectively. A four element quaternion can be written as follows

$$\bar{q} = [q_1 \quad q_2 \quad q_3 \quad q_4]^T = \left[\frac{\theta_x}{\theta_a} \sin \frac{\theta_a}{2}, \frac{\theta_y}{\theta_a} \sin \frac{\theta_a}{2}, \frac{\theta_z}{\theta_a} \sin \frac{\theta_a}{2}, \cos \frac{\theta_a}{2} \right]^T \quad (4.3)$$

The quaternion is the state vector for the analysis carried out. The following is an equation for state *a priori* predictions for subsequent time steps (from Chapter 2)

$$\hat{\mathbf{x}}_k^{kf} = \Phi_{k,k-1}^{kf} \hat{\mathbf{x}}_{k-1}^{kf} \quad (2.7)$$

And it can be applied using quaternions as follows (Gibbs and Wilson, 1960; Goldstein, 1980; Gruben, 1970)

$$\bar{q}_k = (I_{4,4} + \frac{1}{2} \Omega(\bar{\omega}) \Delta t) \bar{q}_{k-1} \quad (4.4)$$

Where $I_{4,4}$ is a four by four identity matrix, subscripts k and $k - 1$ denote subsequent time steps, and as given in Sabatini (2006)

$$\Omega(\bar{\omega}) = \begin{bmatrix} 0 & -\omega_z & \omega_y & -\omega_x \\ \omega_z & 0 & -\omega_x & -\omega_y \\ -\omega_y & \omega_x & 0 & -\omega_z \\ \omega_x & \omega_y & \omega_z & 0 \end{bmatrix} \quad (4.5)$$

Where the constituent elements of $\Omega(\bar{\omega})$ represent raw x, y and z gyroscope data at each time step, respectively, as follows

$$\bar{\omega} = [\omega_x, \omega_y, \omega_z]^T \quad (4.6)$$

When comparing (2.7) to (4.4), it follows that the state transition matrix, $\Phi_{k,k-1}^{kf}$, can be found as follows

$$\Phi_{k,k-1}^{kf} = I_{4,4} + \frac{1}{2} \Omega(\bar{\omega}) \Delta t \quad (4.7)$$

The quaternion (state) covariance matrix, P^{kf} , has the following *a priori* predictions for subsequent time steps (from Chapter 2)

$$P_k^{kf} = \Phi_{k,k-1}^{kf} P_{k-1}^{kf} (\Phi_{k,k-1}^{kf})^T + G_{k-1}^{kf} Q_{k-1}^{kf} (G_{k-1}^{kf})^T \quad (2.8)$$

The three by three matrix Q_{k-1}^{kf} is only populated along the main diagonal by angular random walk values for gyroscopes, found as depicted in Sub-Section 2.4.7 on “Inertial Stochastic Parameters”. These angular random walk values are labeled $\sigma_{av,x,arw}^2(T_{av})$, $\sigma_{av,y,arw}^2(T_{av})$ and $\sigma_{av,z,arw}^2(T_{av})$ for x, y and z gyroscopes, respectively.

$$Q_k^{kf} = \begin{bmatrix} \sigma_{av,x,arw}^2(T_{av}) & 0 & 0 \\ 0 & \sigma_{av,y,arw}^2(T_{av}) & 0 \\ 0 & 0 & \sigma_{av,z,arw}^2(T_{av}) \end{bmatrix} \quad (4.8)$$

The term G_k^{kf} can be found by applying the following to (4.4)

$$\delta \bar{q}_k = \frac{d\bar{q}_k}{d\bar{\omega}} \delta \bar{\omega} \quad (4.9)$$

Which yields

$$G_k^{kf} = \frac{1}{2} \Delta t \begin{bmatrix} -q_4 & q_3 & -q_2 \\ -q_3 & -q_4 & q_1 \\ q_2 & -q_1 & -q_4 \\ q_1 & q_2 & q_3 \end{bmatrix} \quad (4.10)$$

In the above development, d depicts differentiation and δ depicts a small incremental, but finite, change in value.

Applying Kalman filtering updates can be carried out in the standard manner as given in Sub-Section 2.6.3 on “EKF Updates”. As well, Sub-Section 2.6.4 on the “Kalman Smoother” describes the procedure for smoothing the data.

One important consideration when applying the EKF updates is that when low passed accelerometer data are used to update orientation information (for when the thresholding criteria are satisfied) it is not possible to directly apply accelerometer data to update the orientation information stored in quaternions. Generally a design matrix, H_k^{kf} from Equation (2.10), is used so that update and state vector values can be put into a form that they directly correspond with one another (specifically, state vector values are put into a form such that their *theoretically corresponding update values* can be directly subtracted from measurement update data, as is suggested by the form of Equation (2.10)). It is difficult, in this case, to use a design matrix for such a purpose because quaternion values and accelerometer data do not have a simple mechanism that can relate their values to one another. Instead a small angle approximation (specifically, $\sin \theta \approx \theta$) is applied to Equation (4.3) and an iterative approach is used to relate the accelerometer update measurement data directly to the *theoretically corresponding update values* for the state vector (quaternion), so that Equation (2.10) can subsequently be used as part of the update procedure. When the small angle approximation ($\sin \theta \approx \theta$) is applied to Equation (4.3) and θ_x and θ_y are solved for, the following is found

$$[\theta_x \quad \theta_y]^T = [2q_1 \quad 2q_2]^T \quad (4.11)$$

The term θ_x can be related to the y-accelerometer signal in that the sin of the y-accelerometer signal divided by gravity is equal to θ_x . Similarly, the negative sin of the x-accelerometer signal divided by gravity is equal to θ_y . This relationship is the standard manner in which static accelerometer readings are used to deduce inclination.

Finding *theoretically corresponding update values* (to put into Equation (2.10)) involves taking quaternion values (q_1 and q_2) from the state vector and applying Equation (4.11) and the above stated relationship between accelerometer data and angular information (this will produce *theoretically corresponding update values* for the x-accelerometer and y-accelerometer readings). Because Equation (4.11) is only an approximation, it needs to be applied recursively. There are a number of ways of doing this, and generally they involve applying Equation (4.11) to quaternion values to get *theoretically corresponding update values* for the x-accelerometer and y-accelerometer readings. After this, the *theoretically corresponding update values* for the x-accelerometer and y-accelerometer are converted into angles (as described above for inclination measurements) and Equations (4.1) and (4.3) are applied to check and see how close the *theoretically corresponding update values* for the x-accelerometer and y-accelerometer are at producing the correct figures for q_1 and q_2 . Any discrepancy can be found by *subtracting* q_1 and q_2 values found from the (approximation based) estimation technique from the original q_1 and q_2 values of the state vector (respectively). Equation (4.11) can then be applied to this discrepancy to find the *theoretically corresponding update values* for the x-accelerometer and y-accelerometer that corresponds more closely to the original q_1 and q_2 values of the state vector. This technique can be applied recursively as many times as

needed to arrive at the final *theoretically corresponding update values* for the x-accelerometer and y-accelerometer data, that correspond to the original q_1 and q_2 values of the state vector. *Subtraction* of quaternions from one another is a non-trivial matter because one rotation is being subtracted by another (conceptually similar to rotating in one direction and then undoing this rotation partly by rotating in approximately the opposite direction). Even though this is a non-trivial *subtraction* operation, it can be readily performed and is well understood common knowledge.

4.4 Display of Accelerometer Data With and Without Gravity's Impact

Figure 4.2 shows y-accelerometer data before (solid line) and after (dotted line) the effects of gravity are removed for a typical trial involving the laser targeting motion evaluation (as described in Section 3.1). Without any gravitational impact, the data after the removal of gravity generally are close to the zero acceleration mark, as is expected. This result is anticipated because for the remaining accelerometer data after removal of the gravitational impact, lateral tremor is the dominant signal and this signal causes an oscillatory motion about zero acceleration.

It is also clear in Figure 4.2 that in the original data logged, the subject lifted the IMU out of the holster and subsequently tilted the y-accelerometer axis upwards and away from the ground causing the y-accelerometer axis to log a signal with a significant deviation from the zero mark. The IMU axes directions are defined for experimentation in Sections 3.1 and 3.2 on “Laser Targeting Motion Evaluation” and “Eating Simulation Motion Evaluation”, respectively.

At the conclusion of testing, as depicted in Figure 4.2, the subject rotated the IMU such that the y-accelerometer axis was somewhat perpendicular to gravity before placing the IMU back in the holster. This is shown in the figure by an acceleration signal that migrates back towards the zero mark near the conclusion of testing.

To verify that the Kalman smoothing worked appropriately, the accelerometer signal needs to be examined before and after gravity's removal. Accelerometer data with gravity removed should mostly depicted lateral tremor if the smoothing operation was successful. As shown in Figure 4.2, the smoothed signal behaves in the manner that is expected as long term signal deviations from the zero mark, due to the influence of gravity, are mostly removed.

Even though Figure 4.2 clearly depicts that the long term deviations due to gravity have been removed, it is not easy to tell whether or not rotational tremors have been removed. To effectively examine this, spectral data are plotted in Figure 4.3.

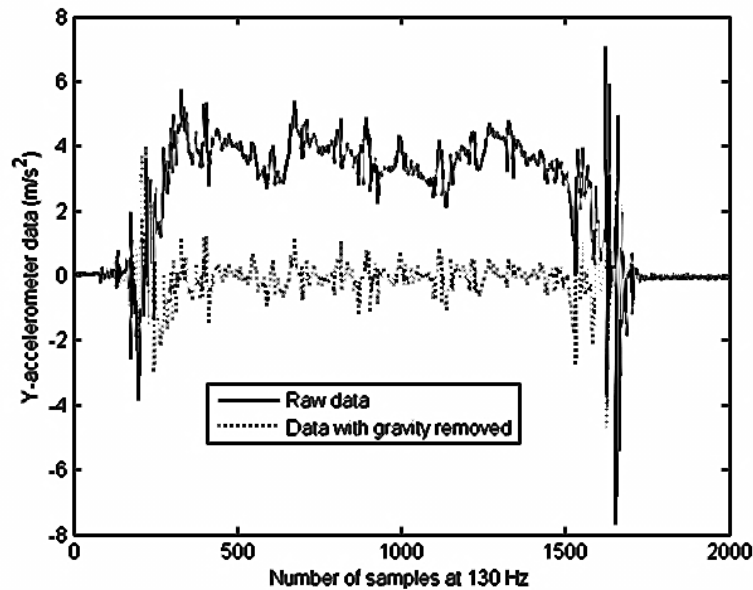


Figure 4.2: Raw y-accelerometer data before and after Kalman smoothing to remove gravity for a typical trial

Taken from Teskey, Elhabiby and El-Sheimy (2010a) – Sensors and Transducers:

http://www.sensorsportal.com/HTML/DIGEST/P_616.htm

For Figure 4.3, and much of the subsequent analysis in this thesis, ET and PD data were partitioned to differentiate patients with *significant tremor* from those with *limited tremor*. This was necessary because patients with *limited tremor* tended to depict similar frequency characteristics to controls in many cases. Data were partitioned according to their frequency content at a wavelet scale of $\gamma = 18$ (approximately 5.1 Hz based on pseudo frequency calculations). This frequency was chosen because it is near the peak frequency for many of the patients examined. The mean for absolute values of continuous wavelet coefficients was examined for each sensor and test subject at a scale of $\gamma = 18$

over the duration of a test. From this evaluation, all mean control data were averaged (creating a mean of means) for each sensor to establish a benchmark against which ET and PD data could be evaluated. If data for any ET and PD subject was more than one standard deviation larger than the benchmark mean control data, then the patient evaluated was considered to have *significant tremor*; otherwise, this patient was considered to have *limited tremor*. To qualify as having *significant tremor*, patients would need to breach one standard deviation above the benchmark mean for at least one of the six sensors examined; 8 of 9 ET patients and 9 of 30 PD patients were found to have *significant tremor*.

Figure 4.3 depicts population averaged x-accelerometer data for controls and patients with *significant tremor* (patients with *limited tremor* had data similar to controls, as will be examined in more detail in the next chapter of this thesis). It can be clearly seen from the figure that data after the removal of gravity showed lower amounts of tremor. This tends to indicate that the Kalman filtering and other mathematical operations applied, as shown in Figure 4.1, successfully removed rotational tremor because in order for the spectral distribution to decrease in magnitude, some tremor would have to have been removed. Figure 4.2 also validates the assertion that rotational motion was removed from the data (as can be seen from the fact that long term signal drifts resulting from gravity's impact during rotation motion are removed, as previously mentioned). From the combined results of Figures 4.2 and 4.3, it can be presumed that the Kalman filtering was applied successfully. Given that the impact of rotational tremor was removed from accelerometer data, the remaining accelerometer data in the 3-12 Hz frequency band

mostly depicts translational tremor; the Kalman filtering has thus allowed for the isolation of translational tremor components for subsequent study. The gyroscope data in the 3-12 Hz frequency band generally depicts rotational tremor so it is not necessary to process gyroscope data with the same rigor as accelerometer data before subsequent frequency analysis can take place.

It is important to note that generally only a small amount of tremor can be attributed to rotational tremor and most of the tremor logged by the x-accelerometers in Figure 4.3 was translational in nature. This can be inferred from the fact that there is only a slight difference in spectral magnitude in the figure for before and after when gravity is removed from each signal. If a large difference in pre and post processed signal magnitude was observed, it would tend to indicate that a lot of rotational tremor had been removed as a result of Kalman filtering and subsequent mathematical operations.

The population y-accelerator data give similar result to what is shown in Figure 4.3 for x-accelerator data. The z-accelerator data show almost no difference in spectral magnitude before and after gravity is removed. This makes intuitive sense since the z-axis is generally parallel to the gravity vector and the x-axis and y-axis are generally perpendicular to the gravity vector during the course of a trial, and thus are more susceptible to gravity's impact.

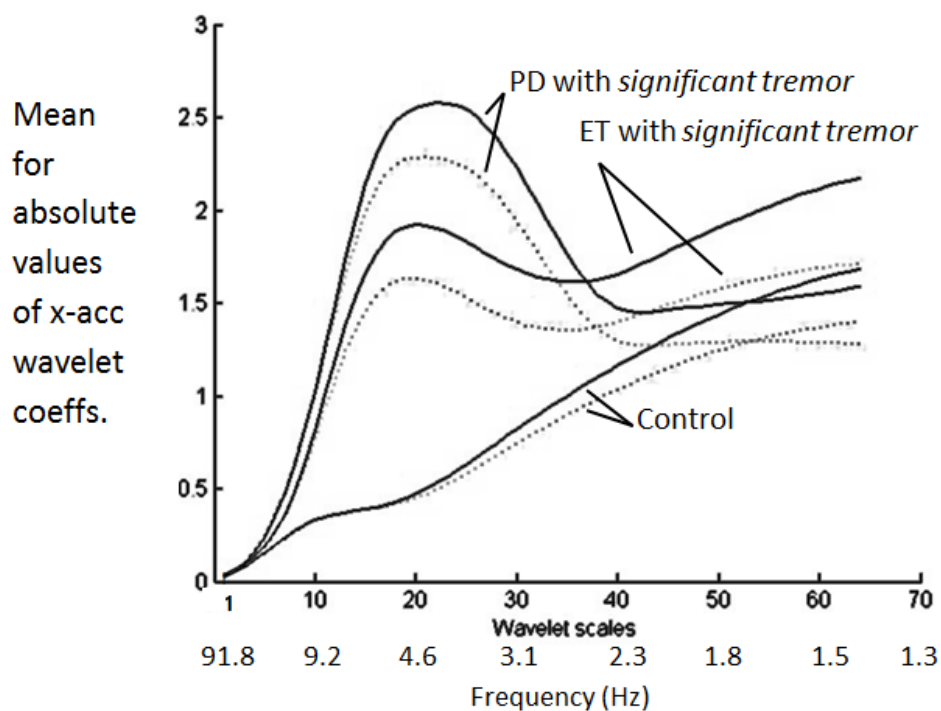


Figure 4.3: Population Coiflets 3 spectral magnitudes for x-accelerometer data before (solid line) and after (dotted line) Kalman smoothing and subsequent mathematical operations to remove gravity

Taken from Teskey, Elhabiby and El-Sheimy (2010a) – Sensors and Transducers:

http://www.sensorsportal.com/HTML/DIGEST/P_616.htm

4.5 Summary

In this chapter, the idea of why Kalman filtering is needed to process IMU data is at first discussed. The phenomenon where accelerometers log both translational and rotational tremor (the latter thanks to the influence of gravity) is examined. As well, the inability of gyroscope data to provide sufficient orientation information to correct accelerometers such that they only display later tremor is discussed. This inability of gyroscope stems

from the errors present in gyroscope signals, and necessitates the use of supplementary data so that Kalman updates can be performed.

Once IMU data are processed, lateral tremor can be represented by the processed accelerometer data, \bar{a}_t , and rotational tremor can be represented by unprocessed gyroscope data (both are generally high pass filtered before subsequent processing to remove non-tremor data).

At the conclusion of this chapter, raw accelerometer data are depicted before and after gravity is removed and the effects of this processing are examined. As well, a spectral evaluation of accelerometer data before and after gravity is removed is given. It is described that x-accelerometer and y-accelerometer tend to log a small amount of rotational tremor, and the z-accelerometer tends to log almost no rotational tremor for the experimentation carried out (i.e. the “Laser Targeting Motion Evaluation”).

Chapter 5: Characterization and Diagnostic Algorithms

This thesis chapter outlines the algorithms and mathematical techniques used to differentiate control from movement disorder data, as well as algorithms used to differentiate ET and PD data from one another. All analysis performed uses data from the laser targeting motion evaluation outlined in Section 3.1. As well, much of the analysis undertaken utilizes the distinction between patients with *significant tremor* and those with *limited tremor*, as defined in Section 4.4.

Figure 5.1 shows a typical population spectral distribution for control, ET and PD data (such spectral distributions will be examined in more detail throughout this chapter).

There are a few very significant points to note from Figure 5.1. Firstly, the auto-spectral distribution for the y-gyroscope data depicted is very similar for both ET and PD patients with *significant tremor* and it is also similar for patients with *limited tremor* and controls. This is not only true of the y-gyroscope data, but other spectral distributions showed similar patterns of motion (for each degree-of-freedom). The fact that population spectral distributions are similar for ET and PD with *significant tremor* is not surprising given that both are reported to be in the range of 3-12 Hz. For patients with *limited tremor*, the fact that spectral distributions are similar to those of controls validates the use of the thresholding outlined in Section 4.4, titled “Display of Accelerometer Data With and Without Gravity’s Impact”. This thresholding successfully differentiated between

patients with data similar to controls (depicting *limited tremor*) and those with data that is not similar to controls (depicting *significant tremor*).

One important finding of this thesis is that peak tremor frequency is similar for all six degrees-of-freedom of motion for a given subject, and spectral distribution also tends to be similar for each degree-of-freedom. This is true for ET and PD patients and this fact is not widely report in the literature (if at all). For anyone studying the pathogenesis of movement disorders, similar frequency of motion tends to indicate the presence of certain biomechanical and neurological phenomenon which will be discussed in Section 6.1, titled “Main Axes of Tremor Motion”.

Note also that the frequency band of peak frequency for *significant tremor* tends to be in the expected 3-12 Hz range. This helps to validate that the data capture was preformed properly.

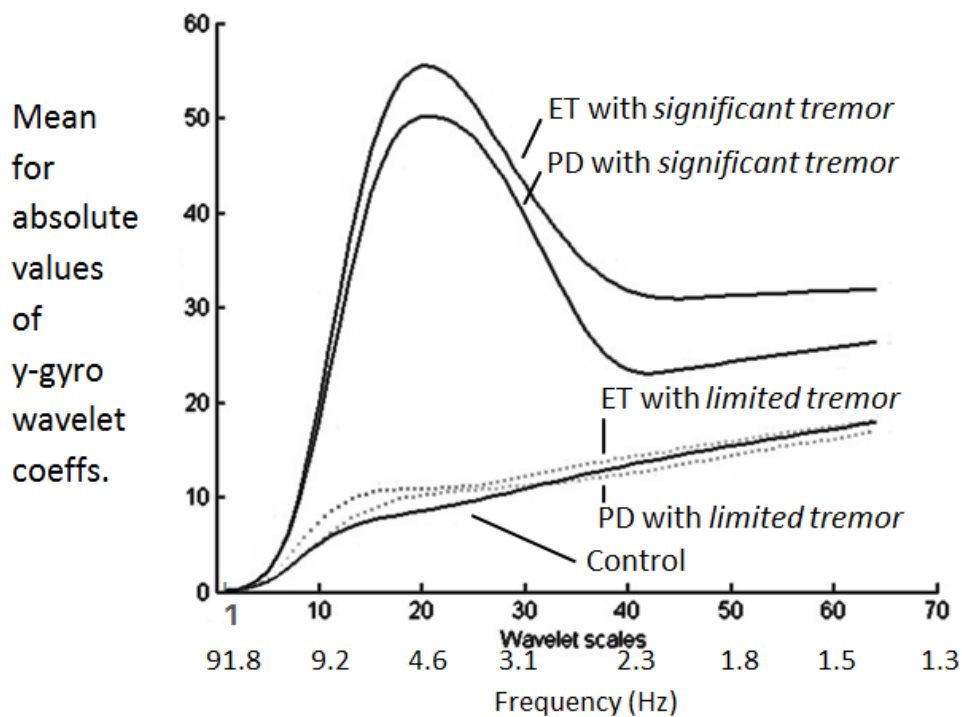


Figure 5.1: Population y-gyroscope data continuous Coiflets 3 spectral distribution

Taken from Teskey, Elhabiby and El-Sheimy (2010a) – Sensors and Transducers:

http://www.sensorsportal.com/HTML/DIGEST/P_616.htm

5.1 Auto-Spectral Fourier Analysis of Tremor

This section and the next (Section 5.2) focus on the difference between control data and movement disorder patient data. Specifically, inertial sensors are examined to determine whether auto-spectral based analysis techniques for inertial data can be used to realize diagnosed hand tremor.

For the purposes of this examination, only ET data for non-medicated patients are displayed in Sections 5.1 and 5.2. ET data are more suited to the analysis carried out in these sections because of the fact that there are many ET patients who were not taking medications (7 of the 9) when compared to PD patients (only 3 of the 30 were not taking medications).

The auto-spectral Fourier analysis that follows in Figure 5.2 is based on Equation (2.16). The population data for controls are shown with solid lines, and the population data for ET patients are shown with dotted lines. Population data are found by adding together data for all controls or ET patients at each frequency plotted and dividing by the number of test subject in each group to obtain a population average. Accelerometer data plotted have had gravitational effects removed as outlined in Chapter 4. As a result, accelerometer data presented represent principally lateral tremor and gyroscope data represent principally rotational tremor (this is the case for all analysis undertaken for this thesis chapter).

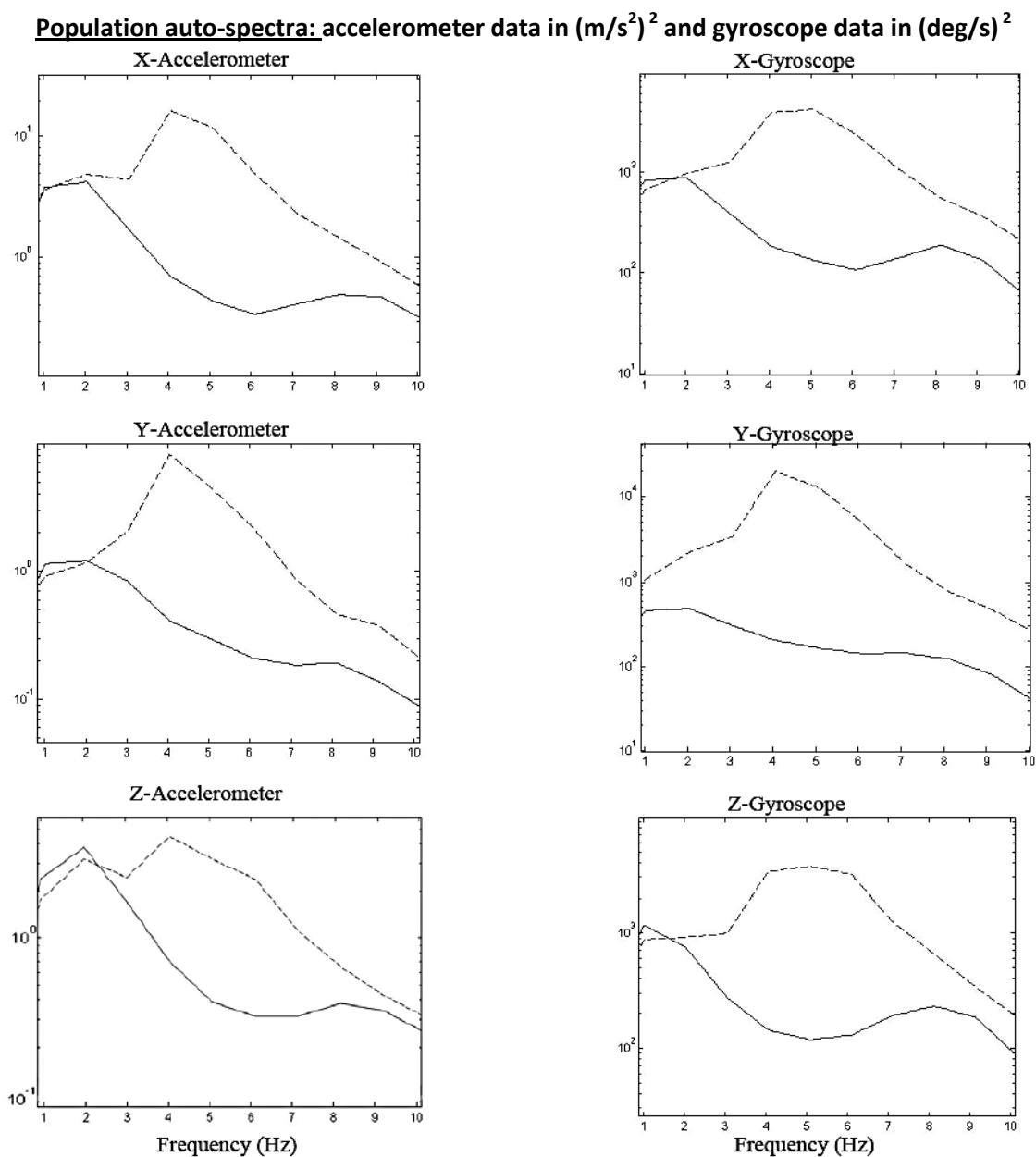


Figure 5.2: Population auto-spectral distributions using Fourier analysis for controls (solid lines) and ET patients (dotted lines)

Taken from Teskey, Elhabiby and El-Sheimy (2010b)

As previously mentioned in this document, population spectral distributions are very similar for all six degrees-of-freedom for control data and separately for all six degrees-of-freedom for ET data. For individual subjects, spectral distributions for all degrees-of-freedom were also similar. Another important point is that ET patient data tended to exhibit significantly more tremor in the frequency band of interest (3-12 Hz); this was often one order of magnitude more than controls.

As a result of such similar spectral distributions across all degree-of-freedom, it is likely that a single axis sensor could be used for many characterization and diagnostic algorithms. It is not necessary to have six sensors if they give such similar information. However, later in this chapter, it will be shown that for other applications, having multiple sensors is a significant asset. For cases when a single axes sensor could be utilized, it would be better to use a gyroscope to avoid cases for when an accelerometer captures both translational and rotational tremor, necessitating the use of Kalman filtering and other mathematical techniques to differentiate the two types of tremor logged (the other alternative is to simply use data with embedded translational and rotational tremor components, but this is intuitively and mathematically difficult to deal with). Another important point about the data in Figure 5.2 is that the x-accelerometer and y-gyroscope generally depicted the most tremor motion. This observation is important for the analysis carried out in Section 6.1, its implications are discussed there. Generally, from what is given in Figure 5.2, it seems that inertial sensors can be used to help diagnose ET. This will be validated in Section 5.2, below.

5.2 Wavelet Spectral Analysis of Tremor

This section validates the use of inertial sensors to assist with the differentiating between diagnosed ET and control motion through the use of wavelet based spectral analysis.

Much of the wavelet analysis depicted is similar to the Fourier analysis from the Section 5.1.

Wavelets are a generally a better tool (than Fourier techniques) with which to undertake spectral analysis for the purpose of differentiating diagnosed ET from control data because their computationally efficient time frequency resolution capabilities allows for the variation in the size of tremor to be considered during analysis. Such variation of the size of tremor is highlighted in Section 3.6, whereby tremor magnitude is shown to increase and decrease for tremor patients, often for a few seconds at a time.

In order to carry out testing to verify the difference in inertial data between controls and diagnosed ET patients, the following mean ($\bar{Q}(\gamma, p)$) and standard deviation ($s(\gamma, p)$) of absolute values for continuous wavelet coefficients are needed for each member of the population examined given N_{sam} samples per member where $\sigma = 1, 2 \dots N_{sam}$

$$\bar{Q}(\gamma, p) = \frac{1}{N_{sam}} \sum_{\sigma=1}^{N_{sam}} |Q(m_{\gamma}, t_{\sigma})| \quad (5.1)$$

$$s(\gamma, p) = \sqrt{\frac{1}{N_{sam}} \sum_{\sigma=1}^{N_{sam}} (\bar{Q}(\gamma, p) - |Q_p(m_\gamma, t_\sigma)|)^2} \quad (5.2)$$

The term $Q(m_\gamma, t_\sigma)$ denotes continuous wavelet coefficients as defined in (2.30) and population members are denoted $p = 1, 2 \dots M$, where there exist a total of M members. The term defined in (5.1), $\bar{Q}(\gamma, p)$, is bolded to distinguish it from a vector which utilizes a similar notation, but without bolding (this notation is used throughout this thesis).

Based on each of the parameters defined in (5.1) and (5.2), a Q-Q plot was used so that control and ET data could be checked for normality (Gnanadesikan and Wilk, 1968); although normality is not strictly needed for the analysis performed, it is good to remove obvious outliers so that end results are not skewed. One ET sample needed to be removed based on the results of the Q-Q plot, and this sample is depicted in Figure 5.3, with abnormally high magnitudes of mean and standard deviation at each given wavelet scale.

Analysis of mean and standard deviation is carried out at a scale of $\gamma = 20$ because this was close to the peak population frequency for the ET data (it has a pseudo frequency of 4.6 Hz). To compare different groups (populations) analyzed (i.e. control and ET) it is constructive to find the mean of the means and mean of standard deviations (within each group examined), as given below, respectively

$$\bar{x}_{\bar{Q}}(\gamma) = \frac{1}{M} \sum_{p=1}^M \bar{Q}(\gamma, p) \quad (5.3)$$

$$\bar{x}_s(\gamma) = \frac{1}{M} \sum_{p=1}^M s(\gamma, p) \quad (5.4)$$

As well, the standard deviation of means and standard deviation of standard deviations is quite useful and can be found, respectively, as follows

$$s_{\bar{Q}}(\gamma) = \sqrt{\frac{1}{M} \sum_{p=1}^M (\bar{x}_{\bar{Q}}(\gamma) - \bar{Q}(\gamma, p))^2} \quad (5.5)$$

$$s_s(\gamma) = \sqrt{\frac{1}{M} \sum_{p=1}^M (\bar{x}_s(\gamma) - s(\gamma, p))^2} \quad (5.6)$$

From the above, the specific terms being utilized for the analysis carried out are $\bar{x}_{\bar{Q}}(20)$, $\bar{x}_s(20)$, $s_{\bar{Q}}(20)$ and $s_s(20)$. The results of applying the above analysis (to produce $\bar{x}_{\bar{Q}}(20)$, $\bar{x}_s(20)$, $s_{\bar{Q}}(20)$ and $s_s(20)$) are shown in Tables 5.1 (a) and (b). What stands out is how different the mean values are from one another in the case of both tables (when comparing control and ET patient data). Most of the time, the ET mean data (mean of mean and mean of standard deviation) are more than double the value of the corresponding control mean data (which lie horizontally across from the corresponding ET data in both tables). Even in cases when the ET mean data are not more than double the control data, they are close to double the control data. Furthermore, the difference

between ET mean data and corresponding control mean data tend to lie outside the relevant standard deviation values given in the tables (relevant standard deviation data is the standard deviation of means and standard deviation of standard deviations data). It is clear from the results that non-medicated ET patients have a tremor magnitude and variation that is quite a bit different from control data. Based on this, any one of the six inertial sensors (three accelerometers and three gyroscopes) used in the examination carried out could be used to differentiate between control and non-medicated ET data.

Another important point stemming from Tables 5.1 (a) and (b) is that as the magnitude of tremor increases for the laser targeting motion evaluation, variation of the size of tremor also increases. This is evidenced by mean of means data in Table 5.1 (a) showing larger magnitudes for ET data over control subject data, which correspond to similar discrepancies in magnitude outlined in the mean of standard deviations data in Table 5.1 (b) (this is described in Section 3.6, where raw data and frequency content are displayed and described). The population member data over all frequencies are shown in Figure 5.3. The figure largely verifies an ET peak frequency in the 3-12 Hz range. It also verifies visually what has been shown above, that the defined wavelet characteristics (based on mean and standard deviation for the absolute value of wavelet coefficients) do a good job differentiating control data from ET data. The data shown in Figure 5.3 are for y-gyroscope data, and similar results could be shown for the other sensors. Figures 5.4 and 5.5 show population results for all sensors.

Table 5.1 (a): Group mean of means ($\bar{x}_{\bar{q}}(20)$) and associated standard deviation of means ($s_{\bar{q}}(20)$) for wavelet coefficients at scale 20

Inertial Sensor	Mean and standard deviation for control data	Mean and standard deviation for ET data
X-accelerometer (gravity removed)	0.515 ± 0.061	1.285 ± 0.438
Y-accelerometer (gravity removed)	0.404 ± 0.083	0.885 ± 0.242
Z-accelerometer (gravity removed)	0.466 ± 0.104	0.980 ± 0.200
X-gyroscope	9.29 ± 2.66	26.4 ± 8.1
Y-gyroscope	9.69 ± 2.87	35.0 ± 17.0
Z-gyroscope	8.79 ± 2.19	31.4 ± 15.9

Adapted from Teskey, Elhabiby and El-Sheimy (2011a)

Table 5.1 (b): Group mean of standard deviations ($\bar{x}_s(20)$) and associated standard deviation of standard deviations ($s_s(20)$) for wavelet coefficients at scale 20

Inertial Sensor	Mean and standard deviation for control data	Mean and standard deviation for ET data
X-accelerometer (gravity removed)	0.528 ± 0.070	1.052 ± 0.344
Y-accelerometer (gravity removed)	0.399 ± 0.078	0.752 ± 0.211
Z-accelerometer (gravity removed)	0.478 ± 0.082	0.818 ± 0.187
X-gyroscope	10.09 ± 3.48	22.05 ± 5.55
Y-gyroscope	10.50 ± 3.17	27.97 ± 12.34
Z-gyroscope	9.77 ± 2.66	26.01 ± 12.11

Adapted from Teskey, Elhabiby and El-Sheimy (2011a)

The most significant things to notice from Figures 5.4 and 5.5 is how similar they are in shape to one another for each degree-of-freedom. This further strongly implies that as magnitude of tremor increases, variation of the size of tremor also increases. Also, to further validate this point, in both sets of plots x-accelerometer and y-gyroscope data were the largest in magnitude.

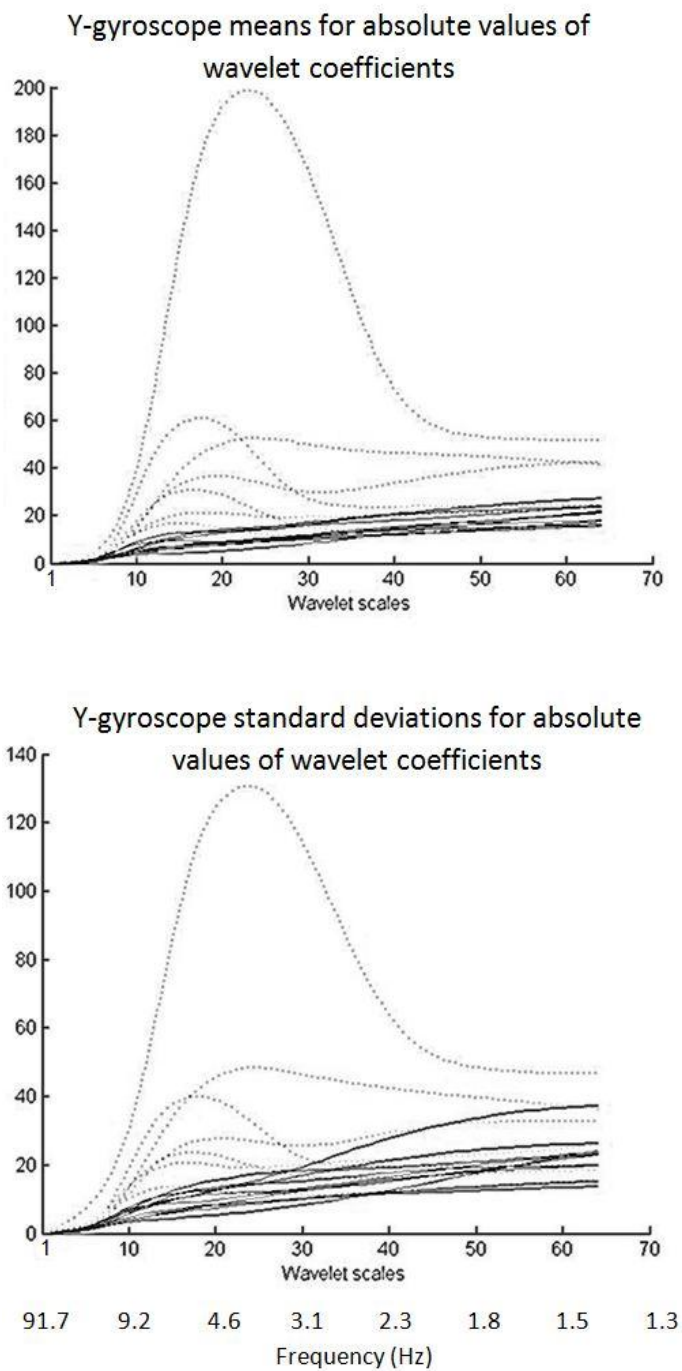


Figure 5.3: Population wavelet coefficient means (from (5.1)) and standard deviations (from (5.2)) for y-gyroscope data of controls (solid lines) and ET patients (dotted lines)

Taken from Teskey, Elhabiby and El-Sheimy (2011a)

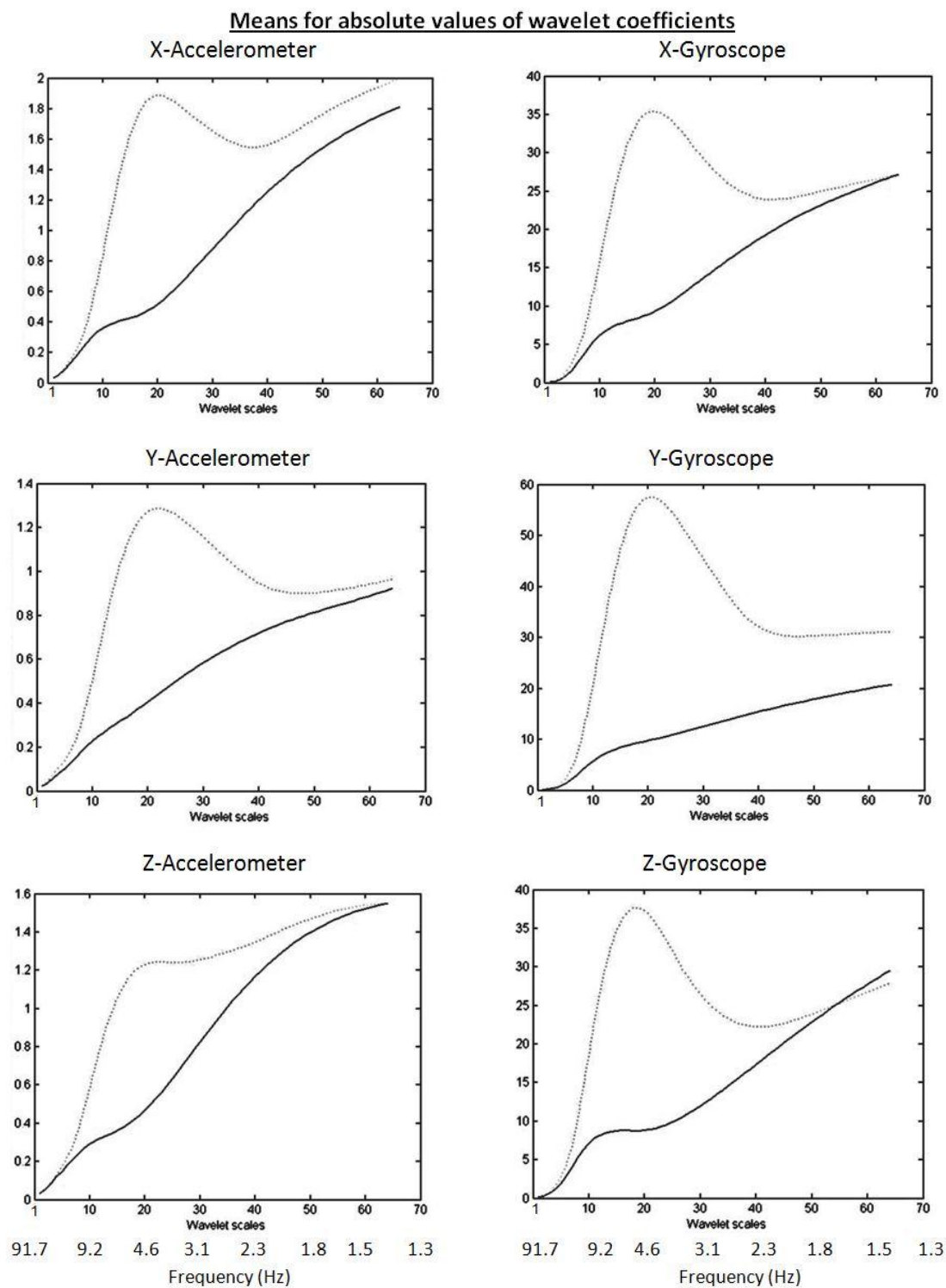


Figure 5.4: Population means from (5.1) for controls (solid lines) and ET (dotted lines)

Taken from Teskey, Elhabiby and El-Sheimy (2011a)

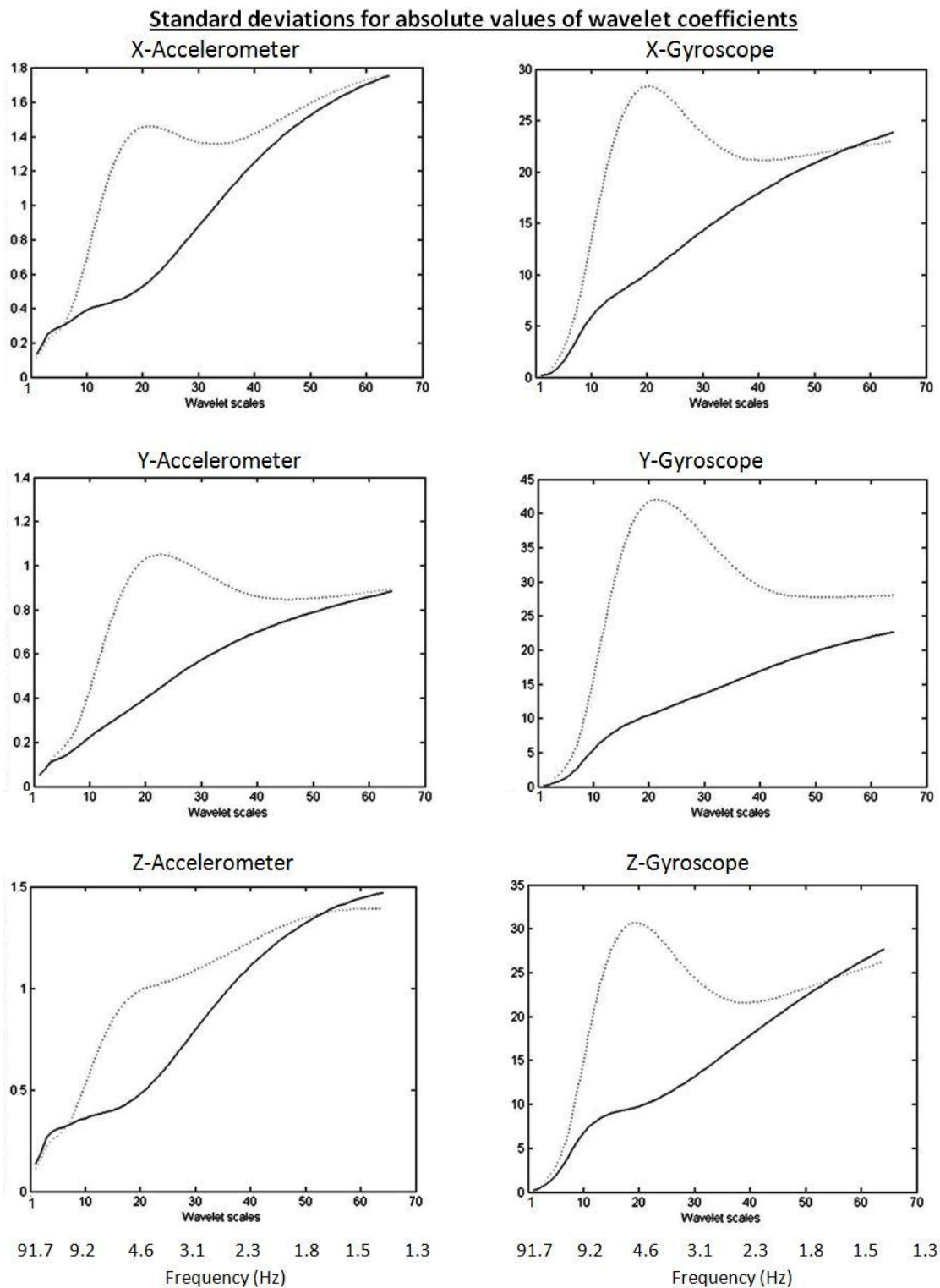


Figure 5.5: Population standard deviations from (5.2) for controls (solid) and ET (dotted)

Taken from Teskey, Elhabiby and El-Sheimy (2011a)

When comparing Figure 5.4 to Figure 5.2 (a Fourier auto-spectral analysis of the sensor data), it is clear that both figures show very similar data (when the manner in which axes are labeled non-linearly are taken into account). Virtually all significant data shown in Figure 5.4, including the overall shape of the spectral distribution and the peak frequency, are shown in Figure 5.2. Both figures also indicate that the x-accelerometer and y-gyroscope contain the most tremor as shown by spectral magnitude in each of the figures. The fact that the data in both figures is so similar strongly implies that for the purposes of auto-spectral analysis, the auto-spectral Fourier based technique produces very similar results to the wavelet based technique. The main advantage of using wavelets, then, is that they easily allow for other parameters to be defined, such as the standard deviation based measure shown in Figure 5.5. Fourier analysis generally cannot as easily allow for computation of such measures with the same computational efficiency as wavelets because Fourier based analysis generally lacks time resolution; therefore, the standard deviation based analysis depicted would likely require multiple Fourier analyses at different signal time frames (which is very computationally expensive).

5.3 Cross-Spectral Fourier Analysis of Tremor

In Section 5.2, above, wavelet spectral analysis was used along with statistical testing to show that ET patients with diagnosed hand tremor had a spectral peak magnitude that is higher than for control data. In this section, Fourier spectral analysis will be used to show that ET and PD data have significant differences for their *motion signature* (as defined by the difference in the pattern of movement consistent with the different groups examined). Specifically, spectral properties derived from ET and PD data will be used in a manner similar to how they might be applied for diagnostic applications.

Cross-spectral analysis is needed to distinguish between PD and ET data because the auto-spectrum of these two data sets can quite similar. Figure 5.6 shows population Fourier auto-spectral plots using the definition in (2.16). Data are given for the x-accelerometer with gravity removed (on the top) and y-gyroscope (on the bottom) for the laser targeting motion evaluation. These data are generally representative for results of data for all six degrees-of-freedom and show that for ET and PD, patients with *significant tremor* had similar auto-spectral distributions over the population, with a peak frequency in the 3-12 Hz range. Control data had similar auto-spectral distributions to PD data with *limited tremor* as both data sets depicted relatively little tremor (ET data with *limited tremor* is not shown here because it consists of only one subject under evaluation and this is not a large enough sample size to draw any conclusions). The fact that there is an auto-spectrum of considerably greater magnitude for *significant tremor* patients than controls in Figure 5.6 validates what was found in Section 5.2, where wavelets and statistical testing were used to indicate diagnosed ET patients had significantly higher magnitudes in there auto-spectral plots than controls.

It is important to keep in mind that a few tremor patients with very high tremors tend to distort the population averages depicted in Figure 5.6 upwards (for patients with *significant tremor*). Table 5.2 shows a number of tremor patients with exceptionally high tremor (sometimes more than an order of magnitude larger than other tremor patients). Despite the variation of size of tremor in the data set examined, the cross-spectral

technique presented later in this section to distinguish between ET and PD motion is quite robust given such varied data.

Table 5.2: ET and PD patients with exceptionally high tremor

Subject	X-accelerometer auto-spectral peak magnitude occurring within 3-12 Hz in unit of $(\text{m/s}^2)^2$	Y-gyroscope auto-spectral peak magnitude occurring within 3-12 Hz in units of $(\text{deg/s})^2$
ET high tremor #1	7.66	8.36×10^3
ET high tremor #2	2.75	2.63×10^3
ET high tremor #3	2.37	1.25×10^3
PD high tremor #1	28.5	6.75×10^3
PD high tremor #2	1.77	0.28×10^3

Taken from Teskey et al. (2011)

The population data shown in Figure 5.6 tends to smooth some of the more important aspects of PD and ET auto-spectra because population based averages tend to obfuscate certain signal characteristics. For this reason, Figure 5.7 shows data for typical ET and PD patients while undergoing the laser targeting motion evaluation; x-accelerometer data has gravity removed as depicted in Chapter 4. For Figure 5.7, auto-spectral data are shown on the top, and coherence (as defined in (2.17)) is shown on the bottom. Data sets with two auto-spectral peaks (local maxima) were not uncommon for ET and PD data (as shown in Figure 5.7), although ET data generally tend to depict single spectral peaks more often than PD data. The main difference noted for PD and ET data is in cases where two auto-spectral peaks are shown. For this case, PD data tended to have a frequency at auto-spectral global maxima that did not coincide with the frequency at the coherence global maxima (as shown in Figure 5.7); whereas, ET data generally depicted that

frequency at auto-spectral global maxima that did coincide with frequency coherence global maxima.

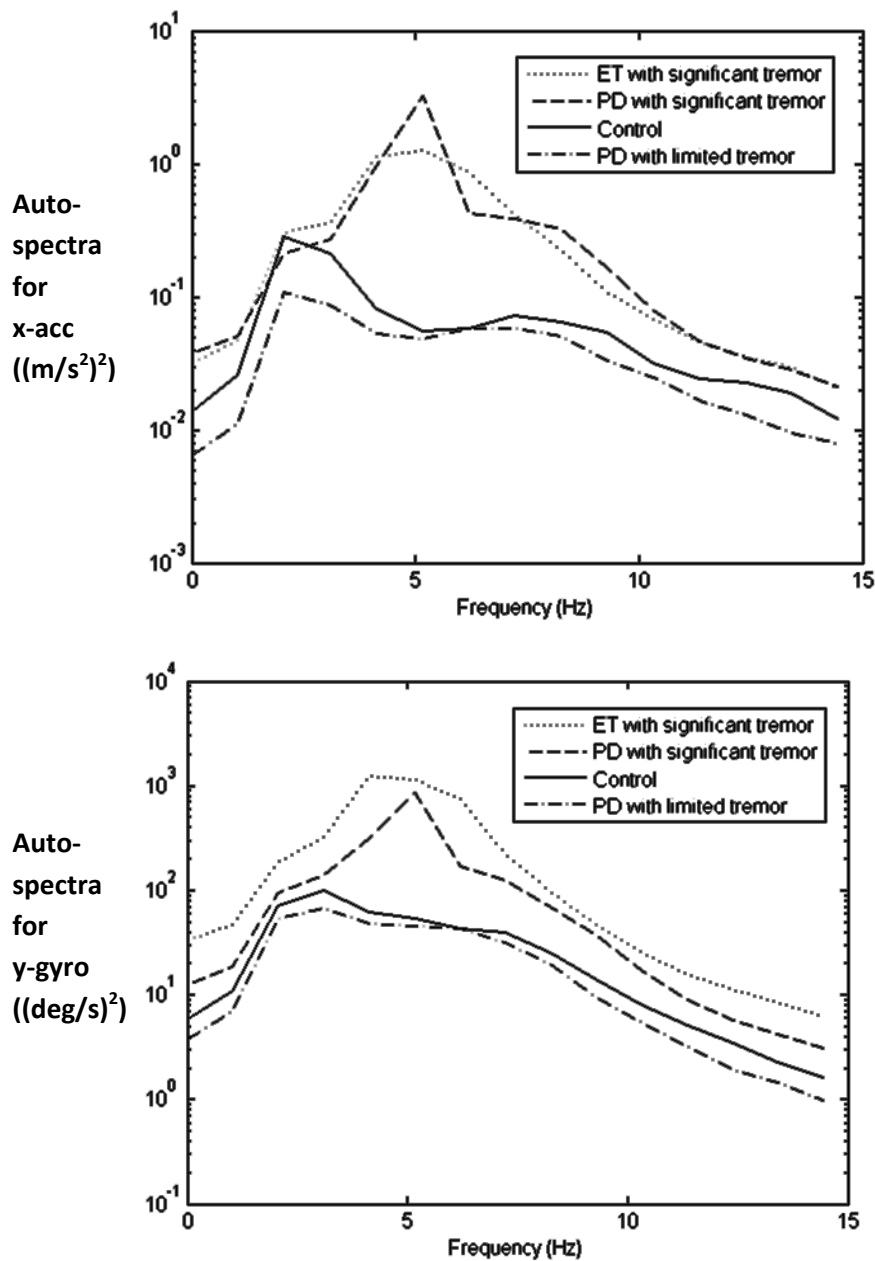


Figure 5.6: Population auto-spectra for x-accelerometer data with gravity removed (top) and y-gyroscope data (bottom) for the laser targeting motion evaluation

Taken from Teskey, Elhabiby and El-Sheimy (2011d)

As well, PD data generally depicted a frequency at auto-spectral local maxima (but not global maxima) that coincided with frequency at coherence local maxima. This highlights a significant difference in the *signature of motion* between ET and PD data that, as far as the author knows, has not been discussed elsewhere in literature.

When other sets of two for the six degrees-of-freedom are analyzed (other than x-translation and y-rotation as depicted in Figure 5.7) very similar patterns emerge, although they tend not to be as pronounced as what is shown in Figure 5.7. This is principally because the two degrees-of-freedom of analysis chosen for Figure 5.7 generally capture more tremor motion for the laser targeting motion evaluation carried out, and thus these two degrees of freedom show a more pronounced *signature of motion*. The fact that the x-translational and y-rotational degrees of freedom captured more tremor is highlighted for the motion observed in the Fourier auto-spectral analysis performed in Section 5.1.

It is difficult to determine why ET data has a consistent frequency at auto-spectral and coherence global peaks while PD data had a frequency at coherence global peaks that coincided only with the frequency of local (but not global) auto-spectral peaks. One important note is that the laser targeting motion evaluation that was utilized for the data analysis had patients undergoing both kinetic and postural motion, these two different motions tended to produce two different sets of tremor. This helps to describe why auto-

spectral plots had two local peaks (representing two different sets of tremor), but still does not fully describe why ET motion has a frequency of maximum coherence at the frequency of largest tremor magnitude. The likely explanation lies in the manner in which ET and PD are generated neurologically and/or as a result of the biomechanics of the human body.

Another important point that can be viewed in Figure 5.7 is that frequency of coherence local peaks almost always coincided with the frequency of local auto-spectral peaks for any tremor motion evaluated. This suggests a very strong relationship for tremor captured among all six degrees-of-freedom; at very least, it highlights that most tremor is of the same frequency when acting along multiple degrees-of-freedom. It also tends to suggest that ET and PD each have a common frequency neurological source and/or that the biomechanical properties of the arm take whatever tremor is produced neurologically and cause the hand motion to display a tremor of consistent frequencies.

A last important note for Figure 5.7 is that the horizontal lines for the plot on the bottom highlight confidence limits for the coherence analysis, as defined in (2.19). These confidence limits imply that any data of greater magnitude coherence (above the confidence limit) is significant in a statistical sense.

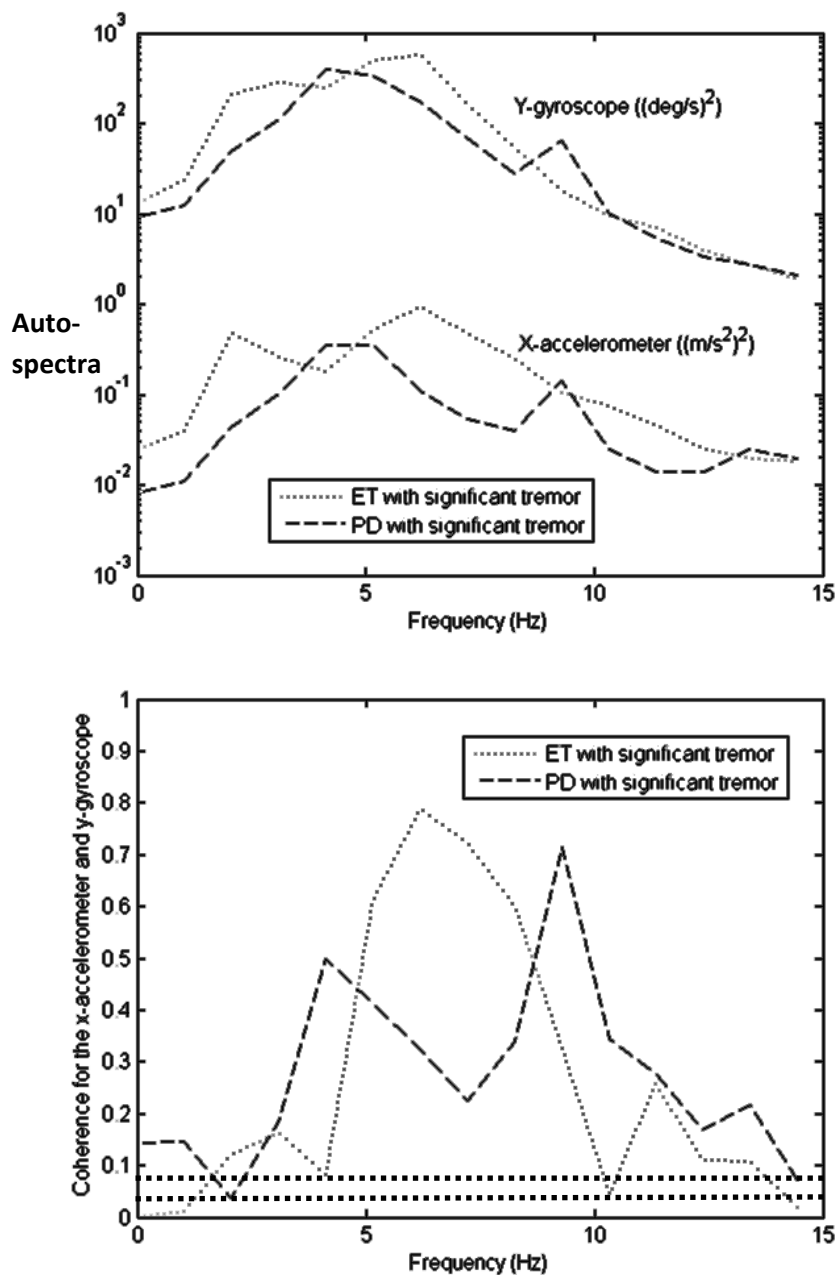


Figure 5.7: Representative individual x-accelerometer data with gravity removed and y-gyroscope data for the laser targeting motion evaluation. Auto-spectra are on top and coherence is on the bottom. Confidence limits (horizontal lines) are shown on the bottom plot, above which coherence is considered significant (ET - upper line and PD - lower line).

Taken from Teskey et al. (2011)

Table 5.3 summarizes population data for the phenomenon discussed and shown in Figure 5.7. The important things to note from the table is the significant difference in ET and PD data, with almost all ET data lying in the rightmost two columns of the table and PD data almost all lying in the remaining column in the table (together with control data). It is important to note that PD has a rate of misdiagnosis of 25% and ET is not precisely defined and has an unknown cause or causes (outlined in Sections 2.2 and 2.3), so the data in Table 5.3 differentiate between ET and PD data as much as is possible given circumstances by which these disorders are diagnosed. In Table 5.3, ET data are generally split in two categories, either having a single frequency of local (and global) maxima for auto-spectral and coherence plots or having one frequency for coinciding global maxima for plots depicting multiple local maxima. PD data generally have non-coinciding frequencies for global maxima in auto-spectral and coherence plots.

Table 5.3: Patterns for auto-spectral and coherence plots given x-accelerometer data with gravity removed and y-gyroscope data for the laser targeting motion evaluation

Subject type	Non-coinciding frequencies for global maxima and two or more local peak frequencies for auto-spectra and coherence	Coinciding frequency for global maxima and two local peak frequencies for auto-spectra and coherence	Coinciding single frequency for local (and global) maxima for auto-spectra and coherence
Control	11	0	0
ET with <i>significant tremor</i>	1	4	3
PD with <i>significant tremor</i>	7	1	1
PD with <i>limited tremor</i>	19	2	0

Taken from Teskey et al. (2011)

An important point to note for the above is that only a few ET patients (2 of 9) were medicated while most PD patients (27 of 30) were medicated. This fact does not significantly skew the analysis presented above. One reason is that PD patients who were medicated often were near the end of active cycle during which medication was affecting their motion significantly. PD patients tend to take medication every few hours, and towards the end of the period of time for which medication was taken, their tremors return. These patients could prevent this by taking medication more often, but they often don't because overuse of medication in the short term tends to lead to its ineffectiveness in the long term. As a result, many of the "medicated" patients were showing tremors as if they were temporarily off their medication, and that is why so many PD patients were showing *significant tremor* (9 of 30 when only 3 of 30 were not on medication at all). This somewhat replicates many studies of PD tremor where patients are asked to go off medication for a period of time.

Another note of significance, as illustrated in Figure 5.8, is that coherence magnitudes for distributions were very similar for all PD patients whether or not they were in the group with *significant tremor* or in the group with *limited tremor*. Figure 5.8 shows coherence population data for the auto-spectra in Figure 5.6. In the latter figure, population auto-spectra for patients with *significant tremor* (ET and PD) are of large magnitude, but population auto-spectra for PD patients with *limited tremor* and controls are of much lower magnitude (the one ET patient with *limited tremor* was omitted from these figures because of a lack of an adequate sample size from which to draw meaningful conclusions). Based on data from Figures 5.6 and 5.8, controls consistently had low

magnitude coherence and auto-spectral distributions, and ET and PD patients with *significant tremor* had large magnitude coherence and auto-spectral distributions.

However, PD patients with *limited tremor* tended to have low magnitude auto-spectral distributions and large magnitude coherence distributions.

In other words, the fact that medication often limited the size of PD tremor did not seem to affect coherence very much. This is a very significant fact that tends to suggest that a lot of the underlying neurological mechanisms causing PD are still present even for medicated patients with mitigated tremor motion. This fact definitely opens up new research avenues in investigating what parts of the *signature of motion* for PD patients are affected by medication and what parts are not. As well, knowledge about how medication affects PD could lead to a better understanding of the neurological mechanism causing PD.

The confidence limit in Figure 5.8, above which coherence is considered significant, is defined mathematically in (2.19). Since each individual data set had its own confidence limit, the worst case scenario was chosen for display in Figure 5.8 (i.e. the individual subject for which the confidence limit is the highest). In this manner, it can be assured that most of the population data shown in Figure 5.8 display significant results.

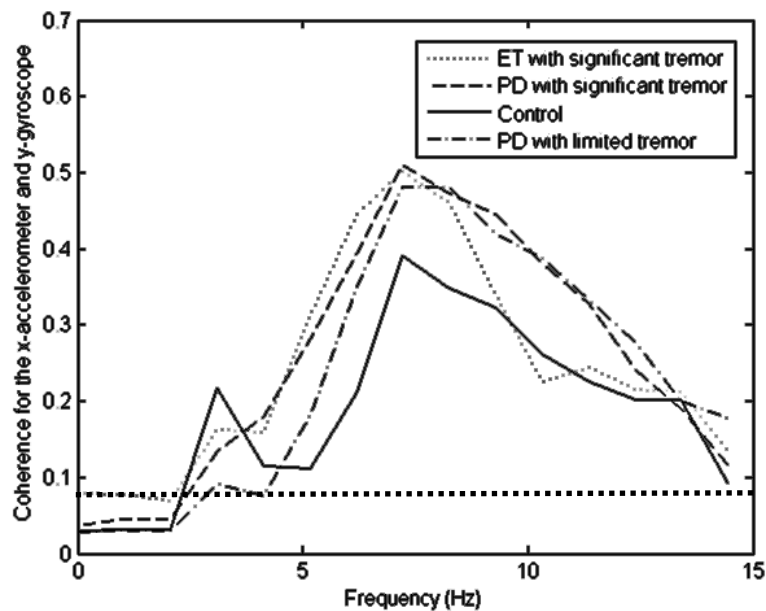


Figure 5.8: Population coherence values for x-accelerometer data with gravity removed and y-gyroscope data for the laser targeting motion evaluation. The horizontal dashed line (confidence limit) indicates the values above which coherence is considered significant for the worst case individual subject (i.e. the subject with the highest value confidence limit).

Taken from Teskey, Elhabiby and El-Sheimy (2011d)

To further validate the results depicted in Figure 5.8, a statistical analysis is performed using the peak coherence values in the 3-12 Hz frequency band for the x-accelerometer and y-gyroscope data. The statistical testing involves the comparison of the control coherence peak values with the peak values of the each of the other three groups examined (ET with significant tremor, PD with significant tremor and PD with limited tremor) using three separate statistical tests. Three Q-Q plots, corresponding to the three

statistical tests, were used to check the data for normality and abnormalities using means and standard deviations provided in Table 5.4 (a similar analysis was performed in Section 5.2). All of the data were found to be suitable for statistical testing.

Statistical testing involved the use of Welch's one tailed t-test; the Student's t-test could not be used because the population variances could not be assumed equal (Walpole et al., 2002; Welch, 1947). The null hypothesis utilized is that data sets of two groups had the same population mean for the individual peak coherence values examined. The statistical testing verified that indeed control data have peak coherence values that are lower than the other three groups examined. The highest p-value from the statistical testing was 0.0854 (for PD subjects with *limited tremor* from Table 5.4). This p-value can be interpreted as meaning that there is only a 8.54% chance of seeing the data observed for controls and PD subjects with *limited tremor* if these two groups examined were not statistically different. The other two statistical tests provide even lower p-values, validating that ET and PD patients with *significant tremor* are indeed statistically different than control patients based on peak coherence values.

An important point to make is that the values for coherence peaks in Table 5.4 are higher than the population averaged data in Figure 5.8 because individual coherence peaks did not all occur at the same frequency and this ensures that the average coherence values over the population are lower than the peak values at any given frequency.

Table 5.4: Population mean, standard deviation and p-values for individual coherence peaks for x-accelerometer and y-gyroscope data occurring within the 3-12 Hz frequency band

Subject type	Mean	Standard deviation	P-value from Welch's one-tailed t-test (null hypothesis is that data sets are statistically the same as control data)
Control	0.480	0.127	-
ET – <i>significant tremor</i>	0.660	0.143	0.0067
PD – <i>significant tremor</i>	0.650	0.136	0.0055
PD – <i>limited tremor</i>	0.548	0.128	0.0854

Taken from Teskey, Elhabiby and El-Sheimy (2011d)

The results in Figure 5.8 and Table 5.4 are significant because they help to partly depict the pathogenesis of PD tremor. Generally, tremor is considered a neurological phenomenon as well as a biomechanical phenomenon. Neurons create the electrical signals that generate tremor and the arm itself also affects tremor because it is a mechanical device with resonant frequencies and mass-spring-damping coefficients. The evidence presented in Figure 5.8 and Table 5.4 tends to suggest a distinct underlying neurological cause for coherence in PD. If coherence was a biomechanical phenomenon only, one would expect that as tremor amplitude decreased, coherence would also decrease. The fact that coherence is still very prevalent at low magnitude tremor suggests that the signature of motion for PD is not completely mitigated with medication, and that a residue of the PD motion still exists for medicated patients.

5.4 Summary

Section 5.1 utilized Fourier based auto-spectra to show that ET generally depicted more tremor data in the 3-12 Hz range than PD. Subsequently, Section 5.2 utilized wavelet analysis to show specific tests that could be used to identify ET tremor from control data. After it was clear from Section 5.2 that ET data and control data were quite different in terms of auto-spectral magnitude, Section 5.3 focused on the use of Fourier auto-spectra and cross-spectra for successful differential diagnosis of ET and PD. As well, a phenomenon whereby medicated PD patients still showed some of the *motion signature* of PD patient with limited tremor mitigation was explored using coherence data.

This chapter largely focused on diagnosis of ET and PD. The next chapter will focus on tremor mitigation and attenuation strategies.

Chapter 6: Attenuation Algorithms

This thesis chapter is divided into two sections. The first section details a methodology regarding how to quantify the main axes of tremor for the six degrees-of-freedom analyzed. This analysis relies heavily on the methodology and data processing outlined in Section 5.3 on cross-spectral Fourier analysis; and as a consequence the analysis in the first section of this chapter uses the same source data as Section 5.3 (from the laser targeting tremor evaluation) and also relies on the results of Section 5.3.

The second section in this chapter outlines how to apply the WFLC analysis for removal of tremor in six degrees-of-freedom. To the knowledge of the author, this is the first time that such an analysis will be carried out in six degrees-of-freedom for movement disorders. This is of particular relevance because the WFLC algorithm is the most popular for tremor removal, as outlined in Sub-Section 2.6.6. The WFLC analysis applied in the second section of this chapter utilizes data for the eating simulation motion evaluation so that tremor removal can be studied for an application in which it could realistically be applied. In the case outlined, removal of tremor from eating using a spoon could be achieved by placing an actuator between the spoon handle and the spoon head such that tremors were not transferred to the food during eating. This could be accomplished using inertial feedback to help generate responses to mitigate tremor.

6.1 Main Axes of Tremor Motion

The tremor investigation carried out here follows from the analysis in Section 5.3, on cross-spectral Fourier analysis of tremor. This previously conducted analysis showed significant coherence between the x-accelerometer (with gravity's impact removed) and y-gyroscope data and noted that x-translational and y-rotational motion had among the greatest coherence for any pair of the six degrees-of-freedom analyzed (for the 3-12 Hz range). As well, it is known from Section 5.1, on auto-spectral Fourier analysis, that x-translational and y-rotational motion had among the most frequency content, particularly in the 3-12 Hz range of interest. Because x-translation and y-rotational motion show such high auto-spectral and cross-spectral values, they are the focus of the analysis performed in this section.

Given that local peaks in both auto-spectral and cross-spectral analyses tended to occur at the same frequency (as outlined in Section 5.3), it is appropriate to speculate that frequencies of tremor were likely identical for the x-translation and y-rotational motion. One of the goals of this analysis is to verify such speculation and to determine the phase lag between the x-translational and y-rotational motion.

In order to achieve the goals of confirming that tremor occurred at the same frequency for the signals analyzed and identifying the phase lag between the signals, (2.18) is applied. This equation gives a phase lag estimate and is used to generate the results in Table 6.1.

Table 6.1: Population phase lag results in radians for the y-gyroscope leading the x-accelerometer at peak coherence for the laser targeting motion evaluation ($\frac{\pi}{2} \cong 1.57$)

Group	Mean for phase lag	Standard deviation for phase lag
Control	1.31	0.30
ET with <i>significant tremor</i>	1.25	0.47
PD with <i>significant tremor</i>	1.55	0.22
PD with <i>limited tremor</i>	1.54	0.17

Taken from Teskey, Elhabiby and El-Sheimy (2011c)

The results shown in Table 6.1 were calculated at peak coherence in order so that the phase lag of the tremor data could be evaluated. The results clearly show that the y-gyroscope leads the x-accelerometer very consistently with a phase shift of $\frac{\pi}{2}$; such consistent results further validate the presence of tremors for different degrees-of-freedom that are at the same frequency. It is important to state that three subjects (one control, one ET patient and one PD patient with *significant tremor*) were not included in the analysis displayed in Table 6.1 because they did not fit the general pattern of motion. Having said this, the consistency of phase lag is quite strong at peak coherence and clearly depicts a commonality in how tremor motion is realized for subjects.

Likely the main factor driving such consistent phase lags for the laser targeting motion evaluation outlined is anatomical in nature. One strong argument supporting this point of view is that control data also depicted a similar phase lag to what pathogenic data displayed. If the phase lag was a factor of neurology, it would be more likely that pathogenic tremor would behave differently (in terms of phase lag) than control tremor. This statement can be validated further by highlighting the fact that all subjects generally

share anatomical features, but not necessarily neurological capabilities. Another strong argument in favor of an anatomical cause of phase lag is the structure of the human body.

The impact of the anatomy of the human body is highlighted by observations made during data collection whereby the subjects all had a much easier time moving their right hand (which was used for data collection) to the left while turning it counter-clockwise, concurrently; and subsequently, subjects tended to move their hand to the right while turning it clockwise concurrently (motion was along the x-axis and about the y-axis). This motion is defined for when looking into the page for Figure 3.1, which outlines data collection (i.e. motion is defined when looking at the subject from behind for the laser targeting motion evaluation). The tremor motion highlighted is common due largely to the structure of the human arm, in that it tends to move more easily in the manner outlined; whereby the subject is moving their hand from side to side at the same time as turning their hand so as to open a door knob. This motion is shown in Figure 6.1.

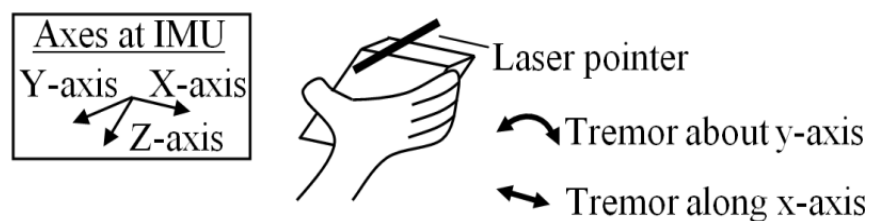


Figure 6.1: The largest two tremors are shown for the laser targeting motion evaluation

Taken from Teskey, Elhabiby and El-Sheimy (2011c)

To verify that the motion shown in Figure 6.1 is consistent with the result in Table 6.1, a mathematical analysis is performed. This analysis verifies that subjects move their hands to the left while turning them counterclockwise and to the right while turning them clockwise during tremor (when looking into the page for Figure 6.1). A sin wave can be used for the mathematical evaluation

$$A_{sin} \sin \omega t \quad (6.1)$$

Where the term A_{sin} is the amplitude of the sin wave in question. This sin wave can be either depicted lateral or rotational tremor; the former will be chosen for analysis first. Lateral tremor was depicted by accelerometer data, as such, any lateral motion much be differentiated twice so that the logged accelerometer data can be appropriately represented. This is given as follows

$$\frac{d^2}{dt^2} (A_{sin,l} \sin \omega t) = -A_{sin,l} \omega^2 \sin \omega t \quad (6.2)$$

Where $A_{sin,l}$ denotes amplitude for a lateral tremor. Note that the signal phase for the lateral tremor is shifted by π after differentiation, representing that lateral tremor and lateral acceleration are out of phase by π radians; lateral acceleration is, of course, what is logged by accelerometers.

Rotation data are initially out of phase with lateral motion data by π radians using a right hand rule sign convention. This can be implied from hand motion to the left while turning counterclockwise and to the right while turning clockwise during tremor (when looking into the page for Figure 6.1). As well, gyroscope data measure rotation rate and thus can

be represented by differentiating rotation motion once (as opposed to twice, which was the case for obtaining acceleration information from lateral motion). When taking the two aforementioned considerations into account, the following can be written

$$\frac{d}{dt}(-A_{sin,r} \sin \omega t) = -A_{sin,r} \omega \cos \omega t \quad (6.3)$$

Where $A_{sin,r}$ denotes amplitude for a rotational tremor. When comparing (6.2) to (6.3), it can be stated that for the motion observed of test subjects, the y-gyroscope signal should lead the x-accelerometer signal by $\frac{\pi}{2}$, and this is indeed the case when examining the results in Table 6.1.

The implications of the fact that it is possible to deduce *closeness* of tremor motion among the six degrees-of-freedom are quite significant. It is very important to know how tremor manifests itself if mitigation is to be carried out. Firstly, knowing the axes along which tremor acts most strongly are important considerations because this is where efforts to reduce tremor should be targeted. Secondly, knowing how different tremors logged relate to one another, specifically in terms of phase, can also add very significant information for anyone designing a tremor mitigation apparatus.

For the case of the motion analyzed here, it was found that hand motion to the left while turning counterclockwise and to the right while turning clockwise was present during tremor (when looking into the page for Figure 6.1). Knowing this, a mitigation strategy

might involve an actuator designed to eliminate both of these tremors concurrently, since they are likely anatomically linked.

Even when designing a passive feedback system, information about the magnitude and phase of tremor for different degrees of freedom would be very useful. This data could be gathered for drinking motion, for example, by having a subject drink water with a cup that had inertial sensors attached. These sensors (capturing all six degrees-of-freedom of motion) would be able to provide data about tremor magnitude along different axes and how these tremors were related to one another in terms of phase and frequency. Once this data were known, it would be possible, using fluid dynamic analysis, to optimize a design of baffles to limit the most significant tremors present for patients drinking.

There were other significant tremors that were correlated for the six degrees-of-freedom examined. In general, tremors tended to share the same frequency for given signal portions, and this was particularly true as the magnitude of tremors increased. For this reason, the most significant phase data available, between different degrees of freedom, stems from data that generally had a large amount of tremor.

One common phase relationship that occurred was for the z-gyroscope leading the x-accelerometer signal by $\frac{\pi}{2}$ radians (in much the same way as how the y-gyroscope signal led the x-accelerometer signal by $\frac{\pi}{2}$ radians). This z-gyroscope relationship with x-

accelerometer data commonly occurred when subjects gripped the IMU from underneath (from its positive z-axis, given axes labels in Figure 6.1). Such a grip was not as common as when subject gripped the IMU from behind (from its positive y-axis, given axes labels in Figure 6.1). Nevertheless, whichever grip was chosen tended to dictate the motion pattern logged. If subjects gripped the IMU from behind, then there was a similar frequency in x-accelerometer and y-gyroscope data (as well as a significant phase shift). If subjects gripped the IMU more from underneath, then there was a similar frequency in x-accelerometer and z-gyroscope data (as well as, again, a significant phase shift). In both cases, the gyroscope data led the accelerometer data by $\frac{\pi}{2}$ radians.

Hand grip also affected the relationship between the x-axis and y-axis lateral tremor. These two tremors were strongly in phase for when subjects wrapped their hand around the left side of the IMU (this is the negative x-axis side of the IMU in Figure 6.1). The reason that this in phase relationship occurred was because when subjects wrapped their hand around the left side of the IMU, the y-axis of the IMU started to capture data that would normally be logged almost completely by the x-axis of the IMU. In other words, the x-axis tremor being logged was quite similar in many cases, but when the IMU positioning shifted, a stronger phase relationship was present between the lateral motion along the x-axis and y-axis. From these results, it is obvious that test subject grip on inertial equipment is very important when logging tremor data and great care should always be taken to obtain consistent results.

All of the tremors detailed thus far have focused on the relationship between the x-lateral tremor and the y-rotational tremor and other data logged from the same relationship due to the test subject grip of the IMU. However, there is a second fundamentally different type of tremor that occurred for the data logged, and this involved a tremor for z-translational and x-rotational motion. These two tremors were out of phase by π radians. This kind of phase relationship implies a downward (positive z-axis) motion occurring concurrently with a negative x-axis rotational motion (using a right hand rule sign convention). The motion captured is thus similar to a cat digging its claw into an object, thrusting downwards and inwards toward an object.

It is interesting to note that there were really only two predominant tremor motion profiles that occurred. One involved a side to side hand motion with a door knob opening motion occurring concurrently and the other involved a clawing motion, as if thrusting downwards and inwards into an object repeatedly. Aside from tremor mitigation, which will be explored further in the next section of this thesis, a lot of useful data for understand both the neurological and anatomical reasons for certain types of tremor motion could be explored based on what was presented here.

6.2 WFLC Based Filtering

The WFLC filtering analysis here was outlined in detail in Sub-Section 2.6.6. It uses iterative steps to solve for frequency, amplitude and phase lock for the signal under evaluation. This analysis method is the most popular for human tremor attenuation, particularly because it can be implemented in real time and because it offers zero phase

lag filtering, both of which are very significant considerations for tremor mitigation. In fact, the WFLC algorithm works well enough that it has been used to successfully remove tremor from a surgeon's hand (Riviere, Radar and Thakor, 1998).

The data collected for WFLC analysis is for the eating simulation motion evaluation, as outlined in Section 3.2. This movement was captured for WFLC analysis because it contained data for which tremor could be realistically mitigated. For example, as mentioned at the beginning of this chapter, it is possible to put an actuator between the head of a spoon and its handle that utilizes real time inertial feedback to help reduce spillage of food.

The data processing utilized first separated lateral tremor from rotational tremor, as outlined in Chapter 4; this required signal analysis so that x-accelerometer data could become representative of lateral tremor. Gyroscope data generally don't need much modification as they mostly represent rotational tremor in their raw form. To achieve the desired signal modification, Kalman filtering and smoothing was employed, as outlined in the top half of Figure 6.2 (which is a summary of the Kalman filtering and smoothing analysis depicted in Figure 4.1).

After Kalman filtering, a critically damped filter was employed to attempt to remove *intended motion* from subjects so that principally tremor motion remained (shown in the

bottom half of Figure 6.2). Once this was carried out, a WFLC filter was used for tremor signal approximation, and then tremor removal was carried out from the lateral and rotational tremor data. At the conclusion of data processing, continuous wavelet spectral analysis was applied to determine how effectively lateral and rotational tremors were removed using the WFLC filter.

Figure 6.3 displays the typical application of a critically damped filter to raw gyroscope data depicting rotational tremor. The application of the critically damped filter to translational tremor data (found from accelerometer data with gravitational impact removed) gives very similar results. The filter produces real time results in a manner somewhat similar to what a low pass filter would provide. The critically damped filter was chosen because it performed best when compared to a number of possible alternatives (Gallego et al., 2009).

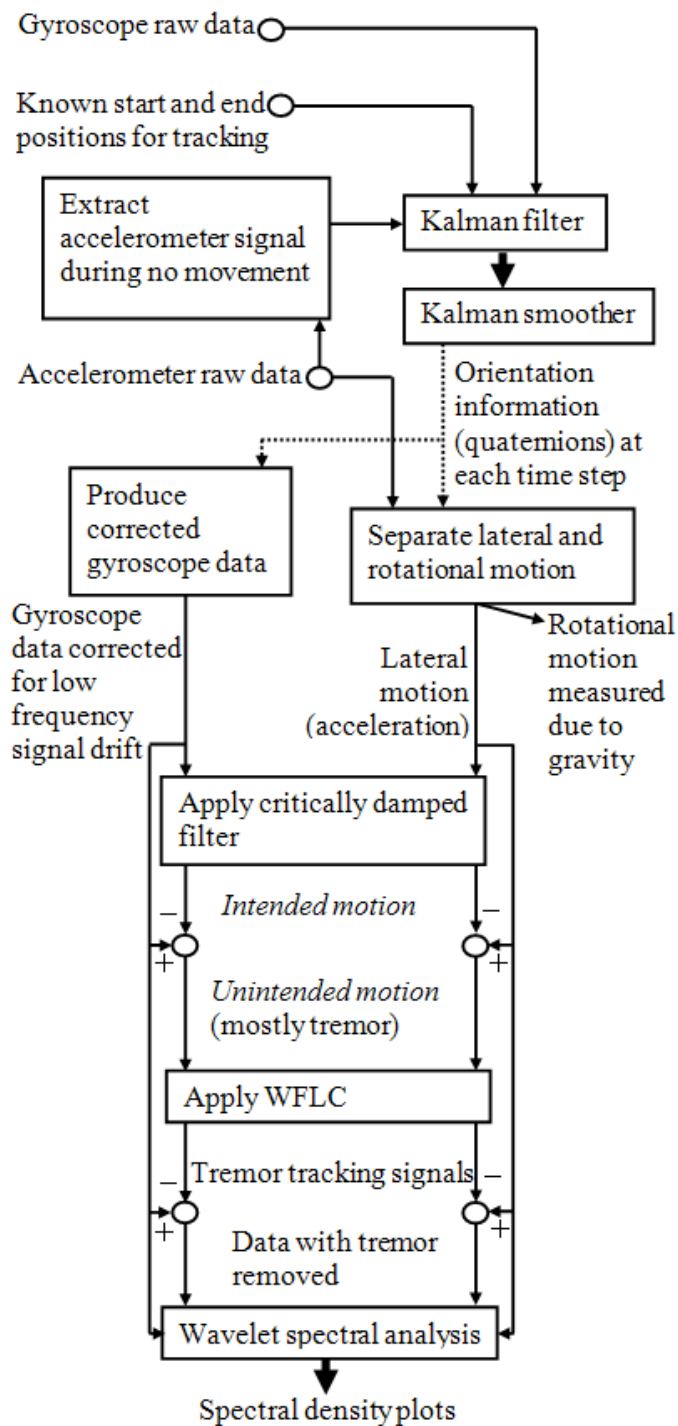


Figure 6.2: Flow chart for WFLC data processing

Taken from Teskey, Elhabiby and El-Sheimy (2011b)

The critically damped filter performs an operation similar to a least squares straight line fit, but with newer data being given a higher weight than older data (i.e. data more recently logged in real time operation has more impact on the fitting parameters than data logged further in the past) (Brookner, 1998). Adjusting the value of the filter parameter that controls how much influence recent data have on filtered results (relative to older data) needs to be done with care. If older data are given too much influence on the filtered results, then quick signal movements are not tracked appropriately. On the other hand, if newer data are given too much influence on the filtered results, then most of the tremor in the filtered signal remains and the filter does not adequately remove unwanted data. A balance needs to be struck so that filtering can be carried out to remove tremor data while still tracking quick signal movements. The data shown in Figure 6.3 depict filtering after adjustments have been made to optimize signal tracking capabilities.

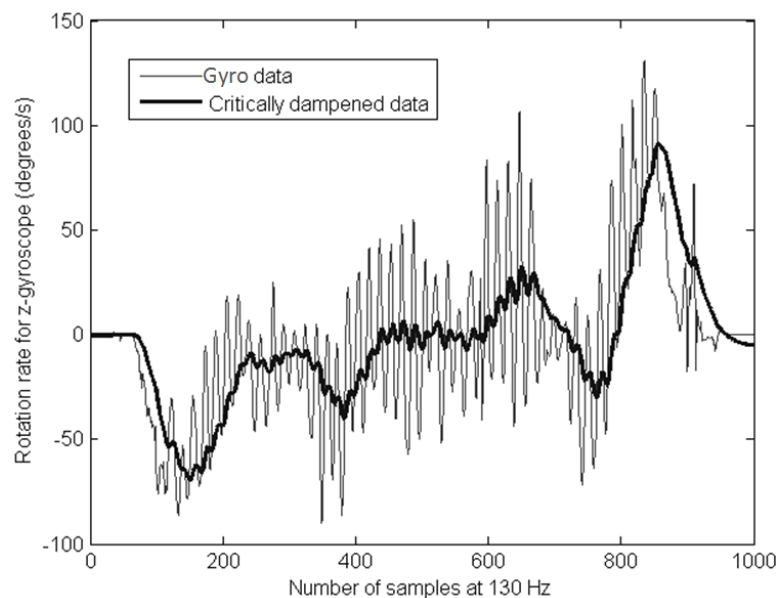


Figure 6.3: Critically damped filtering to remove *intended motion* depicted using representative data from the z-gyroscope

Taken from Teskey, Elhabiby and El-Sheimy (2011b)

After critically damped filtering has been applied, the remaining data can be processed using the WFLC algorithm, which tracks tremor. Adjustments need be made for this algorithm so that tremor tracking does not cause instability during processing. Because the WFLC algorithm is a gradient descent based approach, one of the most significant parameters that can be adjusted controls the speed at which the algorithm converges. If this velocity parameter is set too high, then instability may result from processing. On the other hand, if this parameter is set too low, then the algorithm may not obtain a *lock* on tremor and may not adequately track the signal. As was the case for the critically damped filter, the WFLC algorithm requires a balance to be struck so that the algorithm does not converge on the signal to aggressively or too slowly. Figure 6.4 shows the WFLC typical tracking capability by isolating a signal portion from Figure 6.3; it can usually follow the tremor fairly closely, which helps to achieve the best tremor mitigation results.

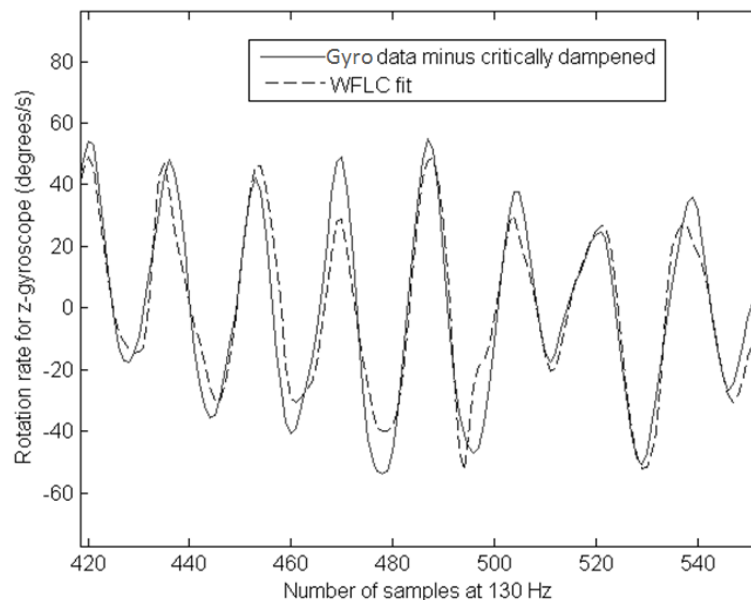


Figure 6.4: WFLC filtering to track tremor, as depicted using representative data from the z-gyroscope

Taken from Teskey, Elhabiby and El-Sheimy (2011b)

The results given in Figures 6.5 and 6.6, for typical accelerometer (without gravity's influence) and gyroscope data respectively, tend to validate the use of the WFLC and critically damped filters as they are presented here. For all three data sets utilized, including controls, as well as ET and PD patients, the results from utilizing the filters outlined tend to suggest that tremor in the 3-12 Hz range was significantly reduced. In fact, all three patient data sets tend to show results whereby data in the 3-12 Hz range have a smaller spectral magnitude after tremor removal than data for controls had before tremor removal. This highlights the fact that tremor was largely removed from the data.

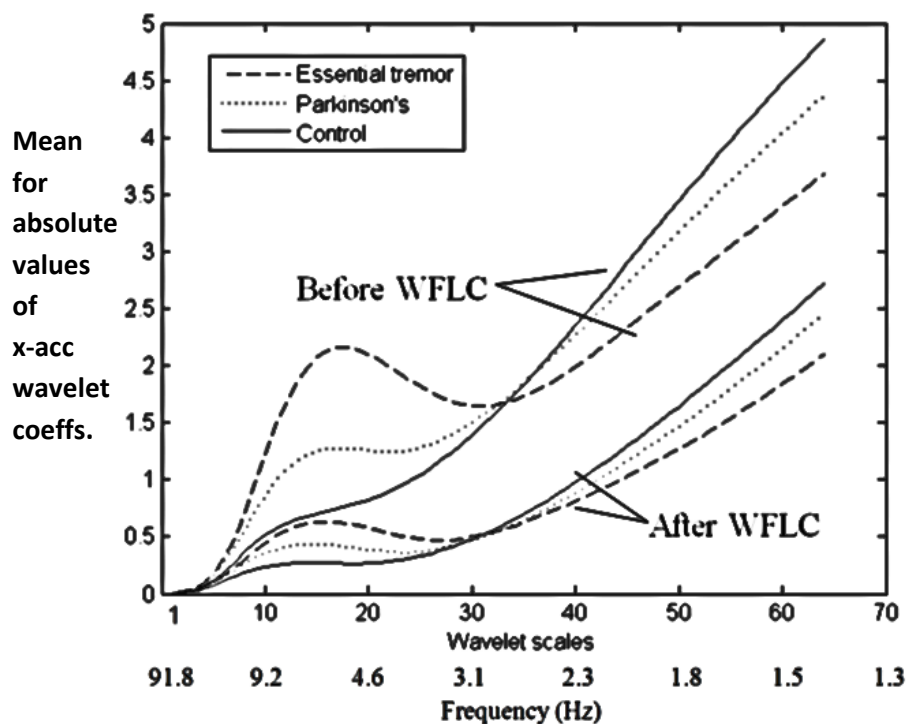


Figure 6.5: Coiflets 3 continuous wavelet analysis to analyze filtering capabilities using representative data from the x-accelerometer (with gravity's impact on the signals removed)

Taken from Teskey, Elhabiby and El-Sheimy (2011b)

It should be noted that only ET and PD patients with *significant tremor* have had their data plotted. The patient data that showed *limited tremor* did not deviate from the data of controls very much when the spectra were plotted as given in Figures 6.5 and 6.6. The terms *significant tremor* is used here as it was defined in Section 4.4, when data from the laser targeting motion evaluation were examined before and after Kalman filtering (this same definition has been used throughout this thesis). Even though the analysis here is based on a different data set than the laser targeting motion evaluation, the patients who exhibited the most tremor did not change substantially when comparing across datasets. For this reason, the same definition of *significant tremor* is used here to make comparison among different thesis sections more straightforward.

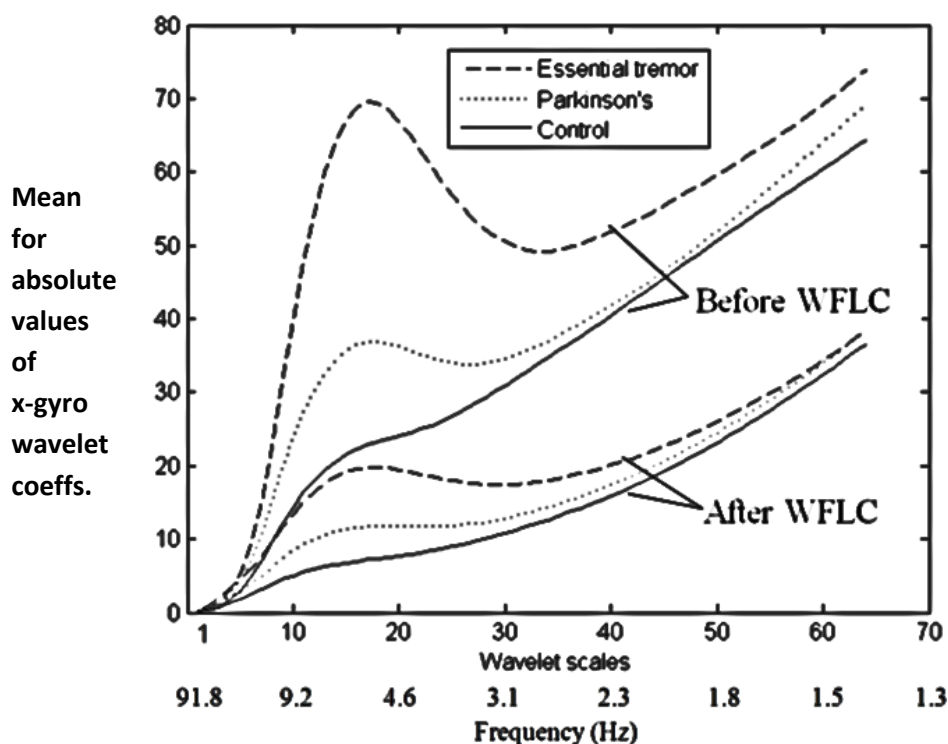


Figure 6.6: Coiflets 3 continuous wavelet analysis to analyze filtering capabilities using representative data from the x-gyroscope

Taken from Teskey, Elhabiby and El-Sheimy (2011b)

The filtering algorithms performed very similarly for all translational and rotational tremor depicted. This was not surprising given that in Chapter 5 it was shown that data collected for motion along the six degrees-of-freedom showed similar spectral properties. As such, it would follow that one should expect tremor removal to operate in a similar manner for all six degrees-of-freedom analyzed.

One of the unfortunate drawbacks of the filtering utilized is that it did not allow data above 12 Hz to go through processing unaltered, which would be ideal since it is the 3-12 Hz range which was targeted for tremor removal. The reason that some of this higher frequency data were removed was due to the WLFC filtering responding to this data. Although removal of this higher frequency data was not ideal, it does not pose a risk to the overall performance of the filtering outlined because limits of the capabilities of mechanical equipment would likely result in data above 12 Hz largely going unfiltered for any real world application. In fact, often some kind of thresholding is utilized in real world applications to limit the types of movements that software can request from mechanical equipment so as to stay within the equipment's operational range.

A much more significant concern for the processing outlined is the inability to leave low frequency data, below 3 Hz, unaltered. This is largely the result of the critically damped filter not adequately tracking *intended motion* of subjects. It is unlikely that for real time applications the problem of tracking this *intended motion* will be solved any time soon. It

has been a topic of significant research for many years and it is difficult to find adequate replacements to the filtering algorithms given here (Rocon et al., 2004).

6.3 Summary

The analysis presented in this thesis chapter highlighted the attenuation (mitigation) methodologies for tremor removal. In the first section of the chapter, the analysis carried out detailed the tremor phase shift between the motion axes (for all six degrees-of-freedom) along which tremor was acting. Not only did this highlight that tremor was largely acting with a given phase shift between pairs of the six degrees-of-freedom of motion, but is also further verified that tremor motion occurs at similar frequencies for the different degrees-of-freedom under examination. This information could assist with designing tremor mitigation equipment by, for example, suggesting a design of actuator that can cancel out all tremor acting along multiple axes.

The second section of this chapter focused on removal of tremor utilizing the critically damped and WFLC algorithms (no actuator was used for this; tremor removal was undertaken on tremor signals logged from subjects instead). These algorithms were generally quite capable of removing tremor for all six degrees-of-freedom analyzed. The biggest difficulty for data processing was the unwanted removal of data outside of the 3-12 Hz range targeted, particularly low frequency data. Given that preserving patient *intended motion* (generally below 3 Hz) has been a significant research topic for many years without complete resolution, it stands to reason that the algorithm presented here

for tremor removal is among the most capable. This algorithm was presented here for the first time given data in six degrees-of-freedom.

Chapter 7: Conclusions and Recommendations

This thesis began with a literature review (Chapter 2) of movement disorders, including different aspects the diseases under consideration (ET and PD), various motion capture technologies that could be used to track the motions and computational methods for evaluating the data captured using inertial sensors. The next chapter (Chapter 3) focused on the inertial data capture techniques from volunteer subjects (ET, PD and controls) and this was followed in Chapter 4 with methods outlining Kalman filtering and smoothing used the help remove the gravitational impact from accelerometer data (i.e. to obtain filtered accelerometer data in which most information remaining is representative of lateral tremor). Characterization and diagnostic algorithms where then highlighted in Chapter 5, and the main finding displayed that ET and PD data have unique *signatures of motion* that can be used to potentially diagnose ET and PD cases. Chapter 6 focused on attenuation algorithms and displayed that not only is attenuation possible, but finding out what motion characteristics to design for in six degrees-of-freedom is also possible.

In conclusion, the main overarching goals of the thesis were achieved. It was shown that inertial sensors can be used for assessment (assistance with diagnosis) and attenuation (active mitigation) of movement disorder motion. The specific objectives realized allow for such a conclusion to be drawn, and these are outlined in the next section of this thesis on the following page.

7.1 Objectives Realized

From all of the analysis highlighted, there were a number of unique objectives that were realized for the research undertaken. These objectives were first outlined in Section 1.1.

One of the key objectives outlined was to *create diagnostic methodologies for assessment of movement disorder motion*; specifically to provide differential diagnosis techniques for when comparing ET and PD data. This task was accomplished within the error rate possible given imperfect capabilities of medical professionals to objectively classify the differences between ET and PD motion. Diagnostic methodologies are given in Chapter 5, and are based on auto-spectral and cross-spectral plots of test subjects when comparing data for the six degrees-of-freedom analyzed.

Another realized objective was to *process and comprehensively analyze tremor data for six degrees-of-freedom of motion*. This goal was realized in that accelerometer data were processed in a manner such that data remaining in the 3-12 Hz frequency band after filtering represented largely lateral tremor motion. Gyroscope data generally did not require extensive processing because in the 3-12 Hz band of interest they mostly captured rotational tremor motion. The processing of accelerometer data to obtain lateral tremor information is highlighted in Chapter 4.

Six degree-of-freedom analysis provided a lot of benefits when analyzing processed data. For one thing, it allowed for the development of a simple technique for differential diagnosis of ET and PD (as outlined in Chapter 5). Another important fact is that in order to mitigate movement disorder motion, its characteristics need to be known and this generally requires six degree-of-freedom analysis (unless an orthosis is used, such that patient motion is significantly restrained). The WFLC analysis carried out in Chapter 6 has an added significance in that the six degree-of-freedom application of this analysis means that it could be readily applied in a real world scenario.

The third and final major objective realized in this thesis was ***algorithm validation for attenuation (removal) of tremor***. The validation was carried out in Chapter 6 which applied critically damped filtering and the WFLC algorithm to track *tremor motion* and remove it so that only *intended motion* of the subject under examination remained. This technique has been used before for tremor removal, but this is the first time it has been applied for all six degrees-of-freedom of motion for pathogenic tremor. The main difficulty encountered with using the processing outlined is that *intended motion* is difficult to judge and therefore it is difficult to tell what part of a patient motion is *tremor motion* and which part is *intended motion*. Differentiating between these two motion types has been an area of significant research for many years and will likely continue to need further study well into the future. Overall, the algorithms used for tremor removal accomplished the stated task quite well and produced results that would yield significant benefits if these algorithms were to ever be applied in a real world scenario; an example of such a real world scenario is the use of an actuator between a spoon head and handle

using inertial feedback to cancel out movement disorders tremors so that a subject could eat more easily.

7.2 Strengths and Weaknesses of the Approach Presented

The approach for data collection and processing utilized MEMS inertial sensors and custom designed processing software. Here, the strengths and weaknesses of using such an approach are highlighted.

A major strength of the data acquisition and processing techniques outlined is that they provide full six degrees-of-freedom motion rendering. This is discussed at length in the previous section (Section 7.1).

Another one of the most significant strengths of the approach presented is the low cost nature of the technology and analysis utilized and its easy accessibility. MEMS inertial sensors capable of performing that analysis can be purchased for as little as a few dollars each and in recent years the technologies to build a platform for data acquisition have become more plentiful. In fact, in many cases a smart phone (worth a few hundred dollars) could be used for both data acquisition and processing (such phones commonly have MEMS inertial sensors built in). This greatly increases the accessibility for an individual wanting to access the algorithms for data processing and also makes distributing these algorithms widely much more realistic. For diagnostic algorithms in particular, all aspects of the data acquisition and analysis could be contained within a

smart phone such that the phone could give a diagnostic result without the need for any supplementary technology or algorithms.

Another similar application stemming from the benefits of low cost and easy accessibility of MEMS inertial sensors involves monitoring patients for tremor motion. This could involve a software application whereby a patient performed a standardized task (such as touching their finger to their nose three times while holding a smart phone). In this manner, tremor could be tracked so that the impact of things such as physical activity and time of day could be analyzed. Even more useful would be analysis of medication to determine the ability of different medications to mitigate tremor for different patients.

Another major strength of the approach presented involves the small size and light weight of MEMS inertial sensors; as previously stated the particular sensors used in this thesis were not larger than 5 mm along their largest dimension and the accelerometer sensor set had a mass of 0.08 grams based on what is given in ST Microelectronics (2006) and Epson Toyocom (2010) (this data is also presented in Table 3.1 of this thesis). The small size and light weight of inertial sensors is, of course, related to the accessibility of MEMS inertial sensors previously outlined in this thesis section (indeed, smart phone manufacturers would not include MEMS inertial sensors in their phones if the sensors were heavy and large). The small size and light weight of sensors allows them to easily track motion without significantly affecting the motion under examination in most cases. Generally, a sensor and data acquisition system can be built to weigh a small fraction of

the limb (or body segment) upon which they are mounted, thereby ensuring that weight of a MEMS inertial sensor does not overburden test subjects. As well, MEMS inertial sensors are often the size of a coin (or sometimes much smaller). This means that they can be mounted without much concern about interfering physically with a subject's *intended motion*.

Another further advantage of the analysis carried out stems from the non-invasiveness of inertial data acquisition; specifically, inertial sensor data can be captured on a data card that is smaller than a coin and weighs less than a coin. Such data cards can often store many hours of data captured at high frequency. This allows for long term data acquisition without the need for cables which can restrict motion.

Inertial sensors are also beneficial for monitoring and attenuation because of their ease of use. Someone can just pick up an IMU or attach it to their body and continue moving. This is in stark contrast to other motion monitoring techniques which can involve time consuming set-ups (such as attaching EMG electrodes to a patient's arm which can take many minutes).

One of the major strengths of the methodology outlined for assessment and attenuation of movement disorders is that it is software based. As a result of this, algorithms can be transferred to various devices utilizing inertial sensors with relative ease and even re-

programming algorithms for different programming languages is relatively straight forward. Such ease of algorithm transfer is a significant consideration given that it allows researchers to network and work in teams more readily when dealing with movement disorder based processing.

Another benefit of using a software based methodology for movement disorders assessment and attenuation is that algorithms can often be defined mathematically and therefore can more easily be communicated to a broad audience. This is a significant factor because it means that researchers (and entrepreneurs) can more readily exchange ideas about algorithm development which tends to accelerate the pace for development of new algorithms.

One of the most significant disadvantage of using inertial sensors for movement disorder motion evaluation is the lack of capacity to obtain long term motion tracking position information (as opposed to tremor motion tracking data and short term motion tracking data, which inertial sensors are well suited to). Inertial sensors generally require supplementary data to provide long term position measurements (such as imaging data or known start and end points for IMUs); the reason for the need for supplementary data is that inertial motion tracking results have errors that grow in a generally exponential nature in time. MEMS inertial sensors are particularly bad at giving long term position measurements because the quality of data that can be obtained from these

sensors is often not sufficient for many applications needing long term position measurements.

Despite the difficulties that inertial sensors (and particularly MEMS inertial sensors) pose in terms of obtaining long term position measurements, this challenge is largely not relevant for tremor related disorders. Only oscillatory signal segments (and not fully processed inertial data to obtain positions) are needed to study most of the aspects of tremor behavior. It will, however, be significant to determine long term positions for subject motion in some cases if non-tremor movement disorders are examined more thoroughly.

Another major disadvantage of using inertial sensors is that the data they provide is difficult to visualize directly. This can pose a significant problem, particularly if one is trying to communicate to patients and medical professionals the differences for movement disorder motion types. This problem is solvable by creating a three dimensional visualization of motion using computer graphics; however, this can be time consuming.

As a further disadvantage of using techniques presented in this thesis, the algorithm based approach for assessment and attenuation of movement disorders has some significant drawbacks. Such an approach is not highly affective for tremor mitigation

and attenuation because it needs to be used indirectly or with the aid of expensive mechanical hardware. An indirect method of using algorithm based data processing for tremor mitigation is to design baffles for a cup taking into account tremor motion data logged. The indirect nature of this technique means that a lot of other analysis needs to be done to make sure baffles work as expected when trying to reduce spillage of a fluidic beverage. For example, to ensure baffles work as expected, a designer may need to use fluid dynamic models to simulate fluid motion.

Using actuators for tremor mitigation and attenuation can be accomplished (this has been carried out for the motion of the hand of a surgeon as mention in the literature review in Chapter 2). However, this requires a lot of extra work so that actuators can be tuned appropriately and so that feedback response times are adequate. As well, actuators needed for tremor removal in real time need to have a very fast response time and therefore are quite expensive (on the order of at least hundreds of dollars).

Despite the drawbacks outlined, the algorithm based approach for assessment and attenuation of movement disorders does generally tend to work well in certain circumstances, such as when evaluating the effectiveness of medication on a patient's motion or when using inertial sensors for diagnostic applications.

7.3 Recommendations

One of the main recommendations for future work is to gather more inertial data from a larger number of patients performing a larger number of tasks; such tasks could

include walking, running, tracing shapes etc. By accomplishing this, more analysis could be applied to the data and methodologies for diagnosing movement disorders could be further extended. Such a large scale accumulation of data should most likely be carried out at a medical research center where there are a large number of patients available daily for examination (this is the easiest way to gather data for hundreds of patients which would not likely be feasible otherwise). As well, such a medical research center would likely have extensive patient records (about the progression of the disease and medications that have been taken). With the use of extensive patient records, analysis of data could provide insight into differences in the motion patterns for different subjects (i.e. there might be, for example, a difference in the motion patterns of patients who had different disease progressions). Other tasks that could be asked of patients (in addition to the clicking on targets on a computer screen and simulating eating as outlined in this thesis) might include touching ones finger to one's nose repeatedly and drawing an Archimedes spiral.

Another recommendation which could prove quite fruitful would involve *tracking tremor motion for patients before and after they are prescribed medication*. This is likely one of the largest areas of commercial application from what is given in this thesis because it would help doctors to objectively monitor patient tremor when patients are on different medications. This would help doctors to not prescribe medications that were ineffective. Furthermore, combined with a database about other patient information (such as age, sex, weight etc.), information about how patients respond to medication can also help researchers to determine aspects about movement disorders that had previously not been

uncovered. For example, a medication affecting production of a certain chemicals in the brain might work better for men than for women, and this would help one to understand more about the disorder under examination.

Another important area of focus for future work is to gather motion (IMU) data concurrently with EMG and, if possible, EEG (Electroencephalography) data. Both of these techniques record electrical impulses (the former records them for muscles while the later records them for electrical activity in the scalp region of the body). It may be very difficult to collect large amounts of data with EMG and EEG because of the large time it takes to properly mount such systems on patients. Also, there are significant challenges when logging IMU, EMG and EEG data concurrently. The largest challenge is to time sequence data streams with one another so that they can be directly compared. Another challenge is having a patient move in a realistic manner when wearing so much monitoring equipment. Despite these challenges, it is worthwhile to try to gather data from an IMU, EMG and EEG concurrently because the data would provide significant information about the relationship between motion and neurological activity.

Another avenue that could be pursued is capturing FMRI (Functional Magnetic Resonance Imaging) data concurrently with IMU data, but this may be less usable in many cases than EMG and EEG data. FMRI data do not provide near real time information about neurological activity (like EMG and EEG), but rather information about the location of blood cells whose resources have been utilized by brain activity

many seconds prior. This means that not only does FMRI introduce a time lag when monitoring brain activity, but it also can be difficult to isolate the area of the brain that has been activated because tracking blood flows through the brain can be difficult. For the purposes of investigating movement disorders, EMG and EEG are likely to yield significant findings more quickly. This is not to say the FMRI data are not useful; indeed, they could provide a breakthrough in movement disorders research. Unfortunately, given some of the drawbacks sighted above and also including the extremely high cost of FMRI (in the hundreds of thousands of dollars or even millions of dollars for a machine), it is clear that gathering FMRI data may be difficult. A further complication also arises if one wants to gather FMRI data concurrently with IMU, EMG and EEG data because it is difficult to take other electrical equipment into an FMRI machine due to the magnetic field used by an FMRI device.

An important area of focus over the long term is monitoring patients over a twenty four hour per day basis. Currently existing inertial technology could certainly accomplish this task, but specific hardware would likely need to be designed. Data capture would likely only take place during a tremor event as defined by the short term standard deviation of an inertial signal above a certain threshold (or using a similar definition for a tremor event). Long term studies of motion are common, but not in six degrees-of-freedom, and gathering such data would be significant.

More processing algorithms for diagnosis and attenuation of movement disorder motion would also be very helpful. There are many possible candidates for other algorithms that would be effective and one very good area to begin with is wavelet analysis. It is quite possible that a wavelet filter would be able to provide real time tremor attenuation (to the knowledge of the author, such filtering has never before been carried out for movement disorder tremor). Another wavelet application is wavelet based coherence analysis (similar to the Fourier based coherence analysis presented in Chapter 5). The wavelet based coherence analysis would be very good at providing time resolution capabilities that Fourier analysis tends to lack.

As a last recommendation, ***providing some sort of physical hardware for tremor mitigation would be helpful.*** Likely drinking and eating are the most suitable tasks for which to provide attenuation because they are common in daily life and a very large number of test subjects complained that their tremors caused problems when drinking and eating. Any device with an active tremor feedback system would likely not be a good place to start for tremor attenuation because actuators that can provide quick instant motion based on inertial feedback are very expensive (often hundreds of dollars). Instead, it would likely be a better idea to design baffles for a drinking cup by logging tremor motion for patients drinking and then simulating the tremor so that different baffles could be tested for tremor mitigation effectiveness. Simulations used to test baffle design could either be computational (i.e. a numerical simulation) or they could use a mechanical actuator and a baffle prototype.

References

- Abeel, P., Coates, A., Montemerlo, M., Ng, A.Y., and Thrun, S. (2005), *Discriminative Training of Kalman Filters*, Robotics; Science and Systems 2005 Proceedings.
- Ai, L., Wang, J., and Wang, X. (2008), Multi-Features Fusion Diagnosis of Tremor Based on Artificial Neural Network and D-S Evidence Theory, *Signal Processing*, Vol. 88, pp. 2927-2935.
- Altmann, S.L. (1986) *Rotations, Quaternions, and Double Groups*, Dover Publications.
- Bain, P.G., Findley, L.J., Thompson, P.D., et al. (1994), A study of heredity of essential tremor. *Brain*; 117: 805–24.
- Begg, R. and Palaniswami, M. (2006), *Computational Intelligence for Movement Science*. Idea Group Publishing: Hershey-London-Melbourne-Singapore.
- Berardelli, A., Rothwell, J.C., Thompson P.D., and Hallet, M. (2001), Pathophysiology of bradykinesia in Parkinson's disease, *Brain*, 124, 2131-2146.
- Bergman, H., and Deuschl, G. (2002), Pathophysiology of Parkinson's Disease: From Clinical Neurology to Basic Neuroscience and Back, *Movement Disorders*, Vol. 17, Suppl. 3, pp. S28–S40
- Bernheimer, H., Birkmayer, W., Hornykiewicz, O., Jellinger, K., and Seitelberger, F. (1973) Brain dopamine and the syndromes of Parkinson and Huntington. Clinical, morphological and neurochemical correlations. *J Neurol Sci* ;20:415–455.
- Bhidayasiri, R. (2005), Differential diagnosis of common tremor syndromes, *Postgrad Med J*;81:756–762
- Bhidayasiri, R., Waters, M.F., and Giza, C.C. (2005), *Neurological differential diagnosis: a prioritized approach*. Oxford: Blackwell.
- Bontranger, E. (1998), Instrumented gait analysis (review of instrumented gait analysis and systems). In J.A. De Lisa (Ed.), *Gait analysis in the science of rehabilitation*, Retrieved January 9, 2005, from <http://www.vard.org/mono/gait/contents.pdf>
- Brennan, K.C., Jurewicz, E., Ford, B., Pullman, S.L., and Louis, E.D. (2002), Is essential tremor predominantly a kinetic or a postural tremor? A clinical and electrophysiological study. *Mov Disord*; 17: 313–16.
- Brookner, E. (1998), *Tracking and Kalman filtering made easy*. John Wiley & Sons, Ltd.

- Brown, R.G., and Hwang, P.Y.C. (1997), *Introduction to Random Signals and Applied Kalman Filtering*, John Wiley & Sons, Inc., third edition.
- Burne, J.A. (1987) Reflex origin of parkinsonian tremor. *Exp Neurol*;97:327–339.
- Cappozzo, A., Cappello, A., Della Croce, U. and Pensalfini, F. (1997), Surface-marker cluster design criteria for 3-D bone movement reconstruction. *IEEE Transactions on Biomedical Engineering*, 44, 1165-1174.
- Cappozzo, A., Catani, F., Leardini, A., Benedetti, M.G. and Della Croce, U. (1996), Position and orientation in space of bones during movement: Experimental artifact. *Clinical Biomechanics*, 11(2), 90-100.
- Chan, Y.T., (1995), *Wavelet basics*. Kluwer Academic, Dordrecht.
- Chang, W.L., Su, F.C., Wu, H.W. and Wong C.Y. (1998), Motion analysis of scapula with combined skeleton and skin-based marker system. *3rd World Congress of Biomechanics*, Sapporo, Japan (pp. 2-8).
- Cohen, L. (1989), Time-frequency distributions – a review, *Proc. IEEE* 77: 941-981.
- Critchley, M. (1949) Observations on essential tremor (heredofamilial tremor). *Brain*; 72: 113–39.
- Critchley, E. (1972) Clinical manifestations of essential tremor. *J Neurol Neurosurg Psychiatry*; 35: 365-72.
- Davis, C.H., and Kunkle, E.C. (1951) Benign essential (heredofamilial) tremor. *Arch Int Med*; 87: 808-16.
- Deuschl, G., Bain, P., and Brin, M. (1998) Consensus statement of the Movement Disorder Society on tremor. Ad Hoc Scientific Committee. *Mov Disord*; 13 (suppl): 2–23.
- Deuschl, G., Krack, P., Lauk, M., and Timmer, J. (1996), Clinical neurophysiology of tremor. *J Clin Neurophysiol*;13:110–121.
- Elble, R.J. (2000), Essential tremor frequency decreases with time. *Neurology*; 55: 1547–51.
- Elble, R.J., Higgins, C., and Hughes, L. (1992), Phase resetting and frequency entrainment of essential tremor. *Exp Neurol*;116:355–361.
- Elble, R.J., and Koller, W.C. (1990), *Tremor*. Baltimore: The John Hopkins University Press.

- El-Sheimy, N., Hou, H., and Niu, X. (2008), Analysis and Modeling of Inertial Sensors Using Allan Variance, *IEEE Transactions on Instrumentation and Measurement*, Vol 57, No 1, 140-149.
- Engin, M., Demirag, S., Engin, E.Z., Celebi, G., Ersan, F., Asena, E., and Colakoglu, Z. (2007), The Classification of Human Tremor Signals Using an Artificial Neural Network, *Expert Systems With Applications*, Vol. 33, pp. 754-761.
- Epson Toyocom, XV-8100CB ultra miniature size gyro sensor data sheet, pp. 1-2, [Online]. Available: http://www.frank-schulte.com/media/Pdf/XV-8100CB_E06X.pdf [Accessed July, 2010].
- Farell, J.L. (2007), *Inertial Instrument Error Characterization*, *Navigation Journal of the Institute of Navigation*, Volume 54, Number 3, pp. 169-176.
- Findley, L.J., and Koller, W.C. (1987), Essential tremor: a review. *Neurology*; 37: 1194–97.
- Frost and Sullivan (2006), *World MEMS Sensors Markets: FA0A-32*, Palo Alto, CA, United States.
- Gallego, J.A., Rocon, E., Roa, J.O., Moreno, J.C., Koutsou, A.D., and Pons, J.L. (2009), On the use of inertial measurement units for real-time quantification of pathological tremor amplitude and frequency. In *Proceedings of the Eurosensors XXIII conference*. *Procedia Chemistry* 1, pp. 1219–1222.
- Gelb, A. (1974), *Applied Optimal Estimation*, MIT Press, Fifth Edition.
- Gelb, D.J., Oliver, E., and Gilman, S. (1999), Diagnostic criteria for Parkinson disease. *Arch Neurol*. Jan;56(1):33-9.
- Gibbs, J.W., and Wilson, E.B. (1960), *Vector Analysis: A Text-Book for the Use of Students of Mathematics and Physics, Founded upon the Lectures of J. Willard Gibbs*, Dover.
- Goldstein, H. (1980), *Classical Mechanics, 2nd ed.*, Addison-Wesley.
- Gonzalez, J.G., Heredia, E.A., Rahman, T. et al. (1995), “A new approach to suppressing abnormal tremor through signal equalization,” in *Proc. RESNA Annu. Conf.*, Vancouver, BC, pp. 707–709.
- Goodall, C. (2009), Improving Usability of Low-Cost INS/GPS Navigation Systems using Intelligent Techniques, PhD Thesis, Department of Geomatics Engineering at the University of Calgary.

- Goswami, J.C., and Chan, A.K. (1999), *Fundamentals of wavelets: Theory, algorithms, and applications*. Wiley series in microwave and optical engineering, Wiley-Interscience, New York, USA.
- Gresty, M. and Buckwell, D. (1990), Spectral analysis of tremor understanding the results. *Electroencephalog. Clin. Neurophysiol.* 53:976-981.
- Griffiths, D., Higham, D., and Watson, A., (1997), The search for a good basis. Proceedings of the 17th Dundee Biennial Conference, June 24-27, Addison Wesley Longman.
- Groves, P.D. (2008), *Principles of GNSS, Inertial and Multisensor Navigation Systems*, Artech House.
- Grubin, C. (1970), Derivation of the Quaternion Scheme via the Euler Axis and Angle, *J. Spacecraft*, Vol. 7, pp. 1251-1263.
- Gnanadesikan, R., and Wilk, M.B. (1968), "Probability plotting methods for the analysis of data". *Biometrika* 55 (1): 1-17. Available at: <http://www.jstor.org/stable/2334448>.
- Gulcher, J.R., Jonsson, P., Kong, A., et al. (1997), Mapping of a familial essential tremor gene, FET1, to chromosome 3q13. *Nat Genet*; 17: 84–87.
- Halliday, D.M., Rosenberg, J.R., and Amjad, A.M. (1995), A framework for the analysis of mixed time series/point process data – theory and application to the study of physiological tremor, single motor unit discharges and electromyograms. *Pro biophys. Melec. Biol.* Vol 64, No 2/3 pp. 237-278.
- Hausdorff, J.M., Peng, C.K., Goldberger, A.L., and Stoll, A.L. (2004), Gait unsteadiness and fall risk in two affective disorders: a preliminary study. *BMC Psychiatry* 4(1) 39.
- Heil, C.E., and Walnut, D.F., (1989), Continuous and discrete wavelet transforms. *Society for Industrial and Applied Mathematics (SIAM) Review*, 31(4), pp. 628-666.
- Herman, T., Giladi, N., Gurevich, T., and Hausdorff, J.M., (2005), Gait instability and fractal dynamics of older adults with a cautious gait: why do certain older adults walk fearfully? *Gait and Posture* 21(2), 178-385.
- Higgins, J.J., Loveless, J.M., Jankovic, J., and Patel, P.I. (1998), Evidence that a gene for essential tremor maps to chromosome 2p in four families [erratum in *Mov Disord* 1999; 14: 200]. *Mov Disord*; 13: 972–77.
- Higgins, J.J., Pho, L.T., and Nee, L.E. (1997), A gene (ETM) for essential tremor maps to chromosome 2p22-p25. *Mov Disord*; 12: 859–64.

- Herskovitz, E., and Blackwood, W. (1969), Essential (familial, hereditary) tremor: a case report. *J Neurol Neurosurg Psychiatry*; 32: 509–11.
- Hubble, J.P., Busenbark, K.L., and Koller, W.C. (1989), Essential tremor. *Clin Neuropharm*; 12: 453–82.
- Jankovic, J., McDermott, M., Carter, J., Gauthier, S., Goetz, C., Golbe, L., Huber, S., Koller, W., Olanow, C., Shoulson, I., et al. (1990), Variable expression of Parkinson's disease: a base-line analysis of the DATATOP cohort. The Parkinson Study Group. *Neurology*;40:1529–1534.
- Jordan, N., Sagar, H.J., and Cooper, J.A. (1992), A component analysis of the generation and release of isometric force in Parkinson's disease. *J Neurol Neurosurg Pshchiatry*; 55: 572-6.
- Kaplan, E.D. (1996), *Understanding GPS Principles and Applications*, Artech House Publishers.
- Keller, W., (2004), *Wavelets in geodesy and geodynamics*. Walter de Gruyter.
- Koller, W.C., and Hubble, J.P. (1990), Levodopa therapy in Parkinson's disease. *Neurology*;40(suppl):40–7.
- Koller, W.C., and Rubino, F.A. (1985), Combined resting postural tremors. *Arch Neurol*; 42: 683–84.
- Koller, W.C., Vetere-Overfield, B., and Barter, R. (1989), Tremors in early Parkinson disease. *Clin Neuropharmacol*; 12: 293–97.
- Kreiss, P. (1912), Uberhereditarentremor. *DtZNervHeilk*;44: 111-23.
- Kuipers, B.J. (1999) *Quaternions and rotation Sequences: a Primer with Applications to Orbits, Aerospace, and Virtual Realit*, Princeton University Press, 1999.
- Kutukcu, Y., Marks, W.J., Goodin, D.S., and Aminoff, M.J. (1999), Simple choice reaction time in Parkinson's disease. *Brain Res*; 815: 367-72.
- Logigian, E., Hefter, H., Reiners, K., and Freund, H.J. (1991), Does tremor pace repetitive voluntary motor behavior in Parkinson's disease? *Ann Neurol*; 30:172-9.
- Lotters, J.C., Schipper, J., Veltink, P.H., Olthius, W., and Bergveld, P. (1998), Procedure for in use calibration of triaxial accelerometers in medical applications. *Sensors and Actuators A*. 68(1-3), 221-228.
- Louis, E.D. (2000), Essential tremor. *Arch Neurol*; 57: 1522–24.

- Louis, E.D. (2000), Essential tremor. *N Engl J Med*; 345: 887–91.
- Louis, E.D. (2005), Essential tremor. *Lancet Neurol*; 4: 100-110.
- Louis, E.D., Barnes, L.F., Albert, S.M., et al. (2001), Correlates of functional disability in essential tremor. *Mov Disord*; 16: 914–20.
- Louis, E.D., Ford, B., and Barnes, L.F. (2000), Clinical subtypes of essential tremor. *Arch Neurol*; 57: 1194–98.
- Louis, E.D., Ford, B., Frucht, S., Barnes, L.F., Tang, M.X., and Ottman, R. (2001), Risk of tremor and impairment from tremor in relatives of patients with essential tremor: a community-based family study. *Ann Neurol*; 49: 761–69.
- Louis, E.D., and Greene, P. (2000), Essential tremor. In: Rowland LP, ed. *Merritt textbook of neurology* (10th edn). Philadelphia: Lea & Febiger: 678–79.
- Louis, E.D., Jurewicz, E.C., Applegate, L., et al. (2003), Association between essential tremor and blood lead concentration. *Environ Health Perspect*; 111: 1707–11.
- Louis, E.D., Ottman, R.A., Ford, B., et al. (1997), The Washington Heights Essential Tremor Study: methodologic issues in essential-tremor research. *Neuroepidemiology*; 16: 124–33.
- Louis, E.D., Ottman, R., and Hauser, W.A. (1998), How common is the most common adult movement disorder?: estimates of the prevalence of essential tremor throughout the world. *Mov Disord*; 13: 5–10.
- Louis, E.D., Tang, M.X., Cote, L., Alfaro, B., Mejia, H., and Marder, K. (1999), Progression of parkinsonian signs in Parkinson disease. *Arch Neurol*; 56: 334–337.
- Louis, E.D., Zheng, W., Jurewicz, E.C., et al. (2002), Elevation of blood -carboline alkaloids in essential tremor. *Neurology*; 59: 1940–44.
- Mallat, S. (1989), A theory for multi-resolution signal decomposition: the wavelet representation. *IEEE Transactions on Pattern Analysis and Machine Intelligence*, 11(7), pp. 674-693.
- Mallat, S. (1999), *A wavelet tour of signal processing, second edition*. Academic Press (an Imprint of Elsevier).
- Mansur, P.H.G., Cury, L.K.P. Andrade, A.O., et al. (2007), A Review on Techniques for Tremor Recording and Quantification, *Critical Reviews™ in Biomedical Engineering*, 35(5), 343-362

- Manto, M., Topping, M., Soede, M., et al. (2003) Dynamically Responsive Intervention for Tremor Suppression, *IEEE Engineering in Medicine and Biology Magazine*, May/June, 120-132.
- Matlab (computational environment) Help Documentation (2008), scal2frq function, [Online]. Available:<http://matlab.izmiran.ru/help/toolbox/wavelet/scal2frq.html> [Accessed 13 July, 2010].
- Maybeck, P.S. (1982), *Stochastic Process and Estimation*, Vol. I and II, Academic Press, Inc., New York.
- Meyer, K., Applewhite, H., and Biocca, F. (1992), "A Survey of Position Trackers," *Presence: Teleoperators and Virtual Environments*, vol. 1, no. 2, 1992, pp. 173-200.
- Nasiri, S. (2005), *A Critical Review of MEMS Gyroscopes Technology and Commercialization Status*, White Paper, InvenSense.
- Navan, P., Findley, L.J., Jeffs, J.A., et al. (2003), Double-blind, single-dose, cross-over study of the effects of pramipexole, pergolide, and placebo on rest tremor and UPDRS part III in Parkinson's disease. *Mov Disord*;18:176–80.
- Norkin, C.C., and White, D.J. (2003), *Measurement of joint motion: A guide to goniometry*. Philadelphia: F.A. Davis.
- Oppenheim, A.V., and Schaefer, R.W. (1989), *Discrete Time Signal Processing*, Prentice Hall, Englewood Cliffs NJ, 879 pp.
- Paulus, W., and Jellinger, K. (1991), The neuropathologic basis of different clinical subgroups of Parkinson's disease. *J Neuropathol Exp Neurol*;50:743–755.
- Pifl, C., Schingnitz, G., and Hornykiewicz, O. (1991), Effect of 1-methyl-4-phenyl-1,2,3,6-tetrahydropyridine on the regional distribution of brain monoamines in the rhesus monkey. *Neuroscience*;44: 591–605.
- Pogarell, O., Gasser, T., van Hilten, J.J., et al. (2002), Pramipexole in patients with Parkinson's disease and marked drug resistant tremor: a randomised, double blind, placebo controlled multicentre study. *J Neurol Neurosurg Psychiatry*;72:713–20.
- Pollock, L.J., and Davis, L. (1930), Muscle tone in parkinsonian states. *Arch Neurol Psychiatry*;23:303–319.
- Popovich, L. and Popovich, M.B., (2008), Extraction of Tremor for Control of Neural Prosthesis, comparison of discrete wavelet transform and butterworth filter, *IEEE - 9th Symposium on Neural Network Applications in Electrical Engineering*, 4 pp.

- Prochazka, A., Elek, J., and Javidan, M. (1992), "Attenuation of pathological tremors by functional electrical stimulation I: Method," *Ann. Biomed. Eng.*, vol. 20, pp. 205–224.
- Rack, P.M., and Ross, H.F. (1986), The role of reflexes in the resting tremor of Parkinson's disease. *Brain*;109:115–141.
- Rajput, A.H., Offord, K.P., Beard, C.M., and Kurkland, L.T. (1984), Essential tremor in Rochester, Minnesota: a 45-year study. *J Neurol Neurosurg Psychiatry*; 47: 466–70.
- Rajput, A.H., Rozdilsky, B., Ang, L., and Rajput, A. (1993), Significance of Parkinsonian manifestations in essential tremor. *Can J Neurol Sci*; 20: 114–17.
- Rajput, A.H., Rozdilsky, B., and Ang, L. (1991), Occurrence of resting tremor in Parkinson's disease. *Neurology*;41:1298–1299.
- Rao, G., Fisch, L., Srinivasan, S., D'Amico, F., Okada, T., Eaton, C., and Robbins, C. (2003), Does this patient have Parkinson disease? *JAMA*.;289(3):347–53.
- Rautakorpi, I. (1978), Essential tremor. An epidemiological, clinical and genetic study. In: Research reports from the Department of Neurology, University of Turku, Finland. Turku: University of Turku: 12.
- Riley, P., and Rosen, M. (1987), "Evaluating manual control devices for those with tremor disability," *J. Rehab. Res., Dev.*, vol. 24, pp. 99–110.
- Riviere, C.N. (1995), "Adaptive suppression of tremor for improved humanmachine control," Ph.D. dissertation, Johns Hopkins Univ, Baltimore, MD.
- Riviere, C.N., Rader, R.S., and Thakor, N.V. (1998), Adaptive Canceling of Physiological Tremor for Improved Precision in Microsurgery. *IEEE Transactions on Biomedical Engineering*, 45(7), pp. 839-846.
- Riviere, C.N., Reich, S.G., and Thakor, N.V. (1997), Adaptive Fourier Modeling for Quantification of Tremor. *Journal of Neuroscience Methods*, 74, pp. 77-87.
- Rocon, E., Belda-Louis, J.M., Sanchez-Lacuesta, J.J., and Pons, J.L. (2004), Pathological Tremor Management: Monitoring, Compensatory Technology and Evaluation. *Technology and Disability*, 16, pp. 3-18.
- Ruiz, P.J.G. (2004), Prehistoria de enfermedad de Parkinson. *Neurologia*;19(10):735–7.
- Sabatini, A.M. (2006), Quaternion-based extended Kalman filter for determining orientation by inertial and magnetic sensing. *IEEE Transactions on Biomedical Engineering*, 53(7):1346-1356.

- Schrag, A., Keens, J., and Warner, J. (2002), Ropinirole for the treatment of tremor in early Parkinson's disease. *Eur J Neurol*;9:253–7.
- Schuurman, P.R., Bosch, D.A., Bossuyt, P.M.M., et al. (2000), A comparison of continuous thalamic stimulation and thalamotomy for suppression of severe tremor. *N Engl J Med*; 432: 461–68.
- Sekine, M., Tamura, T., AKay, M. et al. (2002), Discrimination of walking patterns using wavelet based fractal analysis, *IEEE Transactions on Neural Systems and Rehabilitation Engineering*, VOL. 10, NO. 3, 188-196.
- Shin, E.H. (2005), Estimation Techniques for Low Cost Inertial Navigation, PhD Thesis, Department of Geomatics Engineering, University of Calgary.
- Smaga, S. (2003), Tremor. *Am Fam Physician*;68(8):1545–52.
- ST Microelectronics, LIS3L06AL MEMS Inertial Sensor Data Sheet (2006) pp. 1-17, [Online]. Available: <http://www.st.com/stonline/products/literature/ds/11669.pdf> [Accessed July, 2010].
- Stelmach, G.E., Teasedale, N., Phillips, J., and Worringham, C.J. (1989), Force production characteristics in Parkinson's disease. *Exp Brain Res*; 76: 165-72.
- Stelmach, G.E., and Worringham, C.J. (1988), The preparation and production of isometric force in Parkinson's disease. *Neuropsychologia*; 26: 93-103.
- Strauss, W.A. (1992), *Partial Differential Equations: An Introduction*, John Wiley and Sons, 440 pp.
- Teskey, W.J. (2007), Precision six degree-of-freedom motion tracking using inertial sensors, MSc Thesis, Department of Mechanical and Manufacturing Engineering at the University of Calgary.
- Teskey, W.J., Elhabiby, M., and El-Sheimy, N. (2010a), Kalman smoothing and wavelet analysis for inertial data of human movement disorder motion, *Sensors and Transducers Journal*, Vol. 116, Issue 5, May 2010, pp. 61-75, [Online]. Available: http://www.sensorsportal.com/HTML/DIGEST/P_616.htm [Accessed August, 2011].
- Teskey, W.J., Elhabiby, M., and El-Sheimy, N. (2010b), Wavelet and Fourier Analysis of Essential Tremor Motion using MEMS Accelerometers and Gyroscopes, The 7th IASTED International Conference on Biomedical Engineering, Innsbruck, Austria, Feb. 17-19, 7pp.
- Teskey, W.J., Elhabiby, M., and El-Sheimy, N. (In print: 2011a), Wavelet analysis of essential tremor motion captured using MEMS inertial sensors, submitted to the *Journal of Wavelet Theory and Applications*, 17 pp.

- Teskey, W.J., Elhabiby, M., and El-Sheimy, N. (2011b), Adaptive Human Tremor Assessment and Attenuation: six degree-of-freedom motion analysis utilizing wavelets, INSTICC BIODEVICES Conference, Rome, Italy, January 26-29, 9pp.
- Teskey, W.J.E., Elhabiby, M., El-Sheimy, N., (2011c), Movement Disorders Assessment and Attenuation Techniques for Removal of Tremor, Biomedical Engineering Systems and Technologies 2011- Revised Selected Papers, 12 pp.
- Teskey, W.J.E., Elhabiby, M., El-Sheimy, N., (Accepted: 2011d), Inertial Sensing to Determine Movement Disorder Motion Present Before and After Treatment, Sensors, 12 pp.
- Teskey, W.J., Elhabiby, M., El-Sheimy, N. and MacIntosh, B. (Submitted: 2011), Coherence analysis for movement disorder motion captured by six degree-of-freedom inertial sensing. Submitted to: The Journal of Applied Geodesy, 18 pp.
- Torrence, C., and Compo, G.P. (1998), A practical guide to wavelet analysis. Bulletin of the American Meteorological Society, 79, pp. 61-78.
- Vanicek, P. and Omerbasic, M. (1999), *Does a navigation algorithm have to use a Kalman filter?*, Canadian Aeronautical and Space Institute Journal, Vol. 45, 3, pp. 292-296.
- Walpole, R. E., Myers, R. H., Myers, S. L., and Ye, K. (2002), *Probability and statistics for engineers and scientists, 7th edition*. Prentice Hall.
- Welch, B. L. (1947), "The generalization of "Student's" problem when several different population variances are involved", *Biometrika* 34 (1-2): 28-35. Available at:<http://biomet.oxfordjournals.org/cgi/reprint/34/1-2/28>
- Welch, G. and Foxlin E, (2002), Motion tracking: no silver bullet but a respectable arsenal. IEEE Motion Tracking Survey, Nov/Dec.
- Widrow, B., and Stearns, S.D. (1985), *Adaptive Signal Processing*. Englewood Cliffs, NJ: Prentice-Hall, ch. 12.
- Winter, D.A. (1990), *Biomechanics and Motor Control of Human Movement*, (3rd Edition), New York, Wiley-Interscience Publishings.
- Yang, Y., Niu, X., and El-Sheimy, N. (2006), *Real-Time MEMS Based INS/GPS Integrated Navigation Systems for Land Vehicle Navigation Application*, Institute of Navigation National Technical Meeting 2006, January 18-20, Monterey, California.
- Yazdi, N., Ayazi, F., and Najafi. K. (1998), Micromachined Inertial Sensors, Proceedings of the IEEE, Vol. 86, No. 8, August 1998.